UNIVERSITÁ DEGLI STUDI DI PADOVA

Sede Amministrativa: Università degli Studi di Padova
Dipartimento di Biologia

Dottorato di Ricerca
in
Fisiologia Molecolare e Biologia Strutturale
Ciclo XX

STRUCTURAL STUDIES ON THE C-TERMINAL DOMAIN OF HUMAN PMCA1b

Coordinatore: Ch.mo Prof. Benedetto Salvato
Supervisori:
Ch.mo Prof. Mariano Beltramini
Ch.mo Prof. Luigi Bubacco
Ch.mo Prof. Ernesto Carafoli
Ch.mo Prof. Stefano Mammi

Dottorando: Federico Benetti

1 Table of contents

2 Abstract

Plasma Membrane Calcium ATPases (PMCAs) are P-type pumps involved in calcium homeostasis. Their 3D structures are still unknown but a possible topology has been predicted. PMCAs are predicted to have a cytosolic N-terminal domain, a cytosolic C-terminal domain (regulatory domain), ten transmembrane segments and two cytosolic loops called transduction domain and catalytic domain that connect the 2nd and the 3rd, the 4th and the 5th transmembrane segments respectively. Several mechanisms are responsible of their activation: interaction with Ca^{2+}-calmodulin, interaction with acidic phospholipids and fatty acids, phosphorylation with kinases A and C, proteolysis by calpain and oligomerization. All activation mechanisms decrease the Km values, in particular the oligomerization brings this value around at the value of cytosolic calcium concentration present in the resting cells (50-100 nM). The C-terminal domain is a structural motif that distinguishes PMCAs from all other P-type pumps. It is also the target of all activators and activation mechanisms. In this study we have described the secondary structure and tertiary structure at low resolution of the C-terminal regulatory domain of the human PMCA isoform 1b. We have found that the domain forms aggregates by intermolecular interactions. Moreover, we have studied the reversibility of the oligomerization process and found the best conditions to stabilize the C-terminal domain in the monomeric form. These conditions imply the presence of the lipid mimetic SDS at critical micellar concentration. A structural reconstruction based on Small Angle Neutron Scattering experiments provides a low resolution structure where the C-terminal domain has an hourglass shape. The central cross section compatible with that of an α-helix. This part could correspond at the α-helix of the C28W calmodulin binding region while the downstream and upstream regions could be random coil as also predicted by PSIpred. Binding experiments between the C-terminal domain and the Ca^{2+}-calmodulin have been carried out. The aim was to study whether in a phospholipid mimetic system necessary to stabilize the monomeric form, such as sodium dodecyl sulphate, this domain can still interact with calmodulin. The phospholipid mimetic system that stabilize the domain in the monomeric form prevent its binding with Ca^{2+}-calmodulin. The results suggest that a different aggregation state of the PMCAs exist in diverse membrane rafts: membrane rafts rich in uncharged or zwitterionic phospholipids could contain PMCAs in oligomeric form while membrane rafts rich in acidic phospholipids could contain PMCAs in monomeric form.

3 Abstract

Le calcio ATPasi della membrana plasmatica appartengono alla famiglia delle pompe di tipo P e sono coinvolte nell'omeostasi del calcio. La loro struttura tridimensionale è ancora sconosciuta anche se è stata predetta una possibile topologia. Le PMCA sono predette avere un dominio N-terminale e un dominio C-terminale (dominio regolatorio) citosolici, dieci segmenti transmembrana e due loop citosolici che connettono il secondo segmento transmembrana con il terzo e il quarto segmento transmembrana con il quinto. Diversi meccanismi sono responsabili dell'attivazione delle PMCA: l'interazione con la Ca^{2+}-calmodulina, l'interazione con fosfolipidi acidi e acidi grassi, la fosforilazione per opera delle chinasi A e C, la proteolisi da parte della calpaina e l'oligomerizzazione. Tutti questi meccanismi di attivazione abbassano il valore della Km e, in particolare, l'oligomerizzazione rende questo valore comparabile alla concentrazione citosolica di calcio presente nelle cellule a riposo (50-100 nM). Il dominio C-terminale è il target di tutti questi attivatori e dei meccanismi di attivazione. In questo studio, abbiamo descritto la struttura secondaria e terziaria a bassa risoluzione del dominio C-terminale della PMCA 1b. Abbiamo trovato che questo dominio forma aggregati perciò si è reso necessario studiare la reversibilità del processo di oligomerizzazione e trovare le condizioni ottimali per stabilizzare il dominio in forma monomerica. Queste condizioni implicano la presenza di SDS, che rappresenta un sistema fosfolipide mimetico, alla concentrazione micellare critica. La ricostruzione tridimensionale della struttura a bassa risoluzione basata su dati di *Small Angle Neutron Scattering* ha evidenziato una forma a clessidra con la sezione centrale compatibile con le dimensioni di un'α-elica. Questa parte potrebbe corrispondere alla regione ad α-elica del dominio C-terminale che lega la calmodulina (C28W) mentre le regioni esterne potrebbero essere random coil, come peraltro predetto da PSIpred. Esperimenti di *binding* tra il dominio C-terminale e la calmodulina in presenza di SDS mostrano che a valori della concentrazione di SDS superiori a 0.03% non vi è più interazione. Questi risultati suggeriscono che possono coesistere differenti stati di aggregazione delle PMCA: in regioni della membrana plasmatica ricche di fosfolipidi neutri le PMCA potrebbero trovarsi in forma oligomerica mentre in regioni ricche di fosfolipidi acidi le PMCA potrebbero trovarsi in forma monomerica.

4 Introduction

4.1 Calcium in biological systems

Pluricellular organisms are specialized cells ensemble where their various individual cellular components must communicate to perform specific tasks. This demands the exchange of signals to modulate and coordinate activities. Therefore, multicellular organisms have developed complex ways of generating and processing information, based on messengers that carry the primary signals to cells (first messengers) or decode their information inside them (second messengers). Calcium is a special second messenger because it has great versatility and controls a wide variety of cellular processes including bone mineralization, as in the case of bone, contraction, as in the case of muscle, secretion, glycolysis and gluconeogenesis, ion transport, cell division and growth. In the resting eukaryotic cells calcium concentration is kept low, around 50-100 nM whereas in the extracellular milieu it can be as high as 1-2 mM [**1**]. Calcium is well suited for the role of an intracellular messenger for its high electrochemical gradient across biological membranes and its distinctive coordination chemistry.

Calcium (Ca^{2+}) is defined as a hard ion therefore it prefers oxygen ligands over nitrogen or sulfur ligands: Ca^{2+} – nitrogen bonds are about 0.25-0.3 Å longer than Ca^{2+} – oxygen bonds [**2, 3, 4**]. In a study of 170 X-ray structures of Ca^{2+}-complexes large differences in coordination number and geometry have been observed.

Among the possible ligands, acidic amino acids can coordinate calcium in three different modes:

1. unidentate, when they interact with calcium using only one of the two carboxylate oxygens;
2. bidentate, when they interact with calcium using both carboxylate oxygens;
3. mixed "α-mode", when calcium ion is chelated by one of the carboxylate oxygens and another ligand bound to the α-carbon of amino acid;

Coordination numbers follow the order 8 > 7 > 6 > 9 with irregularly shaped binding cavities. Moreover, the rate of substitution of water molecules in the inner hydration sphere has been determined to be 8.4 s^{-1}. These features permit to distinguish calcium ion from another biologically important ion such as magnesium which tends to demand perfectly octahedral binding cavities and has a rate of substitution of water molecules of 5.2 s^{-1} [**5**].

4.2 Calcium binding proteins

Calcium binding proteins could be subdivided into two broad categories: proteins that regulate calcium concentration in the environment such as parvalbumin and proteins that decode the information carried by the ion such as calmodulin. Calcium acts essentially as an allosteric regulator, so far it was never found to participate as a tightly bound species in catalysis at the active site of enzymes.

4.2.1 EF-hand proteins

The majority of proteins involved in transducing intracellular Ca^{2+} signals are characterized by a common helix-loop-helix structural motif in their Ca^{2+} binding sites, termed the EF-hand [**6**]. EF-hand motifs almost always occur in pairs, packed together in a face-to-face manner. The pairing of sites is believed to stabilize the protein conformation, increase the Ca^{2+} affinity of each site and provide a structural basis for the cooperativity in the binding of Ca^{2+} [**7**]. The classical EF-hand motif consists of a peptide, about 30 residues in length, containing contiguous helix I, a loop around the calcium ion and helix II (**fig. 1**).

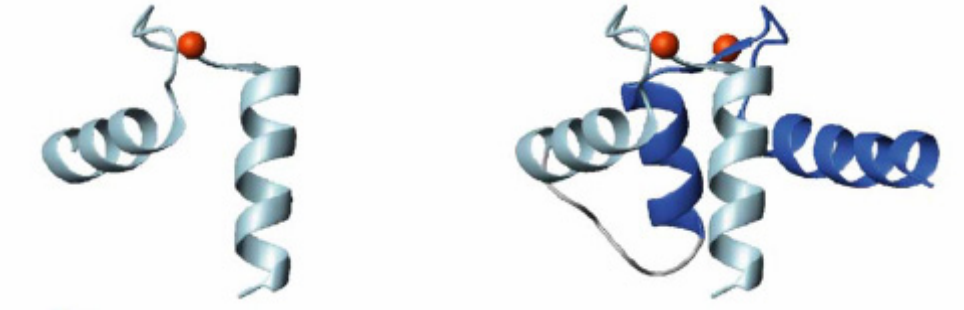

(a) (b)

Fig. 1. 3D reconstruction of: (a), the structure of the isolated EF-hand motif; (b), the structure of the EF-hand domain

Residues 1, 3, 5, 7, 9 and 12 are involved in metal coordination forming a pentagonal bipyramidal array of seven oxygen ligands. These residues are located in the loop of the EF-hand motif and their position are called X, Y, Z, -X, -Y, -Z (**fig. 2**) [7].

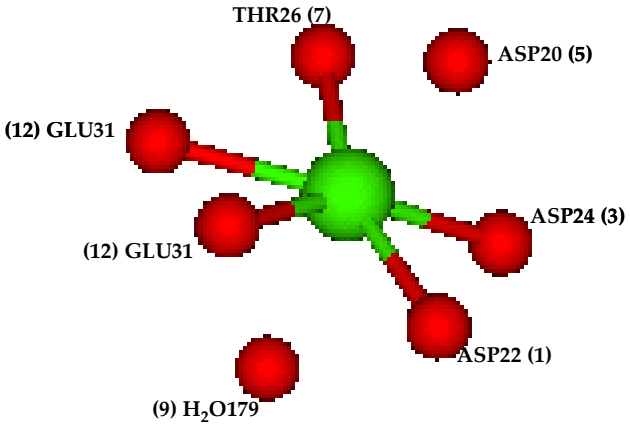

Fig. 2. 3D representation of the calcium binding site of calmodulin (1cll.pdb); the oxygens that participate to the binding are highlighted in red, whereas in green is represented the calcium ion.

Residues 1, 3 and 5 are usually aspartate carboxylate that provide unidentate oxygen ligands. Residue 12 provides bidentate oxygen ligand whereas residue 7 directly coordinates the ion via its main chain oxygen. The oxygen from one water completes the coordination geometry of the EF-hand motif [**8**]. The core of the EF-hand is reasonably conserved, but the outer regions vary and therefore the Ca^{2+} dissociation constant can range from 10^{-7} and 10^{-5} mol/L [**1**].

4.2.1.1 Calmodulin family

The calmodulin family is very large and has been extensively characterized amongst the EF-hand Ca^{2+} sensor proteins **[9, 10]**. Calmodulin, the archetypal EF-hand calcium sensor, is an acidic protein of about 17 kDa. It consists of two EF-hand domains tethered by a flexible helical linker. The two domains share high overall sequence homology (75%), as well as structural similarity both in the presence and absence of Ca^{2+} ions. The differences in the two domains are responsible of distinct biochemical properties as the calcium affinity: CaM-C (kd~10^{-6} M) is 10-fold stronger than CaM-N (kd~10^{-5} M). CaM-C is predominantly acid while CaM-N possesses acidic patches that are partly neutralized by inclusion of basic residues in and around the binding pocket. After the binding with calcium, CaM exposes a hydrophobic surface that interacts with targets (**fig. 3**).

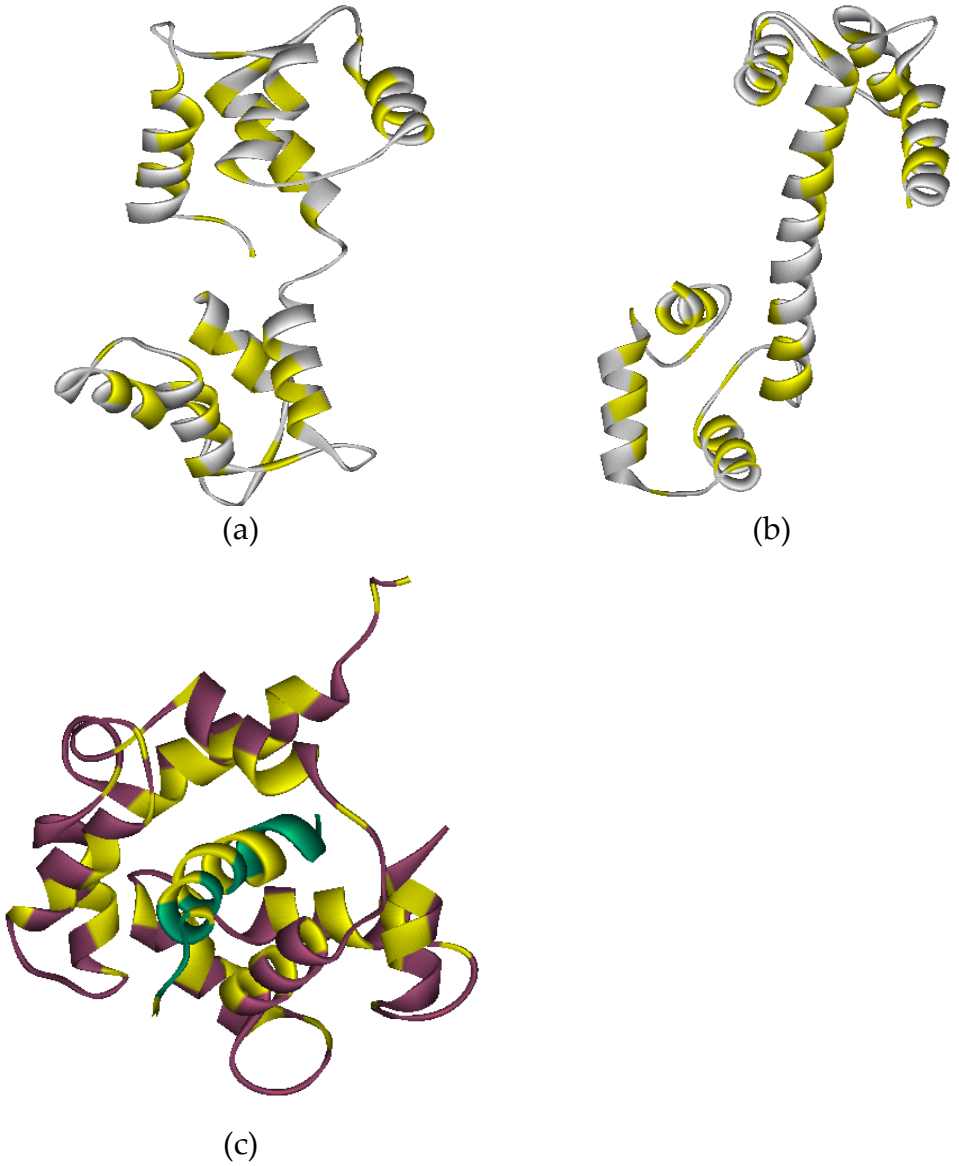

Fig. 3. 3D reconstruction of: (a), tertiary structure of the apo-CaM (1cfd.pdb); yellow patches represent hydrophobic regions. (b), tertiary structure of the holo-CaM (1cll.pdb); yellow patches represent hydrophobic regions. (c), structure of CaM bound to a peptide corresponding to the calmodulin-binding domain of smooth muscle myosin light chain kinase (2bbm.pdb).

Ca^{2+}-bound CaM binds to its targets with high affinity (K_D~10^{-9} M) [**1**]. To form the bound state, the central residues of the link region unwind from their α-helical arrangement to form a hinge that allows the molecule to bend and wrap itself around the target protein. This state persists only as long as calcium concentration remains as high as to saturate the protein. When the concentration falls, the bound calcium dissociates and CaM is quickly released, inactivating the target.

4.2.2 C2 Domains

C2 domains are structures that possess Ca^{2+} binding sites; they are also known as CaLB or Ca^{2+} and lipids binding domains. C2 domains exit in a wide variety of intracellular proteins such as synaptotagmin, phospholipase C and protein kinase C. Like the EF-hands their affinity for calcium is variable. C2 domains consists of a compact ß-sandwich of two four-stranded ß-sheets made from 130 amino acids (**fig. 4**). Ca^{2+}–binding sites are confined to a region that is defined by three loops on one edge of the structure and binds calcium using oxygen atoms of aspartate side chains. The coordination sphere around each Ca^{2+} ion is incomplete, thus explaining the low affinity of these sites for calcium (K_D~1 mM) [**1**]. C2 domains interact with negatively charged phospholipids such as phosphatidylserine, phosphatidylinositol and polyphosphoinositides. The side chains in the loop regions are mostly positively charged. Therefore, when calcium is bound to the C2 domains the negative charges are neutralized and the protein can bind electrostatically to the anionic lipids thus completing the coordination sphere. This mechanism allows soluble proteins with C2 domains to become membrane-associated in presence of high calcium levels. There are not conformational changes induced by calcium to C2 domains suggesting that the calcium signaling transduction is modulated by changes of electrostatic potential as demonstrated on synaptotagmin I. In this case the C2 domains would act as a Ca^{2+}-dependent electrostatic switch, without requiring significant conformational changes. There are variations in the stoichiometry of binding (number of sites) and in the affinity for Ca^{2+}.

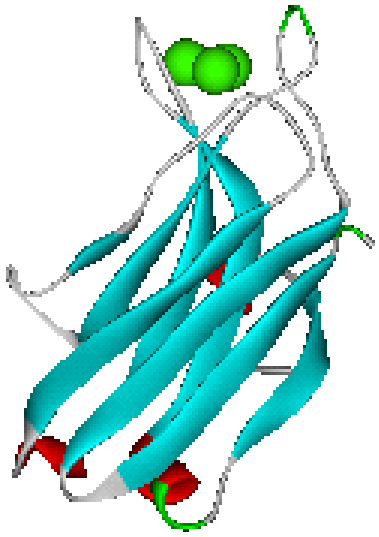

Fig. 4. C2 domain structure with calcium ions in green (1a25.pdb).

4.2.3 Annexins

The annexin family is ubiquitously present in eukaryotic cells except erythrocytes and yeast. Annexins are able to bind to negatively charged phospholipids in Ca^{2+}-dependent manner, and hence to associate reversibility to membranes. *In vitro* studies demonstrated that annexins promote the vesicle aggregation and fusion, inhibit the phospholipase A_2, anticoagulation and ion channel activities. These properties suggest the involvement of annexins in membrane traffic processes such as endocytosis and exocytosis. All annexins contain four highly conserved repeates of 70 residues except the annexin VI that contains eight repeats. Each repeat folds in a compact domain consisting of five α-helices of 7-16 amino acids wound in a right-handed superhelix (**fig. 5**). The four domains are arranged in a cyclic array; strong hydrophobic interactions between domains II and III and I and IV respectively, generate two tight modules that interact more weakly through polar or charged residues. The Ca^{2+}–binding sites are located on the convex side of the protein, which is the membrane-binding side. Ca^{2+} is coordinated to three carbonyl oxygen atoms at the N-terminus of the fold, and to the carboxylate group of an acidic side chain 38 residues down the sequence, water molecules complete the pentagonal bipyramidal coordination sphere. Annexins bind calcium ion with moderate affinity (K_D in the micromolar to millimolar range) and with only three of the four repeats.

Fig. 5. Crystal structure of the annexin V (1avr.pdb) with in green the bound calcium ions.

4.3 Calcium homeostasis

Calcium binding proteins fulfill a wide range of functions. Important members of this family are involved in the intracellular calcium homeostasis maintaining low the cytosolic calcium concentration. There are two systems involved in cellular calcium homeostasis: low affinity, high capacity Na^+/Ca^{2+} exchangers, which are particularly active in excitable tissuses, and a high affinity, low capacity Ca^{2+}-ATPases, which is active in all eukaryotic cells. In addition to membrane pumps and ion exchangers, other proteins act as intracellular Ca^{2+} buffers. Low calcium levels are maintained in the cytosolic compartment by removing Ca^{2+} from the cell and also by pumping it

into the lumen of the endoplasmic reticulum (ER). The pumps are transmembrane proteins that move Ca^{2+} ions across membranes against the electrochemical potential gradient.

4.4 Plasma Membrane Calcium ATPases

Plasma membrane calcium pumps, also known as PMCAs, are a primary system for the specific removal of Ca^{2+} from eukaryotic cells. They belong to the P2 (subtype 2B) subfamily of P-type primary ion transport ATPases, which are characterized by the formation of an aspartyl phosphate intermediate in their reaction cycle. The consensus sequence for the phosphorylation is DKTGT, the same in all P-type pumps [**11**]. P-type pumps exist in two conformational states termed E1 and E2 as shown in **fig. 6**. Generally, in E1 state the PMCAs have higher calcium affinity than the E2 state.

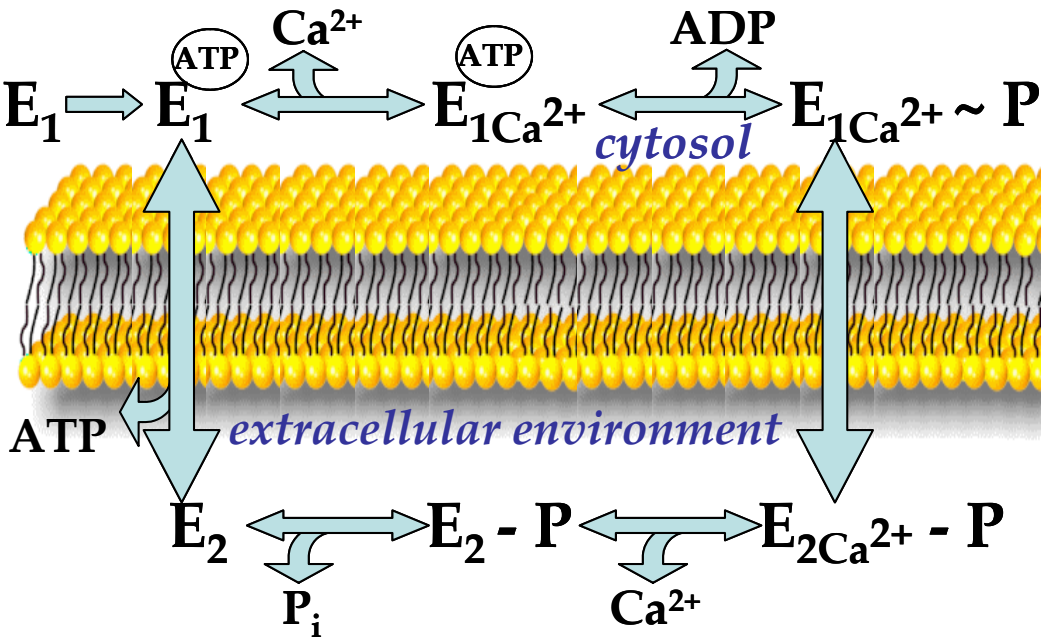

Fig. 6. Catalytic cycle of the PMCA pump: E_1 represents the inactivated PMCA in the resting cells; once activated the PMCA is able to bind ATP (E_1-ATP); calcium is bound to the pump (E_{1Ca2+}-ATP) and ATP transfers its gamma Pi to the protein aspartyl residue to form the phosphorylated intermediate (E_{1Ca2+}~P); E_{1Ca2+}~P has a high energy content and therefore it changes its conformation to generate a low energy conformer (E_{2Ca2+}-P); in this conformation the calcium affinity of the pump is lower and the ion is thus released in the extracellular environment (E_2-P); Pi is also released in the extracellular space (E_2) and the pump returns in E1 state. This cycle works during the stimulus [**12**]. The phospholipidic bilayer represents the plasma membrane.

PMCA differs from its homologues in the sarco(endo)plasmic reticulum (SERCA) for the Ca^{2+}/ATP stoichiometry: PMCA and SERCA extrude one and two calcium ions per hydrolyzed ATP molecule, respectively.

PMCAs are transmembrane proteins of 120-140 kDa. Their structures are still unknown but they are predicted to contain 10 membrane-spanning segments and the NH_2 and COOH termini located in cytosolic side of the membrane [**13**]. There are also two cytosolic loops termed transduction domain and catalytic domain that connect the 2nd and the 3rd and the 4th and the 5th transmembrane segments respectively (**fig. 7**).

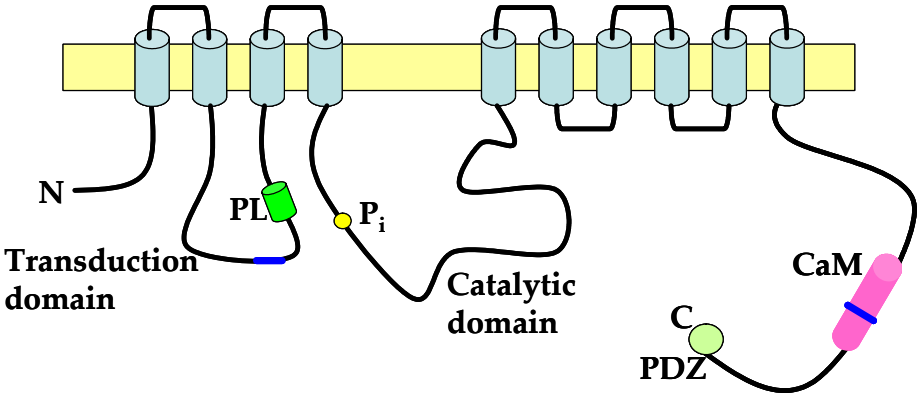

Fig. 7. Putative two dimensional model of PMCAs. PL: indicates the phospholipid sensitive region; Pi: indicates the phosphorylation site; CaM: the calmodulin binding region. The green circle at the COOH terminal denotes the consensus sequence for the interaction with PDZ domains. Blue lines represent the two alternative splicing sites: site A located in the transduction domain and the site C located in the C-terminal domain.

The transduction domain is thought to play an important role in the long range transmission of conformational changes occurring during the transport cycle. The catalytic domain contains the ATP binding site and the aspartate residue that forms the aspartyl phosphate intermediate during ATP hydrolysis. The main part distinguishing PMCAs from all other P-type pump is the C-terminal domain, also referred to as regulatory domain.

4.4.1 Isoforms of the PMCAs

The mammalian PMCAs are composed by four isoforms that are encoded by four non allelic genes. The chromosomal loci for the human genes have been determined: 12q21-q23 for PMCA1, 3p25-p26 for PMCA2, Xq28 for PMCA3 and 1q25-q32 for PMCA4 [**14**, **15**, **16**]. The mammalian genes appear to be very closely related in their exon-intron structure, as demonstrated by the almost perfect conservation of intron locations in all currently known human, rat and mouse PMCA genes and gene fragments. Each of the gene primary transcripts is subject to alternative splicing. There are two alternative splicing site termed A and C located in the transduction domain and in the C-terminal domain respectively. At each splicing site there are many splice options and thus over 20 variants have been identified at the cDNA level.

4.4.1.1 Splice site A

The alternative splicing options at site A is well known in all four human and rat PMCA isoforms (**fig. 8**). Site A is located upstream of one of the two phospholipid sensitive region as shown in **fig. 7** [**17**, **18**].

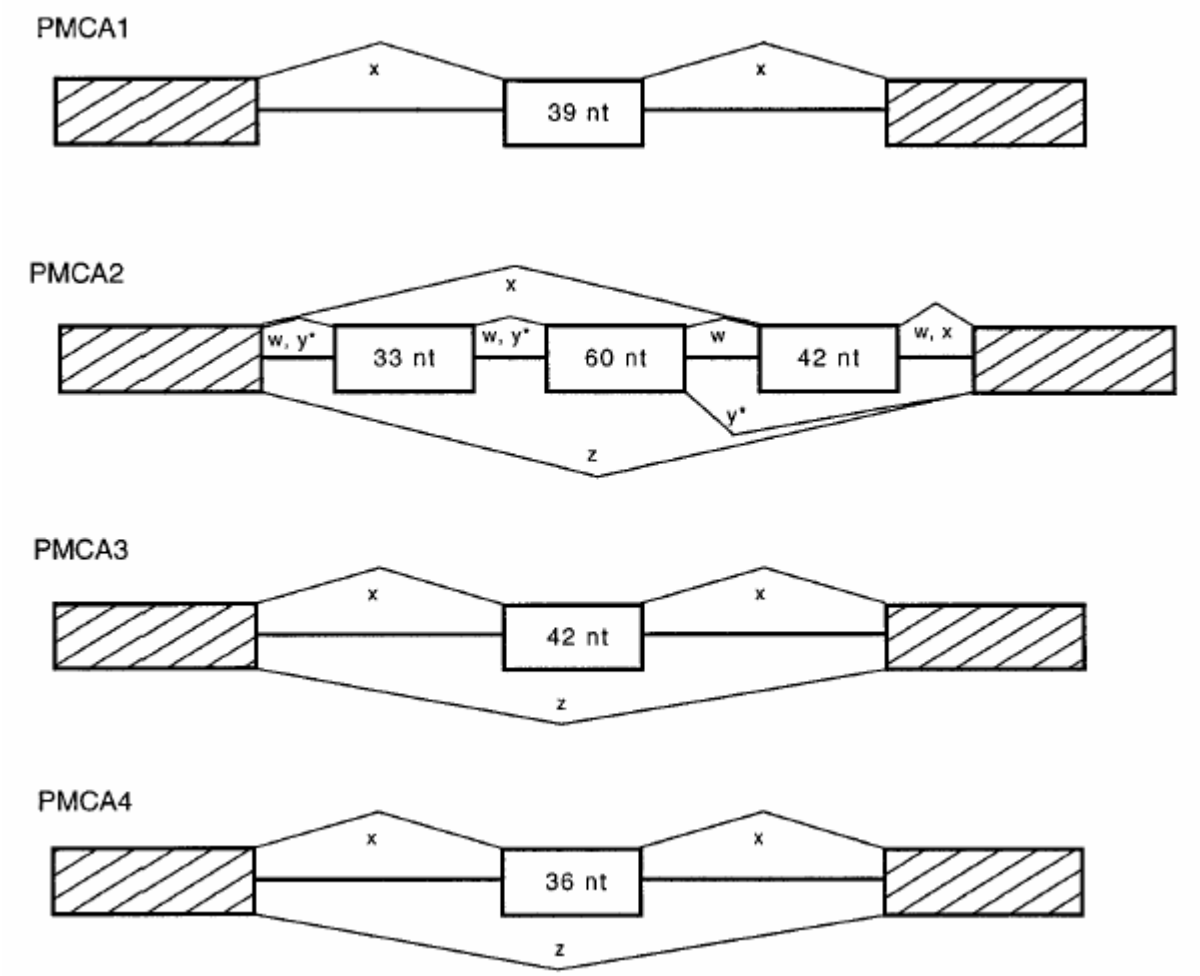

Fig. 8. Alternative splicing options at site A. Open boxes represent the spliced exons, whose number of the included nucleotides (nt) is indicated by Arabian numbers, while the hatched boxes represent the spliced exons flanking site A. Introns are represented by black line that join the boxes. The sizes of the spliced exon are displayed inside the open boxes whereas the resulting splicing variants are labelled by their lowercase symbol [**12**].

The splicing involves an exon of 36-42 nucleotides (nt) that can be optionally inserted or excluded in the mature transcripts of all pumps with the exception of PMCA1, in which a 39 nt exon is always included [**19**]. The splicing options of PMCA2 are more complex because there are three exons of 33 nt, 60 nt and 42 nt and thus many splicing variants. This is possible because all exons contain integral multiples of three nucleotides and any combination does not change the open reading frame of the pump. The lowercase letter **z** indicates the exclusion of all optional exons while the letter **x** indicates the inclusions of the exon 36 (PMCA4), 42 (PMCA3 and 2) or 39 (PMCA1). The additional letters **w** and **y** necessary to describe all alternative splicing variants of the PMCA2 indicate the insertion of all three exons (33 nt, 60 nt and 42 nt) or the inclusion of the 33 nt and 60 nt respectively. In human, only variants **z**, **w** and **x** have been detected while **y** variant has been found in rat [**20**].

4.4.1.2 Splice site C

The alternative splicing site C is located inside the calmodulin binding region of the C-terminal domain as described above. The splicing at the site C occurs in all isoforms although with variable complexity (**fig. 9**).

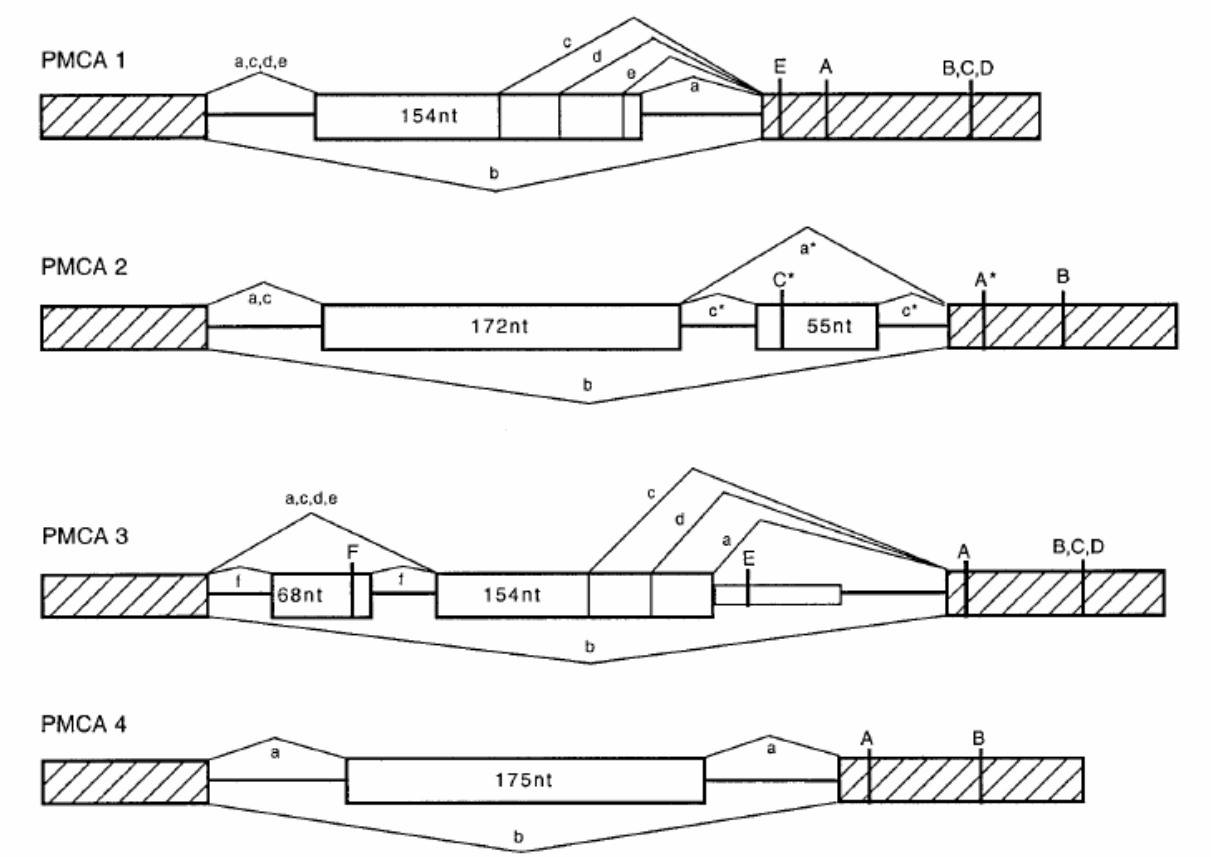

Fig. 9. Alternative splicing options at site C. Open boxes represent the spliced exons while the hatched boxes represent the spliced exons flanking site C. Introns are represented by black line that join the boxes. The number of nucleotides (nt) included in the spliced exon are displayed inside the open boxes whereas the resulting splicing variants are labelled by their lowercase symbol [**12**].

The lowercase letter **b** indicates the exclusion of all alternatively spliced exons whereas the letter **a** indicates the inclusion of the entire large exon of 154 nt, 172 nt, 154 nt and 175 nt, respectively in PMCAs 1, 2, 3 and 4. All splicing variants **a** have a different primary sequence downstream to the insertion site because the large exon does not contain integral multiples of three nucleotides. PMCA1 and PMCA3 present other splicing variants termed **c**, **d** and **e** generated by utilization of multiple internal donor sites within the large exon. All splicing variants except the splicing variant **a** present the consensus sequence X-Thr/Ser-X-Val for the interaction with PDZ domain containing proteins.

The presence of a specific pattern of expression of splicing variants is essential for the normal cellular development as demonstrated by antisense-mediated inhibition experiments on PC12 cells (rat pheochromocytoma 12) [**21**]. In this experiment the expression of PMCA2 and PMCA3 was suppressed causing the decrease of the Vmax from 1.72±0.14 to 1.07±0.11 μmoles Ca^{2+}/mg of protein, the increase of Km (μM) from a value of 1.64±0.17 to a value of 5.88±0.62 and the decrease of the CaM stimulation from x1.43 to x1.06. Experiments performed on other cellular types such as vascular smooth muscle cells [**22**] andMCF-7 cells [**23**] (breast cancer cell line) have induced the apoptosis and suppressed the proliferation respectively. In absence of the correct PMCA expression pattern, other system are involved in calcium homeostasis such as

SERCA and Na^+/Ca^{2+} exchangers while other PMCA splicing variants are not expressed.

4.4.2 Tissue distribution and cellular location of PMCAs

The four PMCA genes are not equally expressed in all tissues: the genes for isoforms 1 and 4 are putative "housekeeping" genes, whereas the genes for the isoforms 2 and 3 have proven to be more limited in their expression [**24**, **25**] (**tab. 1**). Some of the alternatively spliced isoforms of the four PMCA genes have also a tissue specific distribution as shown in **tab. 2**.

mRNA	Spleen	Thymus	Pancreas	Skeletal muscle	Kidney	Liver	Lung	Small intestine	Heart	Adrenal gland	Spinal cord	Brain
PMCA1a				+					+			+
PMCA1b	+	+	+	+	+	+	+	+	+	+	+	+
PMCA1c				+					+		+	+
PMCA1d				+					+			
PMCA2						+				+	+	+
PMCA3a											+	+
PMCA3b										+	+	+
PMCA4a	+	+	+	+	+	+	+	+	+	+	+	+
PMCA4b			+	+			+	+	+		+	+

Tab. 1. Summary of the tissue distribution of PMCA mRNAs [**26**].

Alternative splicing is also responsible to the targeting of the PMCA isoforms in specific membrane domains [**28**]. Experiments performed in polarized MDCK (Madin-Darby canine kidney) epithelial cells have demonstrated that the splicing in the first intracellular loop determine the apical membrane targeting of PMCA2. Only the **w** form, that contains a 45 amino acids residue insertion, showed prominent apical membrane localization (**fig. 10**).

Brain Region	Splice Options																
	1x	1a	1b	1c	1e	2w	2x	2z	2a	2b	3x	3z	3a	3b	4x	4a	4b
frontal cortex	++	+++	++	++	++	-	-	++	+	+++	+++	+	+++	+++	+++	+++	+++
parietal cortex	+++	+++	++	++	+++	-	-	++	+	+++	+++	+	+++	+++	+++	+++	+++
occipital cortex	++	+++	++	++	+++	-	-	++	+	+++	+++	++	+++	+++	+++	+++	+++
temporal cortex	+++	++++	++	+++	++	-	-	++	+	++	+++	++	++++	+++	+++	++++	++
caudate	++	+++	++	++	+++	-	+	+++	+	++	+++	++	+++	+++	+++	++	+++
cerebellum	+++	+++	++	+	++	++	++	++++	+	+++	+++	-	+++	+++	+++	++	++
globus pallidus	+++	+++	+++	+++	-	+	+	+++	+	+++	+++	-	+++	+++	+++	-	++
hippocampus	+++	+++	+	++	-	+	+	++++	+	+++	+++	-	+++	+++	+++	+++	+++
hypothalamus	+++	+	+	-	-	+	+	+	-	++	+++	+	+++	+++	+++	-	++
Inferior olive	+++	+	++	+	-	+++	+++	+++	++	+++	++	-	+++	+++	+++	-	++
olfactory bulb	+++	++	+++	+++	-	+	+	+++	+	+++	++	-	+++	+++	++	-	++
putamen	+++	+++	++	++	-	+	++	++++	+	+++	++	-	+++	+++	+++	-	++
substantia nigra	++	+++	+	-	+++	-	+++	-	++	++	++	++	++	++	+++	-	++
thalamus	+++	+++	++	++	+++	+	++	+++	+	+++	+++	++	+++	+++	++	++	+++

Tab. 2. Distribution of PMCA gene transcripts and splice variants at site A and site C in 14 subregions of the human brain [**24, 27**]. These data do not represent absolute amounts and should not be interpreted as such. The symbols indicate: – not detectable, + weak, ++ present, +++ abundant and ++++ very abundant.

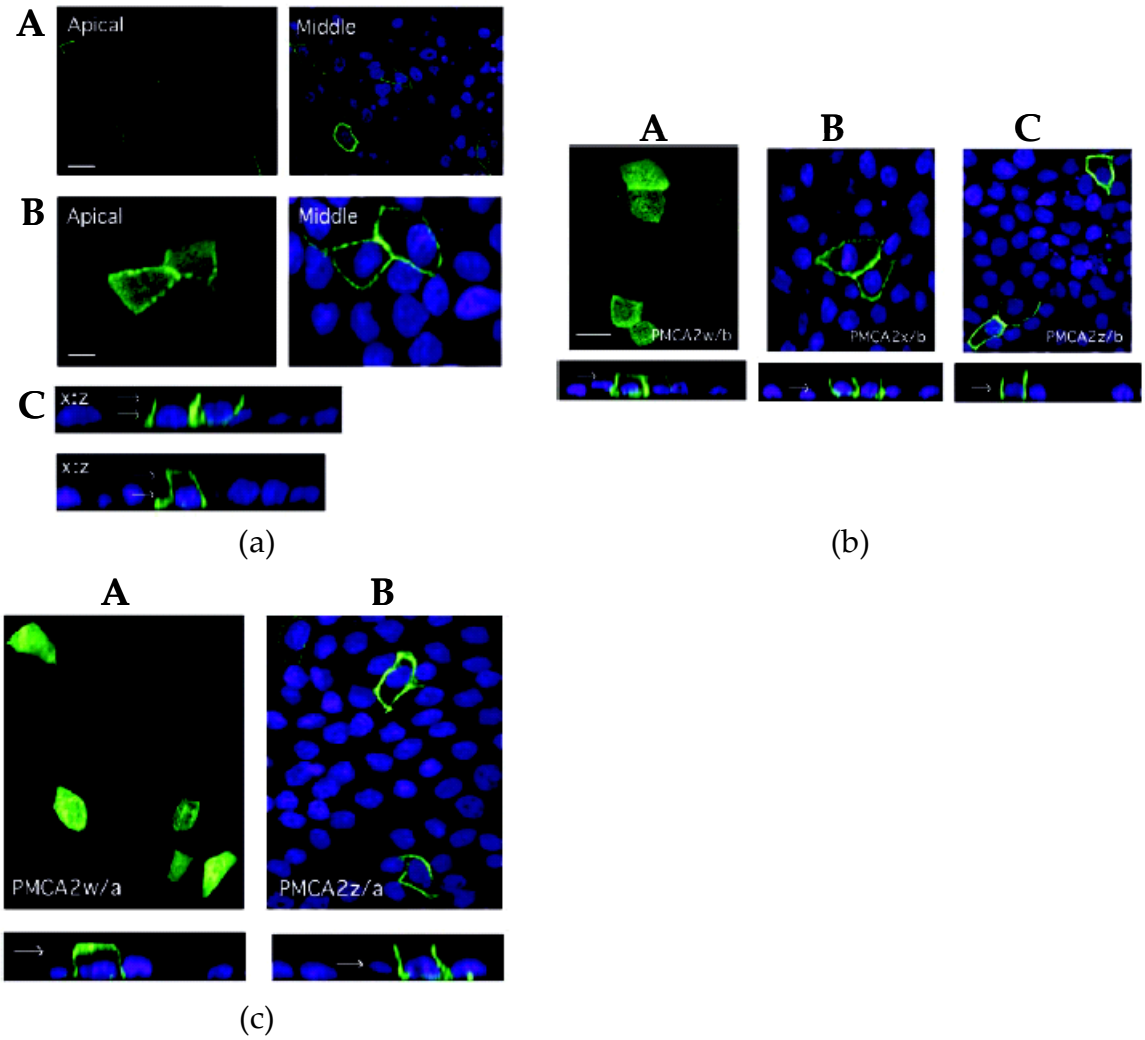

Fig. 10. Different membrane localization of PMCA isoforms. (a), GFP-PMCA4x/b (A) is localized to the basolateral membrane (*right panel*) and not in apical membrane (*left panel*). The basolateral localization of the GFP-PMCA4x/b isoform is obvious from the x:z section of the first box (C). GFP-PMCA2b is localized in the basolateral membrane (*right panel*) and in apical membrane (*left panel*). The apical and lateral localization is also highlighted in x:z section of the second box (C). (b), Different membrane localization of the splice site A variants of PMCA2b: PMCA2w/b (*left panel,* A) is localized in basolateral and apical membrane; PMCA2x/b (*middle panel,* B) is localized only in basolateral membrane whereas PMCA2z/b (*right panel,* C) is also localized in basolateral membrane. (c), The splice site configuration determines the membrane localization of PMCA2 irrespective of the splice site C configuration: PMCA2w/a is always localized in basolateral and apical membranes (*left panel*) while the PMCA 2z/a is only localized in basolateral membrane (*right panel*).

4.4.3 Regulation of the PMCAs

One important aspect of the PMCAs, that distinguishes them from the SERCA pump and all other P-type pumps, is the multiplicity of regulatory mechanisms that act on it. The cytosolic C-terminal domain is the target of all regulatory mechanisms. In the resting cells, the C-terminal domain interacts with the two cytosolic loops stopping the pump activity (autoinhibited form). After a stimulus, activators interact with the C-terminal domain and the pump becomes active (activated form) as shown in **fig. 11**.

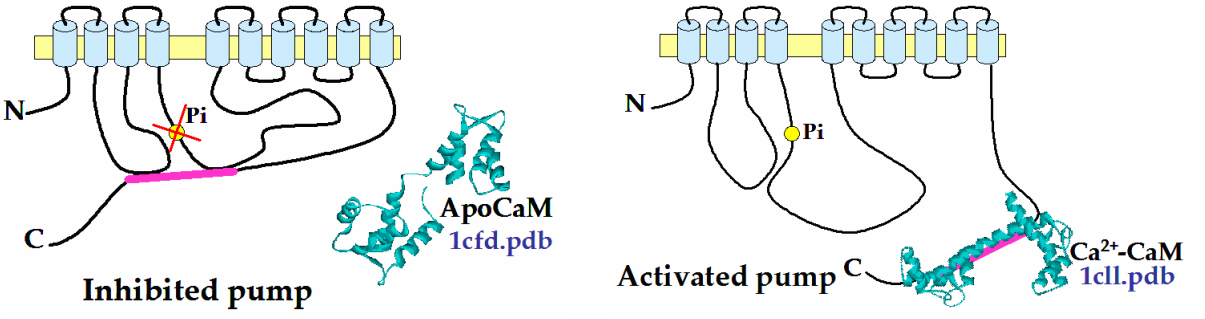

(a) (b)

Fig. 11. Two dimensional model of the PMCA in its autoinhibited form (a) and upon activation by Ca^{2+}-calmodulin (b); in pink is highlighted the calmodulin binding region in the C-terminal domain.

The activators and the regulatory mechanisms are: Ca^{2+}-calmodulin, acidic phospholipids, kinases A and C, oligomerization and proteolysis by calpain.

4.4.3.1 Ca^{2+}-calmodulin

The most important activator of PMCAs is the Ca^{2+}-calmodulin. This activator binds to a region in the C-terminal domain of the pump located ~ 40 residues downstream of the last transmembrane segment [**29**]. Calmodulin decreases the Km_{Ca2+} very significantly, bringing it down from values in excess of 10 μM to 0.4-0.5 μM [**19**]. Some studies on the regulatory domain of PMCA4b have identified a peptide of 28 amino acids that contains all the necessary information to bind calmodulin [**30**] (**fig. 12**).

Fig. 12. C28W sequence of the calmodulin binding peptide

The N-terminal portion (C20W) of this peptide has been structurally characterized by NMR [**31**]. It has an α-helix structure with two different sides: one side is positively charged and the other is predominantly hydrophobic (**fig. 13**).

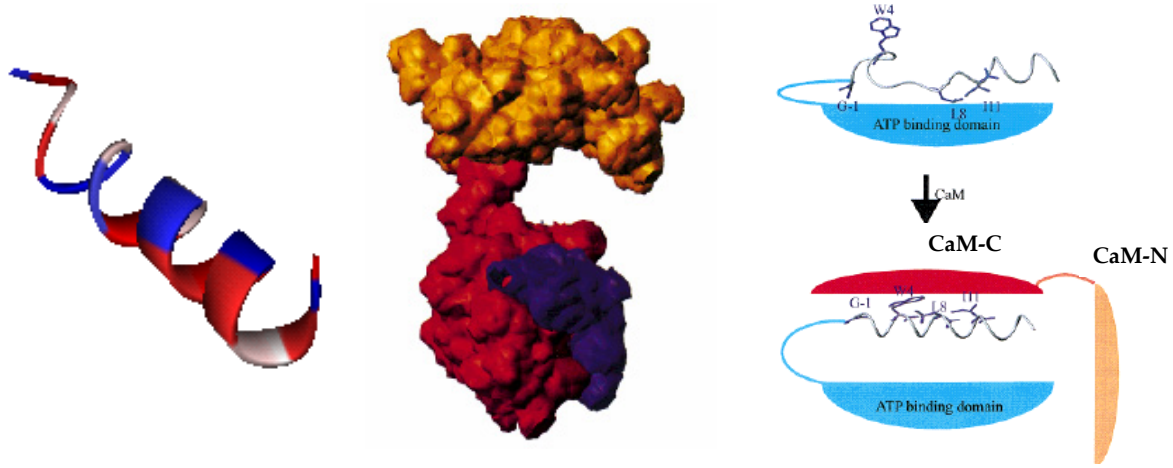

(a) (b) (c)

Fig. 13. (a), NMR structure of a portion of the calmodulin-binding region: polar and positive charged amino acids are represented in red, while hydrophobic amino acids are represented in blue. (b),

Surface representation of the Ca^{2+}-CaM and the C20W peptide; in red is represented the N-terminal domain. (c), Schematic representation illustrating the activation of the PMCA upon binding with CaM.

Inside this region there is the alternative splicing site C. A study of the calmodulin binding to the alternative spliced C-terminal domain of the PMCA1 has demonstrated that the affinity of calmodulin for the C-terminal domain of PMCA1a, 1c and 1d, which contain the histidine-rich inserts, is much higher at pH 5.9 than at pH 7.2 [**32**]. Therefore, alternative splicing in the calmodulin-binding region of the C-terminal domain is proposed to confer pH dependence to the regulation of the Ca^{2+} pump isoforms.

4.4.3.2 Acidic phospholipids and unsaturated fatty acids

Acidic phospholipids and long chain unsaturated fatty acids are activators of the PMCA [**33**]. Negatively charged phospholipids such as phosphatidylserine (PS), cardiolipin, phosphatidylinositol (PI), phosphatidylinositol 4-phosphate (PIP), phosphatidylinositol 4,5-bisphosphate (PIP_2) and phosphatidic acid (PA) induce profound changes in Vmax, $K_{0.5}$ and Hill coefficient of the PMCA [**34**]. PI and PS stimulate the PMCA in a concentration-dependent manner. PIP, PIP_2 and PA stimulate the pump activity only at low concentrations while at high concentrations they act as inhibitors as shown in **fig. 14**.

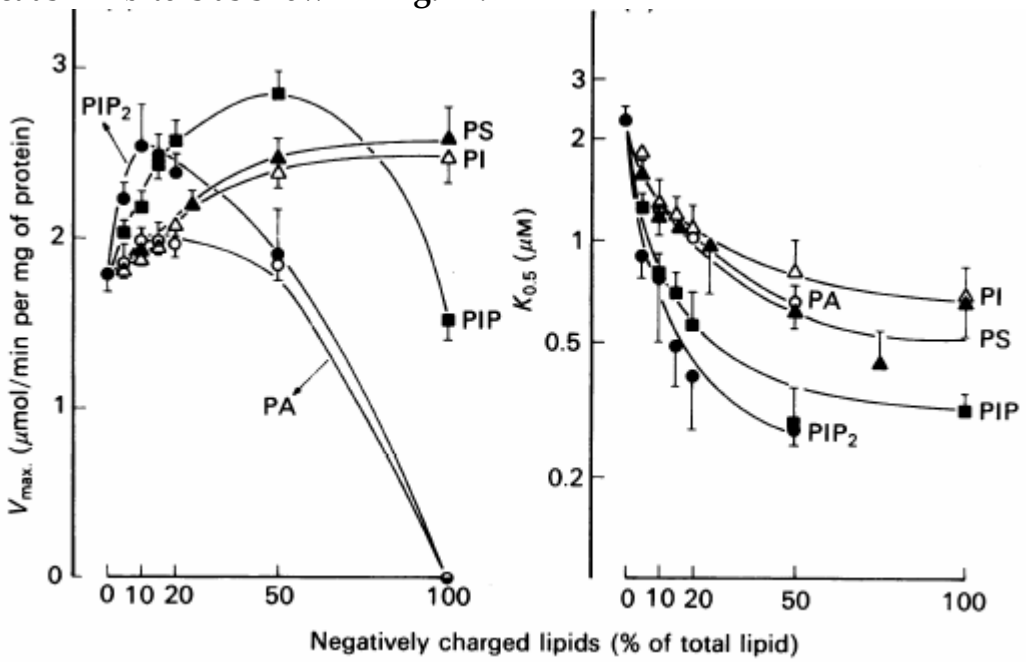

Fig. 14. Effect of negatively charged lipids on the calculated kinetic parameters of the smooth-muscle plasma-membrane Ca2+-transporting ATPase.

In the absence of acidic phospholipids (100% of phosphatidylcholine, PC) the Vmax is 1.79 ± 0.08 μmol/min per mg of protein whereas the $K_{0.5}$ for Ca^{2+} is 2.28 μM and the Hill coefficient for Ca^{2+} is 0.87 ± 0.05. PI and PS increase the Vmax of 1.39 folds and 1.45 folds respectively. In the presence of low concentrations of PIP, PIP_2 and PA, the Vmax increases of 1.6 folds, 1.42 folds and 1.12 fold respectively. In the low concentration range, the order of effectiveness of stimulation is PIP_2 > PIP > PI ≈ PS ≈ PA. The calcium affinity ($K_{0.5}$) of PMCA decreases proportionally with the acidic phospholipids concentration. Furthermore, the negatively charged lipids induce a

slight increase in the cooperativity (Hill coefficient), which is, however, smaller in the case of PIP_2 and PA. The cooperativity decreases at high acidic phospholipids concentration. The minimal percent abundance of acidic phospholipids in the environment of the enzyme, necessary for full stimulation, is 40%. These lipids stimulate the PMCA reducing the Km_{Ca2+} to around 0.25 μM [**35**]. Therefore, the activation of PMCAs by acidic phospholipids is very important when the free cytosolic calcium level decrease to levels where calmodulin activation is not significant. PMCA contains two regions that interact with acidic phospholipids: the first is located in the transduction domain and the second is located in the calmodulin-binding region of the C-terminal domain [**36**]. Calmodulin has no further activating effect when added to the enzyme after acidic phospholipids. Unsaturated fatty acids such as oleic and linoleic acids are able to activate the PMCA at lower concentrations than acidic phospholipids: 6 nmol of fatty acids per μg of protein are sufficient to activate the basal ATPase activity optimally [**33**].

4.4.3.3 Phosphorylation by kinases A and C

Pump phosphorylation by cAMP-dependent kinase (PKA) was detected *in vitro* and *in vivo* [**37**, **38**]. The phosphorylation increases the Vmax and the calcium affinity of the pump, decreasing the Km_{Ca2+} to about 1 μM in absence to calmodulin. The KRNSS consensus sequence of phosphorylation by PKA is located between the calmodulin-binding region and the C-terminus of the ATPase [**39**]. Phosphorylation by Ca^{2+}/phospholipid-dependent enzyme (PKC) has been also determined [**40**, **41**]. The site of phosphorylation has been identified around a threonine within the C-terminal calmodulin-binding domain. The phosphorylated calmodulin-binding domain is unable to bind calmodulin [**42**].

4.4.3.4 Proteolysis by calpain

In vitro, several proteases, e.g. trypsin, catalyze the controlled degradation of the PMCA inducing its irreversible activation. *In vivo*, a calcium-dependent protease such as calpain is able to cut the pump [**43**]. Calpain exists in two molecular forms characterized by different calcium sensitivities: calpain I and calpain II, also defined as micromolar (μ) and millimolar (m), respectively, due to their activity at micromolar and millimolar calcium concentrations. Both μ-calpain and m-calpain are heterodimers containing an identical 28-kDa subunit and an 80-kDa subunit that shares 55–65% sequence homology between the two proteases. The crystallographic structure of m-calpain reveals six "domains" in the 80-kDa subunit: 1) a 19-amino acid NH2-terminal sequence; 2) and 3) two domains that constitute the active site, IIa and IIb; 4) domain III; 5) an 18-amino acid extended sequence linking domain III to domain IV; and 6) domain IV, which resembles the penta EF-hand family of polypeptides [**44**]. PMCAs have two different cut sites: the first is located in the middle of calmodulin-binding region and the second closer to the N-terminus of the domain. In the presence of bound calmodulin the first cut site is located downstream of the first cut site without calmodulin (**fig. 15**).

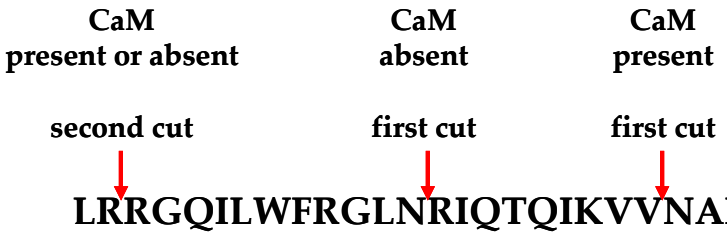

Fig. 15. Splitting pattern of the synthetic calmodulin-binding peptide by calpain in the absence or presence of calmodulin.

Calpain become active in the presence of calcium concentrations at least in the μM range. Therefore, degradation by calpain occurs under conditions of pathological cytosolic Ca^{2+} overload, possibly to provide cells with an efficient means to extrude calcium. Then, the truncated pump product, initially generated by calpain, is further degraded by other proteases to smaller, inactive fragments.

4.4.3.5 Oligomerization

Activation by oligomerization has been demonstrated by studying the dependence of PMCA activity on the enzyme concentration using the calcium ATPase purified from human erythrocytes [**45**]. These experiments have highlighted the transition from a calmodulin dependent form (low enzyme concentration: 15 nM) to a fully active calmodulin independent form (high enzyme concentration: 75 nM) as shown in **fig. 16**. Oligomers activity has been also demonstrated using the calmodulin inhibitor 48/80 that is unable to decrease their activity.

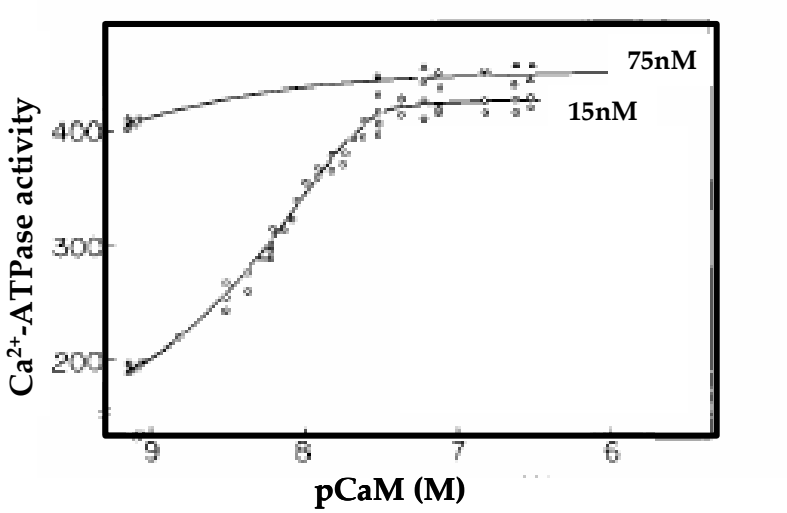

Fig. 16. Effect of Ca^{2+}-calmodulin on PMCA activity.

Oligomers are still able to interact with calmodulin as demonstrated by binding experiments carried out using a calmodulin-Sepharose 4B resin (**fig. 17**).

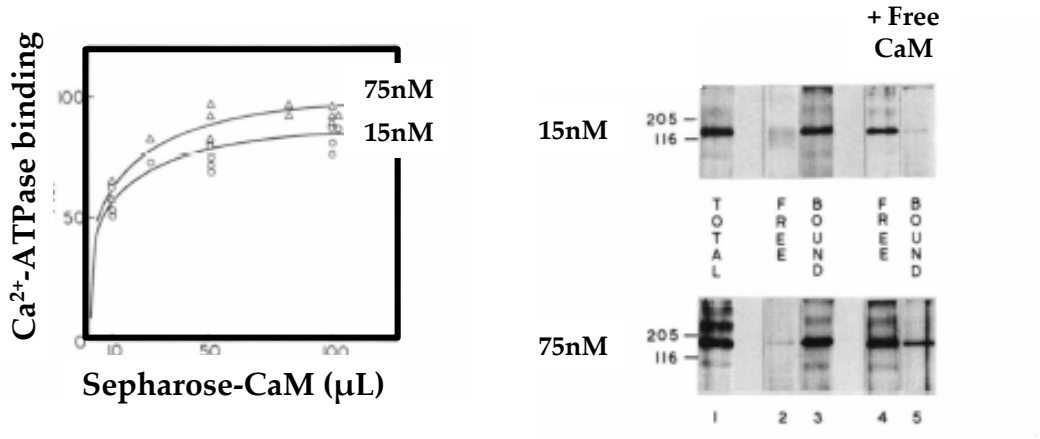

(a) (b)

Fig. 17. Binding experiments of PMCA to calmodulin-Sepharose 4B resin: (a), binding curve of PMCA in oligomeric (75 nM) and monomeric (15 nM) forms; (b), SDS-PAGE of PMCA after binding experiments: lane 1 represents the total amount of protein used in the experiment; lane 2 represents the unbound (free) PMCA; lane 3 represents the bound PMCA after elution with EGTA; lane 4 shown the unbound fraction of PMCA when 6 μM of calmodulin was added to the enzyme at the lower and higher concentration before the binding experiment; lane 5 represents the bound fraction of PMCA when 6 μM of calmodulin was added to the enzyme at the lower and higher concentration before the binding experiment.

FRET technique has been used to study the oligomerization process. These experiments have demonstrated that the oligomerization is a calcium dependent process. Furthermore, pump activity is proportional to the enzyme concentration [**46**, **47**] as shown in **fig. 18**.

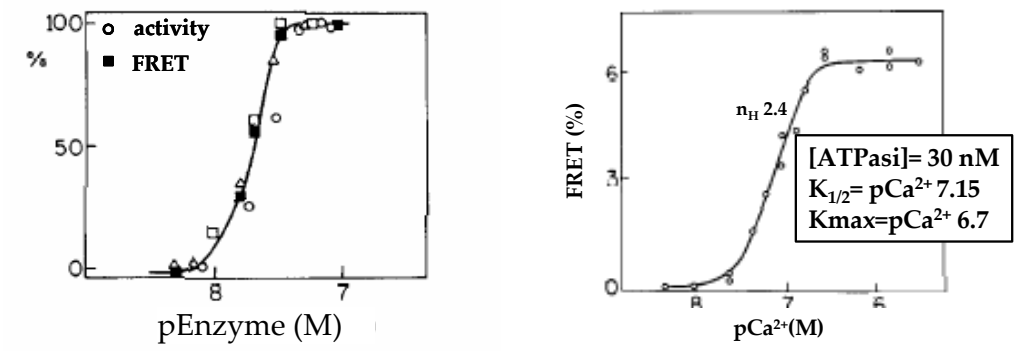

(a) (b)

Fig. 18. FRET studies on the oligomerization process: (a), Enzyme concentration dependence of PMCA activity (white circle) and oligomerization as measured by polarization of the FITC-labelled enzyme (white triangle) or energy transfer efficiency (white and black squares); (b), Ca^{2+} dependence of oligomerization as measured by energy transfer efficiency between the FITC- and EM- labelled enzyme molecules.

Ca^{2+} dependence of oligomerization process is very steep showing a n_H of 2.36 ± 0.24, $K_{½}$ of pCa 7.15 and a maximum at pCa 6.7. These values are compatible with the *in vivo* calcium concentrations. Several experiments have highlighted that the calmodulin binding region, located inside the cytosolic C-terminal domain of PMCA, mediates the oligomerization process of the pump [**48**, **49**, **50**, **51**]. These experiments have been carried out by increasing the PMCA concentration, to study the transition from monomer to oligomer, and in presence of calmodulin, of the C-terminal domain calmodulin binding region (C28W) and of calpain (**fig. 19**).

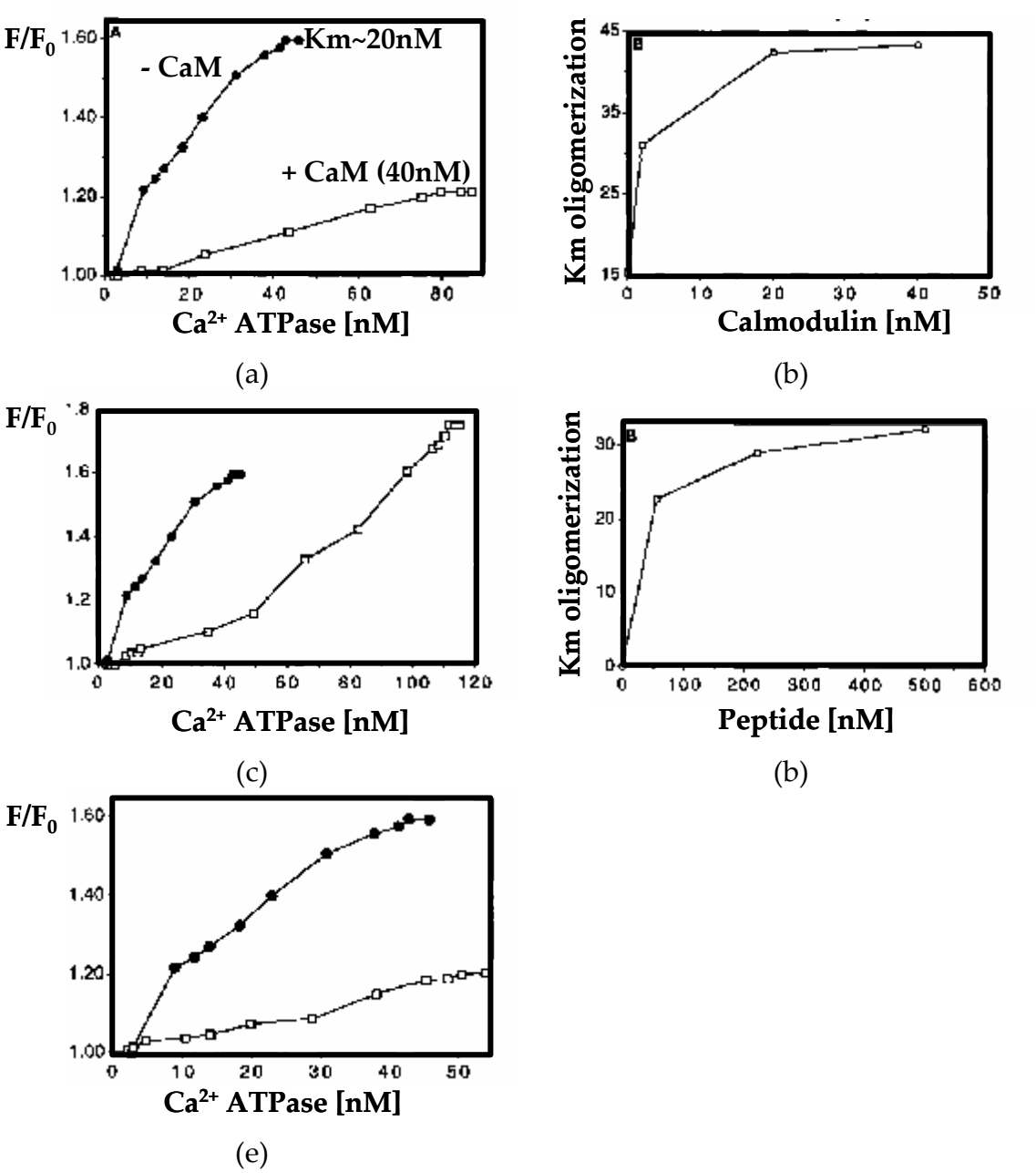

Fig. 19. (a), Fluorescence titrations of the pump to monitor the oligomerization process in the presence (+CaM) or in the absence (-CaM) of calmodulin. (b), Km curve as a function of the calmodulin concentration; (c), Fluorescence titrations of the pump to monitor the oligomerization process in presence of the calmodulin-binding peptide (C28W); (d), Km curve as function of the calmodulin binding peptide concentration; (e), Fluorescence titrations of the pump to monitor the oligomerization process after proteolysis by calpain.

All molecules used for these experiments interact with the C-terminal domain and inhibit that oligomerization process. Since self-association occurs only at concentration of PMCA much higher than those that can be expected in the native membrane environment, its physiological significance appears doubtful. However, immunocytochemical studies have demonstrated that the Ca^{2+} pump is localized in caveolae and its concentration is 18-25 folds higher than that present in noncaveolar portion of the plasma membrane [**52**, **53**]. Thus, in caveolae the conditions favouring the oligomerization process could be met. An inositol 1, 4, 5-triphosphate receptor-

like protein has been also found in caveolae [**54**] and thus these plasmalemmal invaginations could represent a specialized apparatus for the calcium intake and extrusion from the cytoplasm.

4.4.4 PMCA and PDZ domain containing proteins interaction

The last four C-terminal residues of the **b** splice form contain the minimal consensus sequence (Ser/Thr-X-Val-COO^-) for binding to the PDZ protein interaction domain (**fig. 20**) and more exactly for the interaction with channel-clustering proteins of the membrane associated guanylate kinase (MAGUK) family such as SAP97/hDlg, ß2-syntrophin and PSD-95 family (SAP90/PSD95, SAP97/hDlg, and PSD93/Chapsyn-110) [**55**, **56**, **57**].

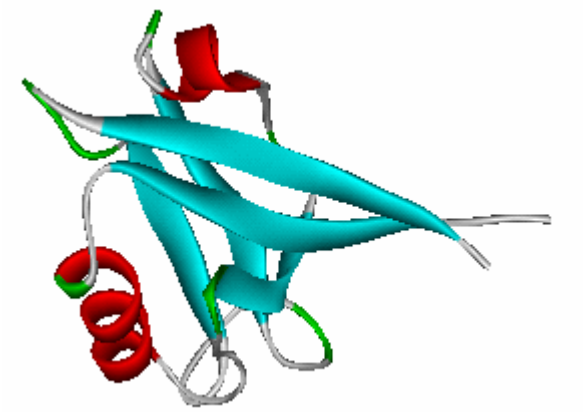

Fig. 20. Ribbon representation of the second PDZ domain of PSD95 (1qlc.pdb). This PDZ domain shows five ß-strands and two α-helix. The peptide containing the consensus PDZ-binding sequence interacts with the surface groove between a helical segment and one ß-strand [**58**, **59**].

The MAGUKs are a large family of proteins involved in sequestering protein complexes at the plasma membrane and formation of different cell junctions. Members of this family occur in all multicellular organisms and have specific domain organization: one or three PDZ domains, a SH3 domain and GUK (guanylate kinase) domain [**60**]. These interactions are very important for the signaling transduction networks of the cell as demonstrated for example by the interaction between PMCA4b and NOS-I [**61**]. PMCA4b is a negative regulator of nitric oxide synthase I (NOS-I, nNOS) stopping the production of the second messenger nitric oxide (NO) most important for the regulation of the synaptic signalling and plasticity, muscle contractility and local blood flow [**62**]. PDZ domain of the NOS-I is responsible of the interaction with the C-terminal consensus sequence of the PMCA4b.

5 Human PMCA1b C-terminal domain: cloning, expression, purification and structural characterization

5.1 Materials and Methods

5.1.1 Cell culture and RNA extraction

Neuroblastoma cell line SHSY5Y was used for the amplification of the human PMCA1b C-terminal domain. RNA was extracted by TRIZOL® reagent (Sigma). A volume of 1 mL of this reagent was directly added to culture and the lysate incubated at room temperature for 5 minutes. A volume of 0.2 mL of chloroform was added to the sample and the mixture was vigorously shook and incubated at room temperature for 10 minutes. The resulting mixture was centrifuged at 14000g for 15 minutes at 4 °C. The colorless upper aqueous phase was transferred to a fresh tube and 0.5 mL of isopropanol were added to the sample. The sample was incubated at room temperature for 10 minutes and then centrifuged at 14000g for 10 minutes at 4 °C. The RNA containing pellet was rinsed with 1 mL of ethanol 75% in H_2O DEPC (Diethyl pyrocarbonate) twice and, when completely dried, resuspended in 20 μL of nuclease-free water. Isolated RNA was tested in 1% agarose gel electrophoresis that was run in TAE buffer.

5.1.2 RT-PCR

In order to obtain cDNA from mRNA a reverse transcription polymerase chain reaction (PCR) was performed. 20 pmol of primer oligo dT_{18} were added to 1 μg of RNA template in a final volume of 5 μL of nuclease-free water. The mixture was incubated at 70 °C for 5 minutes and cooled at 4 °C for 5 minutes. A volume of 15 μL of reverse transcription mix made from ImProm-II™ reaction buffer, $MgCl_2$ 3 mM, dNTPs 0.5 mM, recombinant RNasin® Ribonuclease Inhibitor 1u/ μL, ImProm-II™ reverse transcriptase was added to the mixture. The reaction conditions were:

Annealing	25 °C for 5 minutes
Extension	42 °C fro 60 minutes
Inactivation	70 °C for 15 minutes

cDNA was analyzed in 1% agarose gel electrophoresis that was run in TAE buffer.

5.1.3 PCR amplification

cDNA was used to amplify the PMCA 1b C-terminal domain nucleotide sequence by PCR. Specific primers were designed on nucleotidic sequence NM_001682 and their sequences are reported below:

Primer	Sequence	Tm °C
CterFor	5′- ACA↓TATGACAATTCCAACTAGC – 3′	58
CterRev	5′ – TC↓TCGAGTCAGAGTGATGTTTC – 3′	62

Each primer contains a specific restriction site necessary for the cloning in the expression vector pET21b: CterFor contains NdeI whereas CterRev contains XhoI. The mixture of PCR was made from:
10 µL of GoTaq® Flexi Buffer (5X)
3 µL $MgCl_2$ (1.5 mM)
5 µL dNTPs (200 µM)
3.75 µL each primer (0.75 µM)
0.2 µL cDNA
0.3 µL GoTaq (1.25U)
24 µL nuclease-free water
50 µL final volume
Thermal cycling conditions for the C-terminal domain amplification were as follows:

Step	Temperature	Time	Number of cycles
Initial denaturation	95 °C	5 min	1
Denaturation	95 °C	30 sec	30
Annealing	60 °C	1 min	
Extension	72 °C	1 min	
Final extension	72 °C	10 min	1
Soak	4 °C	Indefinite	1

PCR reaction was carried out using a BIO RAD My Cycler™ Thermal Cycler while the PCR products were analyzed by 1% agarose gel electrophoresis made in TAE buffer and visualized with ethidium bromide. The length of the amplified band was compared with a 100 bp ladder (Promega).

5.1.4 Purification of PCR products

PCR product was purified by Wizard® SV Gel and PCR Clean-Up System kit (Promega). The mixture containing the PCR product was transferred to the SV Minicolumn, incubated at room temperature for 1 minute and then centrifuged at 14000g for 1 minute. After a first wash by flow through, 700 µL of Membrane Wash Solution, previously diluted with ethanol 95%, were added to the SV column containing PCR product. The SV minicolumn was centrifuged at 14000g for 1 minute. The wash was repeated a second time with 500 µL of Membrane Wash Solution. PCR product was resuspended with 50 µL of nuclease-free water. The quality and quantity of purified PCR product were tested by 1% agarose gel electrophoresis. Purified PCR product was stored at -20 °C.

5.1.5 Ligation

PCR product was used to perform a ligation reaction with pGEM®-T easy (**fig. 21**).

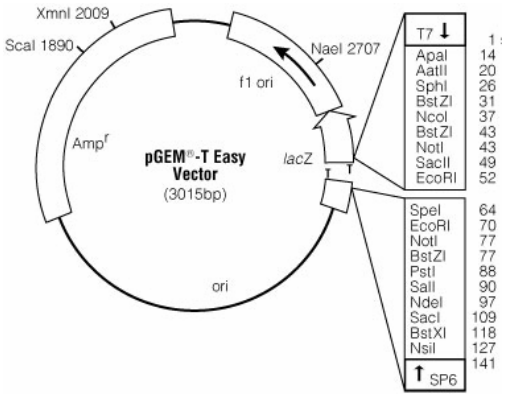

Fig. 21. pGEM-T easy map (Promega)

The molar ratio of the PCR product to the vector used in the reaction was 3:1 calculated as:

PCR product (ng) = (50 ng of pGEM · bp PCR products (500)) · 3 / bp pGEM (3015)

The ligation reaction was carried out overnight at 14 °C and the products of ligation were used to transform competent InvαF' *E. coli* cells. The transformed cells grew on agar plate containing ampicillin 100 μg/ mL were tested by PCR screening to select the positive clones. PCR screening conditions were the same used for the amplification.

5.1.6 Isolation of plasmid DNA

Positive clones in the PCR screening were inoculated in 5 mL of liquid LB medium selective for ampicillin and incubated at 37 °C overnight. Plasmid DNA was extracted by Wizard® Plus Minipreps DNA Purification System (Promega). Cells were harvested by centrifuging the culture at 2700g for 5 minutes (Microcentrifuge® 18 centrifuge Beckman Coulter) and the pellet was resuspended with 250 μL of Cell Resuspension Solution (Tris-HCl 50 mM, EDTA 10 mM, RNase A 100 μg/ mL, pH 7.5). To this suspension, 250 μL of Cell Lysis Solution (NaOH 0.2 M, SDS 1%) were added to destroy the cells followed by 10 μL of Protease Alkaline Solution. The solution was incubated at room temperature for 5 minutes, then 350 μL of Neutralization Solution (potassium acetate 1.32 M, pH 4.8) were added and it was centrifuged at 14000g for 10 minutes. Cleared lysate was transferred into spin column and centrifuged at 14000g for 1 minute. Once removed the flow through, the plasmid containing Spin column was washed with 750 μL of Wash Solution (potassium acetate 80 mM, Tris-HCl 8.3 mM, EDTA 40 μL, ethanol 55%, pH 7.5) twice. Plasmid DNA was recovered with 100 μL of warm (60 °C) nuclease-free water. The quality and the quantity of plasmid DNA was analyzed by 1% agarose gel electrophoresis and UV measurements using a UV/vis mod. 8452A Diode Array spectrophotometer (Hewlett Packard). The plasmid was sequenced using T7 universal primers.

5.1.7 Cloning in pET21b

Double digestion of the pGEM-C-teminal domain plasmid using NdeI and XhoI restriction enzymes was performed. This step was carried out at 37 °C for 2 hours and the digested material was loaded on 1% agarose gel electrophoresis that was run in TA buffer. The band corresponding to the C-terminal domain was extracted from gel, purified as described above and used to perform a ligation reaction with the digested expression vector pET21b (**fig. 22**). The optimum molar ratio used in this reaction was always 3:1. Also in this case, the reaction was carried out overnight at 14 °C. The products of ligation were used to transform competent InvαF' cells and the cells grew on agar plate containing ampicillin 100 µg/ mL were tested by PCR screening. Positive clones were inoculated in 5 mL of liquid LB medium selective for ampicillin and incubated at 37 °C overnight. C-terminal domain containing pET21b was purified using Wizard® Plus Minipreps DNA Purification System (Promega). Purified plasmid was sequenced to test the accuracy of the cloned insert.

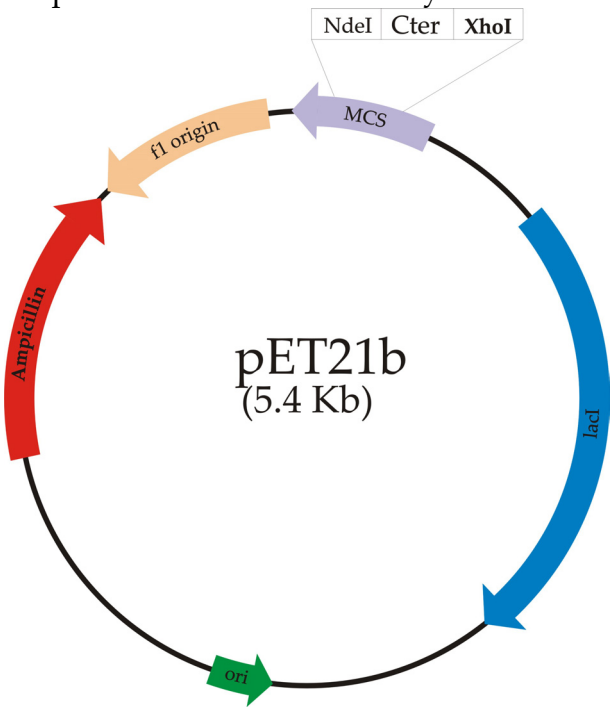

Fig. 22. pET21b map (Novagen)

5.1.8 Tests for expression of the recombinant C-terminal domain

Competent *E. coli* BL21 (DE3) cells were transformed with 1 µL (273 ng) of pET21b-C-terminal domain, streaked on agar plate containing ampicillin (Amp) 100 µg/mL and incubated at 37 °C overnight. Clones were inoculated in three Erlenmeyer flasks containing 25 mL of LB, ampicillin 100 µg/mL and incubated at 37 °C until an optical density at 600 nm (OD_{600}) of 0.6. The expression tests were carried out at increasing concentration of IPTG: 0.4 mM, 0.6 mM, 0.8 mM at 30 °C for 5 hours. 1 mL of each culture was collected every hour and centrifuged at 2700g (Beckman Coulter Microfuge® 18 Centrifuge) at 4 °C for 5 minutes. The pellets were stocked at -20 °C for next SDS PAGE analysis.

In order to produce the ^{2}H labelled C-terminal domain necessary for the small angle neutron scattering experiments were performed expression tests in M9 minimal

medium. Tests were performed at two different ampicillin concentrations (100 μg/mL and 50 μg/mL) and in presence of increasing IPTG concentration: 0.4 mM, 0.6 mM and 0.8 mM. The inductions were carried out for 4 hours. The pellets were stocked at -20 °C for next SDS-PAGE analysis.

5.1.9 Large-scale expression of the recombinant C-terminal domain

Once obtained the best conditions to produce recombinant C-terminal domain, large-scale inductions were made. To this aim, clones were inoculated in 500 mL of LB-ampicillin 100 μg/mL until an OD_{600} of 0.6 and induced with IPTG 0.4 mM at 30 °C for 4 hours. The growth was stopped at 4 °C for 30 minutes and the bacteria were centrifuged at 2700g (Beckman TJ-25 Centrifuge) for 30 minutes. The C-terminal domain containing pellet was stored at -80 °C.

5.1.10 Large-scale expression of ^{2}H labelled C-terminal domain

Once obtained the best conditions to produce ^{2}H labelled C-terminal domain, large-scale inductions were made. Clones were inoculated in 5 mL of selective LB and incubated overnight at 37 °C. A volume of this culture was transferred into 100 mL of selective LB until an OD_{600} of 0.15 was reached. The culture was incubated at 37 °C until an OD_{600} of 0.9 was reached and then centrifuged at room temperature at 3700g for 5 minutes. The pellet was resuspended in 200 mL of M9 minimal medium and incubated at 37 °C until an OD_{600} of 0.8 was reached. The culture was centrifuged at room temperature at 3700g for 5 minutes and the pellet resuspended in 50 mL of M9 minimal medium prepared using D_2O water. Reached an OD_{600} of 4.1, the culture was centrifuged as indicate above and the pellet resuspended in 450 mL of M9 minimal medium in D_2O. The suspension was incubated at 37 °C until an OD_{600} of 0.6 was reached and then IPTG 0.4 mM was added to culture. The culture was incubated overnight at 30 °C, stopped at 4 °C for 30 minutes and centrifuged at 4 °C at 3700g for 5 minutes. The pellet was stored at -80 °C.

5.1.11 Purification of the C-terminal domain

C-terminal domain containing pellet was resuspended with 20 mL of Tris-HCl 50 mM, NaCl 0.15 M, $CaCl_2$ 2 mM, PMSF 1 mM and 20 μL of protease inhibitor cocktail (4-(2-aminoethyl)benzenesulfonyl fluoride, bestatin, pepstatin A, E-64, and phosphoramidon), pH 7.5. *E. coli* BL21 cells were disrupted by French Press (Inlabo American Instrument Company) applying three passes at 1000 psi (68.95 bar). The lysate was centrifuged at 15871g (Beckman Coulter Allegra 64R Centrifuge) for 30 minutes to separate the soluble and insoluble fractions. The soluble fraction was filtered using a 0.22 μm cut off filter and loaded onto Calmodulin-Sepharose 4B, previously equilibrated with Tris-HCl 50 mM, NaCl 0.15 M and $CaCl_2$ 2 mM pH 7.5, with a flow rate of 0.5 mL/min. Unbound proteins were washed using the equilibration buffer with a flow rate of 1 mL/min whereas the C-terminal domain was eluted using Tris-HCl 50 mM, NaCl 0.15 M, EGTA 2 mM, pH 7.5 with a flow rate of 1.5 mL/min. Purified C-terminal domain was analyzed by SDS-PAGE together with all fractions collected during the purification. Protein concentration was determined by UV/vis spectroscopy using an extinction coefficient of 6990 M^{-1} cm^{-1}.

Purified C-terminal domain was stored to -20 °C in presence of sucrose 20%. When necessary, the purified C-terminal domain was dialysed using benzoylated cellulose dialysis bags (D7884-10FT, SIGMA) with cut off of 1000 Da.

5.1.12 SDS-PAGE

Expression tests of the C-terminal domain and all purification steps were analyzed by 12% SDS-PAGE. Gels composition is reported below:

Stock solutions	Resolving gel 12%	Stacking gel 4%
Acrylamide 40%	3 mL	0.5 mL
Bisacrylamide 1.6%	2.35 mL	390 µL
Tris 3M	1.67 mL	1.25 mL
SDS 10%	100 µL	50 µL
Sucrose	1.125 g	-
APS 10%	70 µL	35 µL
TEMED	7	3.5 µL
H_2O	2.82 mL	2.77 mL
Total volume	10 mL	5 mL

Pellets of the samples collected during the expression tests were resuspended with a volume of running buffer proportional to the OD_{600}. To 40 µL of sample were added 10 µL of loading buffer (5X) and the mixture was boiled at 100 °C for 5 minutes. Then, 20 µL of denaturated samples were loaded onto gel. 10 µL of loading buffer (5X) were also added to 40 µL of each sample collected during all purification steps. Samples were boiled at 100 °C for 5 minutes and 20 µL of denaturated samples loaded onto gel. Insoluble fraction was resuspended in 100 µL of running buffer and 25 µL of loading buffer (5X) and boiled at 100 °C; also in this case 20 µL were loaded onto gel. Samples were run at 4 °C at 20 mA per gel using a BIORAD mini Protean 3 cell. Proteins were visualized by Blue Comassie staining. The ultralow range marker kit (M-3546, SIGMA) was used to estimate the molecular weight of the recombinant proteins.

5.1.13 Reverse phase HPLC and mass spectrometry

Reverse phase HPLC chromatography was performed followed by mass spectrometry analysis. A C4 Phenomenex Jupiter (150 x 4.6 mm) column was used in reverse phase chromatography. The column was equilibrated with 95% of solvent A (H_2O mQ and 0.1% Trifluoroacetic acid, TFA) and 5% of solvent B (acetonitrile and 0.1% TFA). Purified C-terminal domain was eluted with the gradient reported below:

Time (minutes)	0	4	8	25	27	30	32	45
% B	5	5	34	50	90	90	5	Stop

The chromatography was carried out with a flow rate of 0.6 mL/min and the elution was observed at 226 and 280 nm corresponding to the absorption of the peptide bond and of aromatic amino acids respectively. The fraction of C-terminal domain was

collected and lyophilized using a Savant Speed Vac concentrator. The protein was resuspended in 10 μL of solution made from 49% H2O mQ, 50% acetonitrile and 1% formic acid for electrospray ionization mass spectrometry analysis using the Mariner System 5220 (Applied Biosystem) spectrometer, in collaboration with Dr.ssa. Polverino De Laureto (C.R.I.B.I., University of Padova). Reverse phase chromatography and ESI mass spectrometry were also performed to ^{2}H labelled C-terminal domain. Non linear gradient used for the elution of the ^{2}H C-terminal domain is reported below:

Time (minutes)	0	4	8	35	37	40	42	52
% B	5	5	34	50	90	90	5	Stop

5.1.14 N-terminal sequencing

C-terminal domain run in 12% SDS-PAGE was transferred to a PVDF membrane (Immobilon-P) by tank transfer blotting at 50 V overnight at 4 °C using Bio-Rad Trans-blot cell®. The membranes were stained in Ponceau Red and subsequently dried in air in order to excise the band. Amino acid sequences were determined by automated Edman degradation in a pulsed liquid-phase sequencer (Model: Procise HT-491, Applied Biosystems, Foster City, CA, USA) equipped with an online HPLC system for PTH-amino acid identification. C-terminal domain electroblotted on PVDF membrane was excised and washed successively with methanol, water and methanol. For analysis, 10 pmoles were introduced in the sequencer reaction chamber. Sample was run in the pulsed liquid-phase mode of Edman chemistry, with n-heptane/ethyl acetate as the extraction solvent for anilinothiazolinones. A total of 6 sequencing cycles were performed and amino acid positions assigned by means of peak area and retention time. N-terminal sequencing was performed in collaboration with prof. O. Marin.

5.1.15 Atomic Absorption measurements

Purified C-terminal domain was dialysed against a solution made from Tris 50 mM, NaCl 0.15 M and EGTA 5 mM, pH 7.5. Absorption measurements of buffer and protein were recorded on a Perkin Elmer AAnalyst100 instrument and normalized with 4 ppm calcium standard absorption. Measurements were recorded using a wavelength of 422.7 nm with a slit of 0.7 nm. Protein concentration used for atomic absorption measurements was 0.6 mg/ mL.

5.1.16 Circular Dichroism

Secondary structure of purified C-terminal domain was studied by far UV (190-260 nm) circular dichroism on JASCO J-715 spectrophotometer. CD spectra were recorded at room temperature in Tris 10 mM, NaCl 0.15 M, pH 7.5 using 0.01 cm pathlength cells. Data were analysed with the jwstda32 software. CD spectra were performed with a protein concentration of 0.2 mM in absence or in presence of 1 mM of free calcium.

CD spectroscopy was used to study the effect of SDS on the secondary structure of the C-terminal domain. Samples composition used for CD experiments are reported below:

	Blank composition			Sample composition			
Sample name	Buffer (μL)	SDS 1% (μL)	SDS 10% (μL)	C-ter (μL)	SDS 1% (μL)	SDS 10% (μL)	[C-ter] mM
C-ter	100	-	-	100	-	-	0.2
C-ter -SDS 0.005%	99.5	0.5	-	99.5	0.5	-	0.199
C-ter -SDS 0.01%	99	1	-	99	1	-	0.198
C-ter -SDS 0.05%	95	5	-	95	5	-	0.19
C-ter -SDS 0.1%	99	-	1	99	-	1	0.198
C-ter -SDS 0.5%	95	-	5	95	-	5	0.19
C-ter -SDS 1%	90	-	10	90	-	10	0.18

C-ter abbreviation of C-terminal domain

Each CD spectrum was obtained as average between two replicates. The percentages of α-helix, ß-sheet and random coil were calculated using two different softwares based on neural network, CDNN and k2d, and the formula described by Greenfield and Fasman.

5.1.17 Small Angle X-Ray Scattering (SAXS)

Small Angle X-Ray Scattering measurements were performed to investigate the tertiary structure at low resolution of the C-terminal domain. Experiments were carried out increasing the C-terminal domain concentration from 0.21 mg/mL to 1.59 mg/mL, increasing the ionic strength from 0.15 M NaCl to 1 M, in presence of physiological and Hofmeister calcium concentrations, 10 μM and 2 mM respectively, and in presence of imidazole and N-acetyl tryptophanamide. All measurements were recorded at the synchrotron of Hamburg (Germany) in collaboration with Dr. Ivan Micetic (Dipartimento di Biologia, Università degli studi di Padova).

5.1.18 Electron microscopy

Transmission Electron microscopy was performed on negatively stained samples using a transmission electron microscope (TEM) FEI Tecnai T12. Uranyl acetate 1% was added to 0.2 mg/mL of C-terminal domain. All images were made in collaboration with Mr. G. Tognon of C.N.R.

5.1.19 Native PAGE

Native PAGEs at 12% in presence of non polar detergents such as TRITON X-100 and NP40 and in the presence of increasing SDS concentration (0-1%) were performed.

Bovine serum albumin (A-2153, SIGMA) was used as positive control because it has an isoelectric point (pI) of 5.82 that is similar to the pI of the C-terminal domain, 5.06, and a molecular weight of 69293.4 Da. Denaturated C-terminal domain was also used as marker. A volume of 10 μL of loading buffer (glycerol 100% and bromophenol blue) was added to 40 μL of each sample (0.327 mg/mL). Samples were run at 4 °C at 20 mA per gel using a BIORAD mini Protean 3 cell. Gels were stained with Blue Comassie.

5.1.20 Determination of Critical Micelle Concentration (CMC)

Critical Micelle Concentration (CMC) of SDS in Tris 10 mM, NaCl 0.15 M, pH 7.5 was determined by surface tension measurements. Buffer was titrated with increasing SDS concentrations (0.2%-0.6%).

5.1.21 Small Angle Neutron Scattering

Small Angle Neutron Scattering measurements were performed to investigate the tertiary structure at low resolution of ^{2}H labelled C-terminal domain in the presence of SDS. Experiment was carried out at matching point conditions calculated from scattering density plots. In these conditions is possible to subtract the water and SDS signals as background and to see only the protein signal. Scattering density for the protonated protein was calculated using the coherent scattering length (10^{-12} cm) and volume ($Å^3$) for each residue value reported in [**63**]. Scattering density was plotted as function of D_2O volume fraction considering that exchangeable ^{1}H were replaced by ^{2}H. In order to increase the contrast, ^{2}H labelled C-terminal domain was expressed. In this case, the scattering density plot was calculated considering that most unchangeable ^{1}H were substituted by ^{2}H. Scattering density plot of SDS was calculated as function of SDSd25 fraction considering that polar and paraffinic parts have different behaviour due to interaction between sulphur and protons. Scattering length density was determined using the Scattering Length Density Calculator available online at http://www.ncnr.nist.gov/resources/sldcalc.html site. Matching point corresponds to the scattering density obtained from intersection between polar SDS and paraffinic SDS curves plotted on water curve. In this way, the SDSd25 and D2O volume fractions were determined. Sample compositions are reported below:

Sample composition	A	B	C	D	E	F	G
Buffer D_2O-H_2O (μL)	300	299.1	297	270	0	0	0
SDS % (SDSd25-SDSh25)	0	0.03	0.1	1	0.03	0.1	1
SDSd25-SDSh25 (μL)	0	0.9	3	30	0.9	3	30
Protein volume (μL)	0	0	0	0	177.6	177.6	177.6
Buffer D2O (μL)	0	0	0	0	121.5	119.4	92.4
Final volume (μL)	300	300	300	300	300	300	300

A, buffer made from Tris 10 mM, NaCl 0.15 M, pH 7.5
B, buffer with 0.03% of SDS mixture
C, buffer with 0.1% of SDS mixture

D, buffer with 1% of SDS mixture
E, ^{2}H labelled C-terminal domain and 0.03% of SDS mixture
F, ^{2}H labelled C-terminal domain and 0.1% of SDS mixture
G, ^{2}H labelled C-terminal domain and 1% of SDS mixture

Stock protein concentration	6.79 mg /mL
Sample protein concentration	4.02 mg/mL
Stock SDSd25-SDSh25 concentration	10%
$D_2O/(D_2O+H_2O)$	0.408
SDSd25/(SDSd25+SDSh25)	0.357

All measurements were recorded at Laboratoire Leon Brillouin (LLB) of Saclay, France in collaboration with prof. F. Carsughi (Dipartimento di Scienze Applicate ai Sistemi Complessi Università Politecnica delle Marche and SoftComp Project Institut fuer Festkoerperforschung). SDSd25 was kindly provided by prof. Stefano Mammi (University of Padova) whereas D_2O water was bought from Euriso-top with a 99.85% of deuteration degree.

5.2 Results

In order to clone the human PMCA1b C-terminal domain, RNA from SHSY5Y neuroblastoma cell line was extracted (**fig. 23**, panel a). cDNA was obtained using oligo dT_{18} primer (**fig. 23**, panel b) whereas specific primers, designed on deposited PMCA1b sequence, were used to amplify the domain from cDNA (**fig. 23**, panel c).

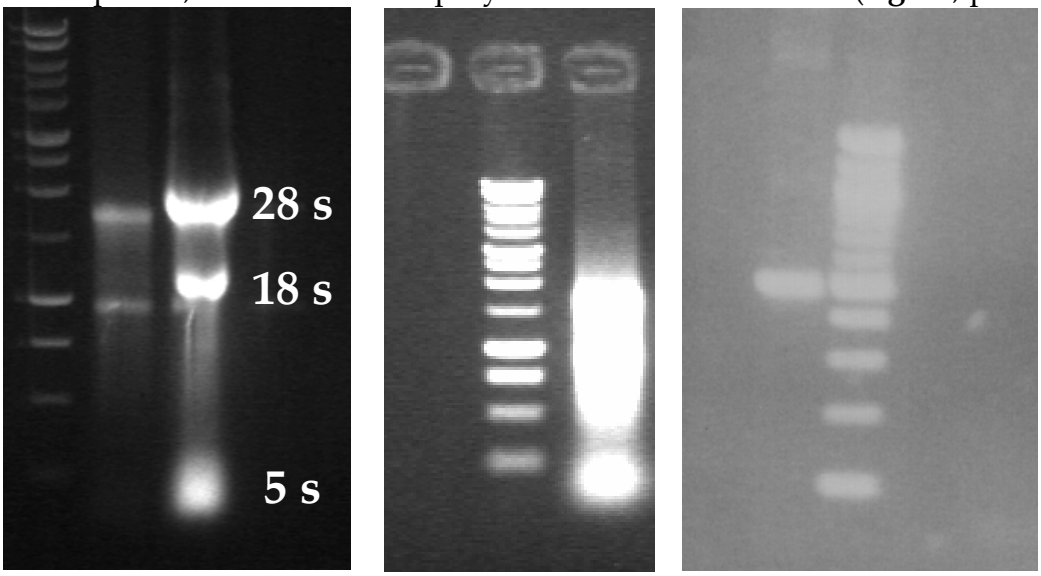

(a) (b) (c)

Fig. 23. (a), 1% agarose gel electrophoresis of extracted RNA from SHSY5Y neuroblastoma cell line. (b), 1% agarose gel electrophoresis of cDNA. (c), amplified nucleotidic sequence coding PMCA1b C-terminal domain.

Agarose gel electrophoresis of the extracted RNA presents three bands corresponding to 28s, 18s and 5s of ribosomal RNA because they constitute 80-85% of total RNA. Bands are included between 1500 bp and 200 bp indicating that there is not degradation of the extracted RNA. cDNA was also included in the range 1500 bp-200 bp because RT-PCR amplify all cellular mRNA. PCR of the C-terminal domain nucleotidic sequence using specific primers had produced a single band corresponding to 500 bp. Amplified sequence was cloned into the expression vector pET21b and sequenced at BMR Genomics of University of Padova. The result of sequencing was translated and aligned with the C-terminal domain of the human PMCA1b (NM_001682) using the ClustalW program (**fig. 24**).

```
NP_001673       TIPTSRLKFLKEAGHGTQKEEIPEEELAEDVEEIDHAERELRRGQILWFRGLNRIQTQIR 60
sequenced       TIPTSRLKFLKEAGHGTQKEEIPEEELAEDVEEIDHAERELRRGQILWFRGLNRIQTQIR 60
                ************************************************************

NP_001673       VVNAFRSSLYEGLEKPESRSSIHNFMTHPEFRIEDSEPHIPLIDDTDAEDDAPTKRNSSP 120
sequenced       VVNAFRSSLYEGLEKPESRSSIHNFMTHPEFRIEDSEPHIPLIDDTDAEDDAPTKRNSSP 120
                ************************************************************

NP_001673       PPSPNKNNNAVDSGIHLTIEMNKSATSSSPGSPLHSLETSL 161
sequenced       PPSPNKNNNAVDSGIHLTIEMNKSATSSSPGSPLHSLETSL 161
                *******************************************
```

Fig. 24. Alignment of sequenced recombinant C-terminal domain with the deposited sequence NP_001673.

Competent BL21 (DE3) cells were transformed with the expression vector pET21b containing the human PMCA1b C-terminal domain. Expression tests at increasing

IPTG concentrations, 0.4 mM, 0.6 mM and 0.8 mM were performed. The growth rate at different IPTG concentration is reported in **fig. 25**.

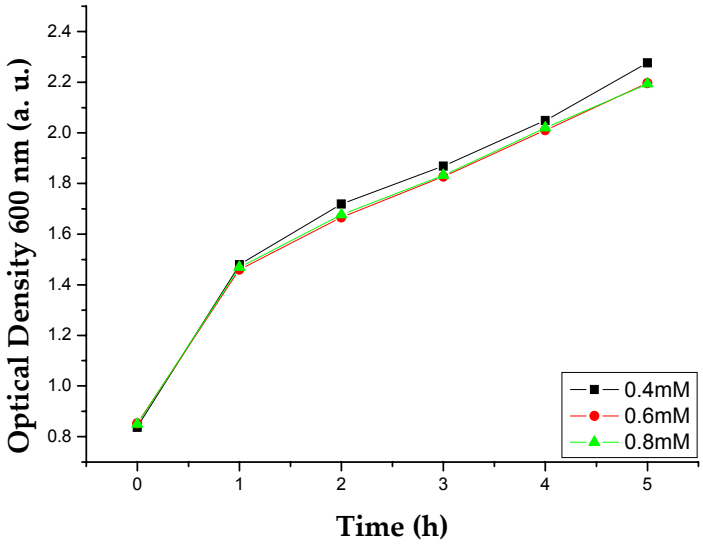

Fig. 25. Growth curves of the *E. coli* BL21 (DE3) strain for the expression of the human C-terminal domain.

The curves at different IPTG concentrations are very similar indicating that there is no toxicity by IPTG to the culture. SDS-PAGE analysis of cellular extracts obtained at various time of growth shows an increase of C-terminal domain expression (**fig. 26**).

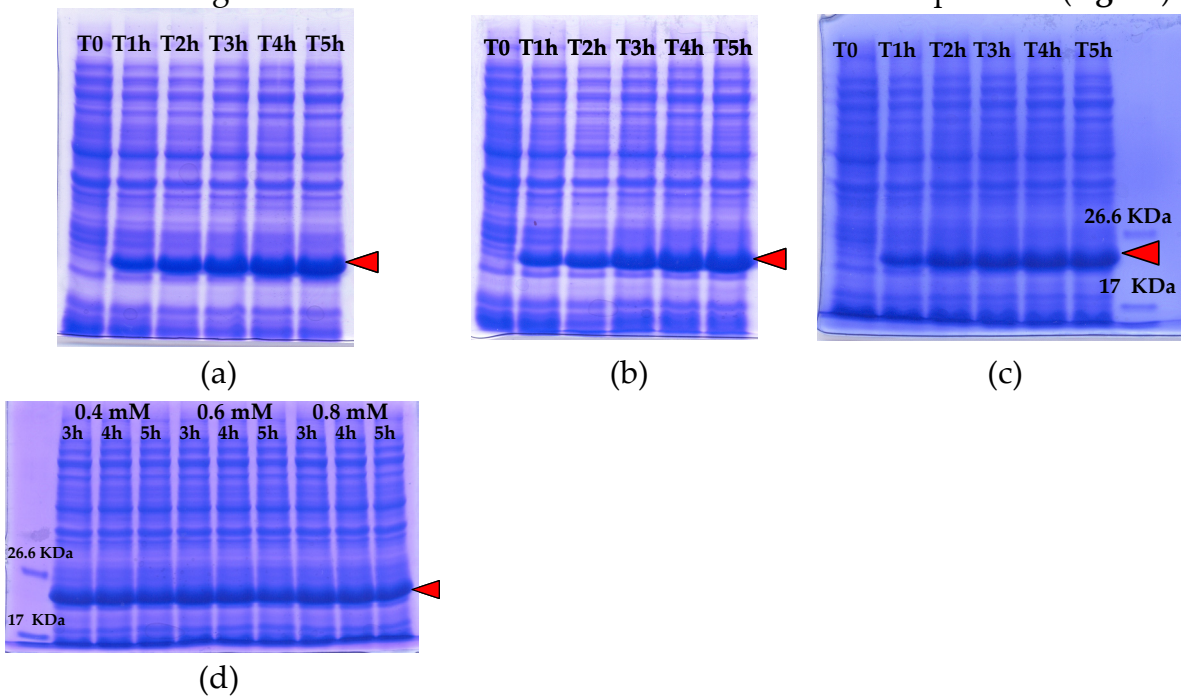

Fig. 26. Expression tests of the C-terminal domain at different concentrations of IPTG: 0.4 mM (a), 0.6 mM (b) and 0.8 mM (c). T0 is the positive control whereas T1h, T2h, T3h, T4h and T5h correspond to the bacterial lysate collected after 1, 2, 3, 4 and 5 hours. Gel in panel (d) represents the total proteins after an induction of 3 hours, 4 hours and 5 hours respectively at different IPTG concentrations. Arrow indicates the C-terminal domain.

Levels of C-terminal domain as function of time (**fig. 26**, panels A, B, C) and as function of IPTG concentration (**fig. 26**, panel D) indicate that the maximum yield of protein is obtained inducing the bacteria with IPTG 0.4 mM for 4 hours (16 mg/L).
The C-terminal domain was purified using a CaM affinity column as described in 5.1.11. EGTA, a specific calcium chelator, was used to elute the bound C-terminal domain. The gel (**fig. 27**) shows the purified C-terminal domain.

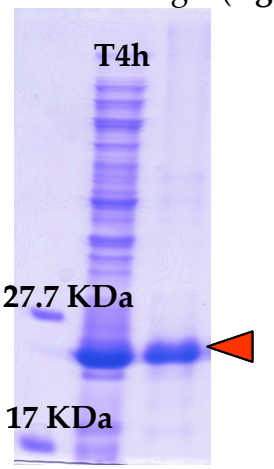

Fig. 27. 12% SDS-PAGE stained with Blue Comassie. Lane 1, molecular mass markers (low range SDS-polyacrylamide gel electrophoresis standards, SIGMA); Lane 2, cellular extract after 4 hours of induction; Lane 3 of the purified C-terminal domain of PMCA1b also indicated by red arrow.

The purification process produced a highly purified C-terminal domain that run into the gel with an apparent molecular weight of 22-23 kDa instead of the calculated 18.264 kDa. Therefore, electrospray mass spectrometry and N-terminal sequencing were performed. The purified C-terminal domain was applied on a reverse phase column and eluted with a non linear gradient as show in **fig. 28**.

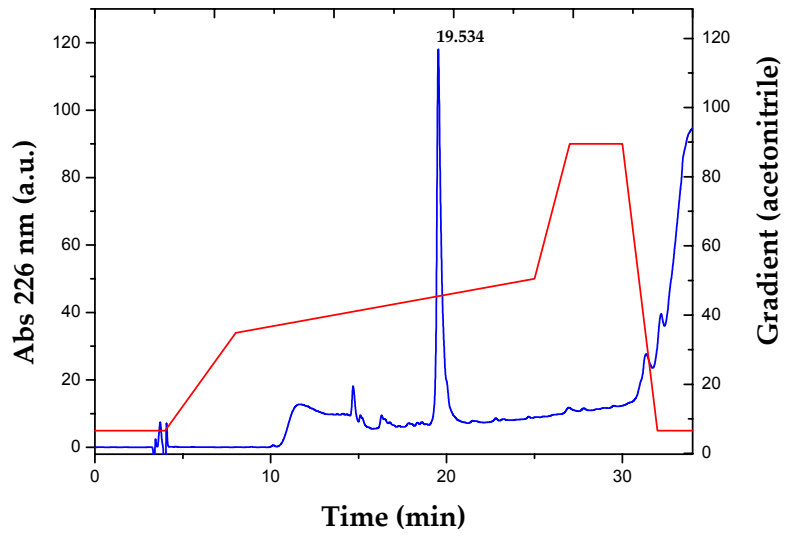

Fig. 28. Reverse phase chromatogram of purified C-terminal domain; red line represents the non linear gradient of acetonitrile used for the elution.

The single sharp peak corresponding to the C-terminal domain was subjected to an ESI mass spectrometry (**fig. 29**).

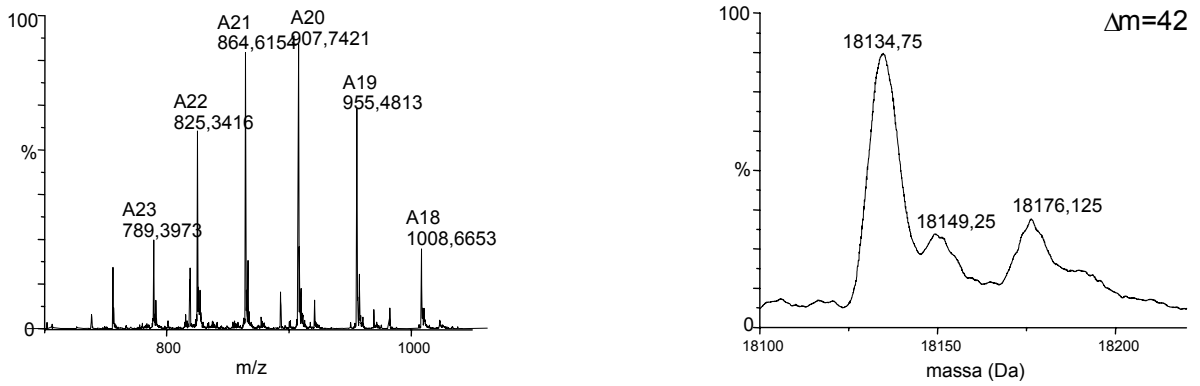

(a) (b)

Fig. 29. (a) Multi-charge ESI spectrum of the purified C-terminal domain. (b) Single-charge ESI spectrum of the purified C-terminal domain (deconvoluted spectrum).

Recombinant C-terminal domain has a molecular weight of 18.134 kDa that differ from calculated molecular weight of 132 Da probably due to the lack of the initial methionine. Furthermore, there is another small peak of 18.176 kDa that could correspond to the acetylated protein. The absence of the initial methionine was also confirmed by N-terminal sequencing. The result of sequencing was TIPT that correspond to the amino acids downstream of the last transmembrane helix.

C-terminal domain seems to contain three calcium binding sites with affinity corresponding to K_D values of about 300 nM, 30 nM and EGTA-insensitive. EGTA-insensitive calcium binding site was determined in CaM binding region E1079-P1180, inside the C-terminal domain, by mass spectroscopy that shown an increase of 39 Da compared to calculated mass [**64**]. Therefore, atomic absorption measurements after dialysis against an EGTA containing solution were performed. Atomic absorption measurements are reported below:

Ca^{2+} standard 4 ppm (Abs)	Buffer (Abs)	C-terminal domain (600 ppm) (Abs)	Ca^{2+} concentration (ppm)	Ca^{2+}/protein Ratio
0.184	0.012	0.028	0.3478	0.00058

The Ca^{2+}/protein ratio was 0.00058 indicating that there is not the EGTA resistant calcium binding site. In order to study the secondary structure of the C-terminal domain, circular dichroism experiments in presence and in absence of calcium were performed (**fig. 30**).

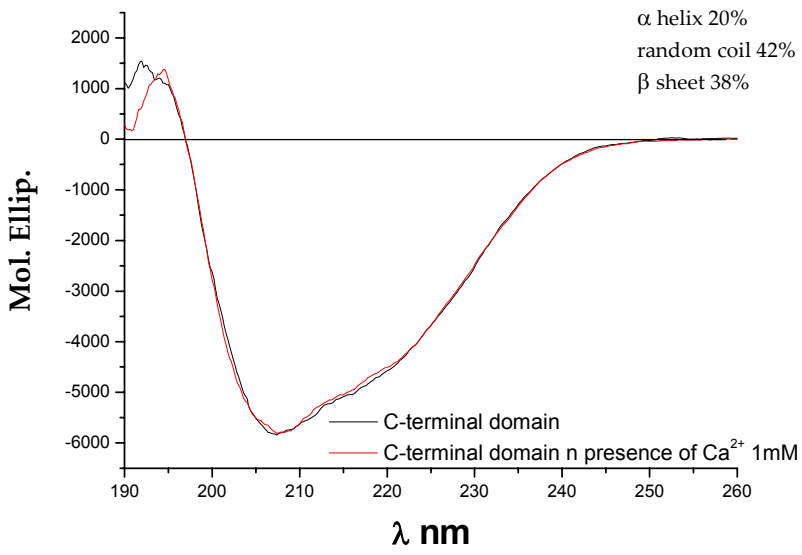

Fig. 30. Circular dichroism spectra performed in absence (black line) or in presence (red line) of free calcium. CD experiments were carried out in Tris 10 mM, NaCl 0.15 M, pH 7.5.

CD spectra in absence or presence of free calcium show a percentage of 20% α-helix, 42% random coil and 38% ß-sheet. The percentages were calculated using the neural network CDNN.

SAXS experiments, to determine the shape at low resolution of the C-terminal domain, have shown the tendency of the protein to aggregate (**fig. 31**).

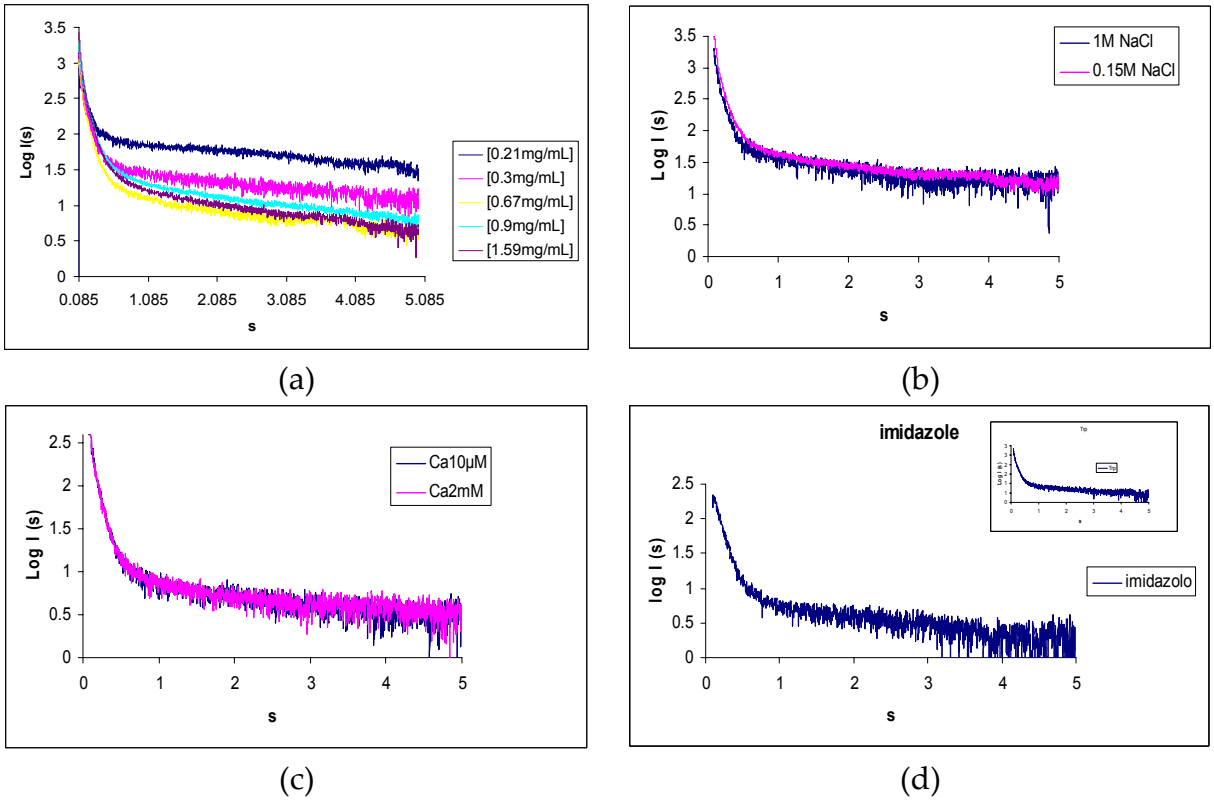

Fig. 31. (a), scattering patterns at different protein concentrations; (b), scattering patterns at different ionic strength; (c), scattering patterns in presence of 10 μM and 2 mM of $CaCl_2$; (d), scattering patterns in presence of imidazole and N-acetyl triptophanamide (inset).

All scattering patterns highlight that the C-terminal domain in all experimental conditions is in oligomeric form.
Aggregates were also visualized by electron microscopy negative staining (**fig. 32**).

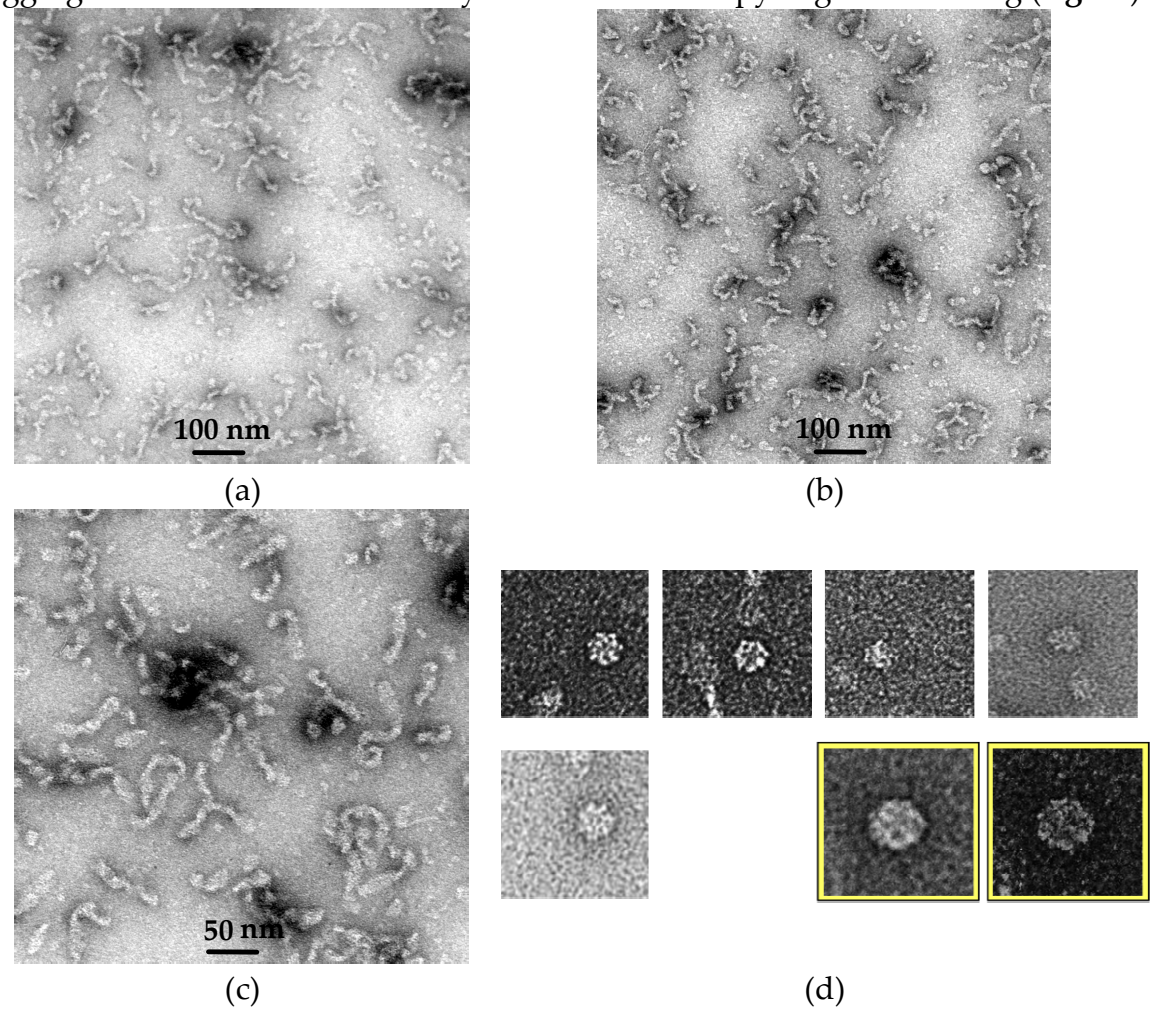

Fig. 32. (a), (b), electron microscopy images of C-terminal domain 0.2 mg/mL. (c), enlargement of previous images. (d), cross section of filaments; images emphasized by yellow represent the average (left) and the variance (right) of the five cross sections.

Electron microscopy images show aggregates as unstructured filaments larger than 100 nm with a cross section radius of 8.75 nm. Average and variance of several cross sections were obtained using SPIDER software. The non perfect overlap could be due to low number of cross section used for the analysis. However, the question was to understand whether the oligomerization process is reversible. To this aim, electron microscopy images in presence of sodium dodecyl sulphate (SDS) were collected (**fig. 33**).

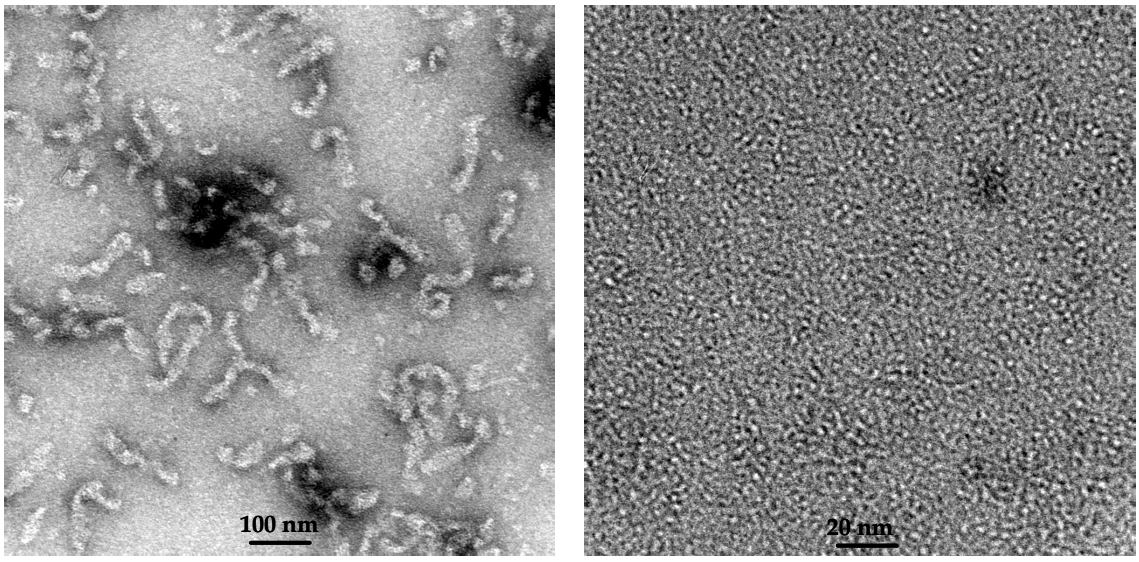

(a) (b)

Fig. 33. (a), electron microscopy image of the C-terminal domain. (b), electron microscopy image of the C-terminal domain in presence of SDS.

Oligomers were disrupted by Sodium Dodecyl Sulphate as shown in **fig. 33** where it is possible to note the absence of filaments. In order to study the minimal SDS concentration necessary to maintain the C-terminal domain in monomeric form, a titration of the protein with increasing detergent concentrations was performed. Non ionic detergents effect on the C-terminal domain was also studied. The aggregation state of the C-terminal domain was analyzed by native PAGE (**fig. 34**).

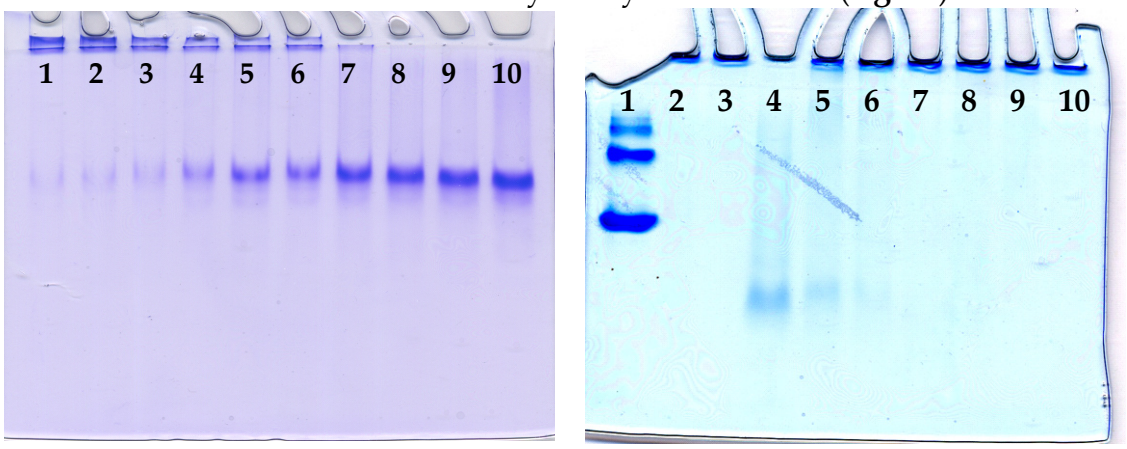

(a) (b)

Fig. 34. (a), 12% native PAGE of the C-terminal domain in presence of increasing SDS concentrations. Lane 1: 6.5 μg of C-terminal domain; lane 2: 6.5 μg of C-terminal domain and SDS 0.01%; lane 3: 6.5 μg of C-terminal domain and SDS 0.02%; lane 4: 6.5 μg of C-terminal domain and SDS 0.03%; lane 5: 6.5 μg of C-terminal domain and 0.04%; lane 6: 6.5 μg of C-terminal domain and 0.05%; lane 7: 6.5 μg of C-terminal domain and SDS 0.1%; lane 8: 6.5 μg of C-terminal domain 0.5%; lane 9: 6.5 μg of C-terminal domain and 1%; lane 10: 6.5 μg of denaturated C-terminal domain. (b), native PAGE of the C-terminal domain in presence of non ionic detergents. Lane 1: BSA (positive control); lane 2: 4 μg of C-terminal domain; lane 3: 4 μg of C-terminal domain in presence of NP40; lane 4: 4 μg of denaturated C-terminal domain; lane 5: 4 μg of C-terminal domain and SDS 0.01%; lanes 6-10: 4 μg of C-terminal domain in presence of increasing TRITON-X100 concentrations.

In the presence of SDS 0.1% the C-terminal domain is stabilized in monomeric form as shown by native PAGE. Under these conditions, the C-terminal domain has the same electrophoretic mobility of the denaturated domain. In the presence of non

ionic detergents such as NP40 and TRITON-X100, the C-terminal domain remains in aggregated form as indicated by blue line in the wells. BSA was used as positive control because it has an isoelectric point similar to that of the C-terminal domain (5.82 vs. 5.06). To determine the critical micelle concentration (CMC), measurements of surface tension were performed (**fig. 35**). The CMC was determined in Tris 10 mM, NaCl 0.15 M, pH 7.5.

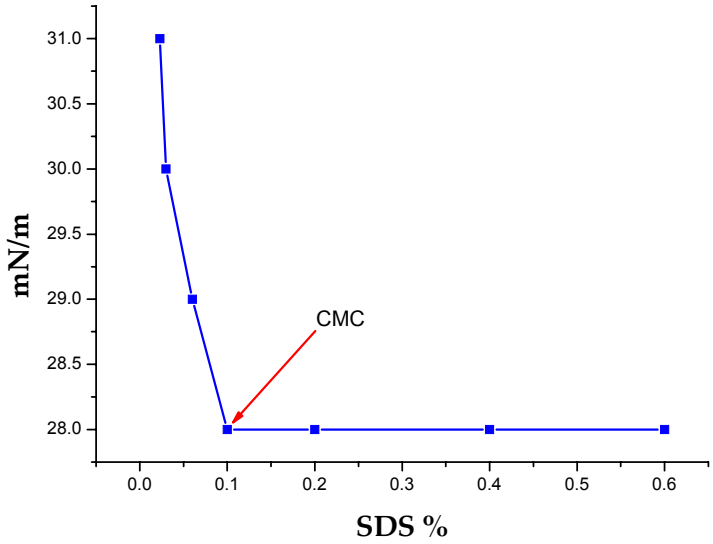

Fig. 35. Determination of the surface tension as function of SDS concentration.

CMC of SDS determined by surface tension measurements corresponds to 0.1% (3.5 mM). This data indicates that the C-terminal domain is completely stabilized in monomeric form at the CMC of SDS. Secondary structure of the C-terminal domain in presence of SDS was studied. Therefore, far-UV CD experiments were performed (**fig. 36**).

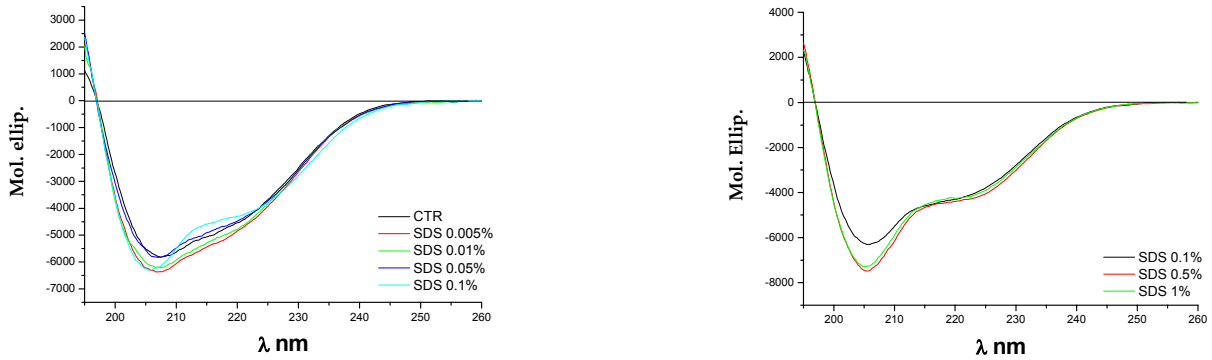

(a) (b)

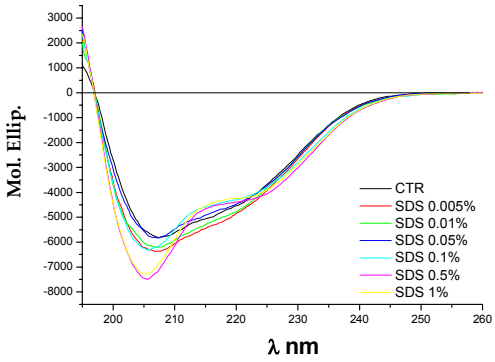

(c)

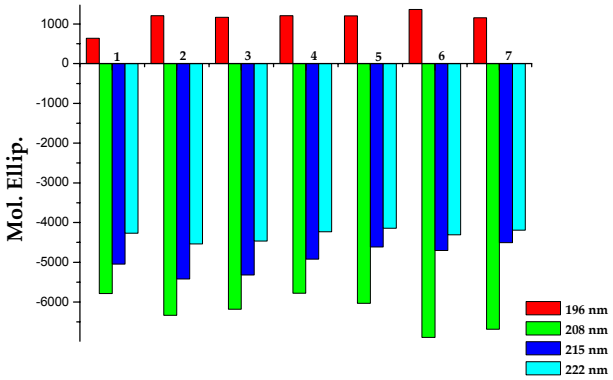

(d)

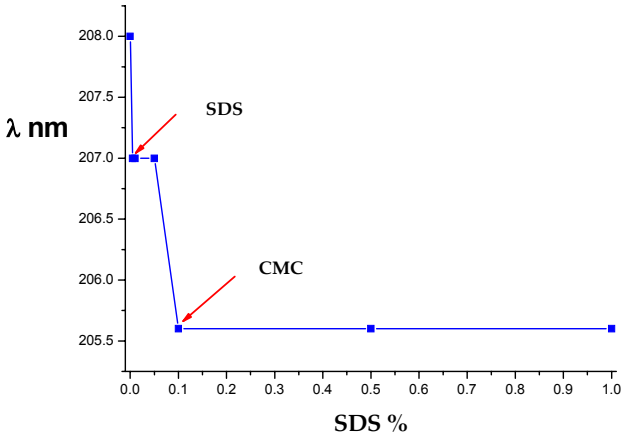

(e)

Fig. 36. (a), CD spectra of C-terminal domain below the CMC of SDS. (b), CD spectra of C-terminal domain above the CMC of SDS. (c), Total CD spectra of C-terminal domain in presence of increasing SDS concentrations. (d), Molar ellipticity of C-terminal domain at 196 nm, 208 nm and 222 nm. Lane 1: C-terminal domain; lane 2: C-terminal domain and SDS 0.005%; lane 3: C-terminal domain and SDS 0.01%; lane 4: C-terminal domain and SDS 0.05%; lane 5: C-terminal domain and SDS 0.1%; lane 6: C-terminal domain and SDS 0.5%; lane 7: C-terminal domain and SDS 1%. (e), Shift of the peak at 208 nm in presence of SDS.

CD spectra shapes below the CMC are very similar. They are characterized by a strong molar ellipticity at 208 nm compared to that at 222 nm but, in presence of SDS, there is a shift of the peak from 208 nm to 207 nm. CD spectra above the CMC present a decrease of the molar ellipticity at 215 nm and a shift of the peak from 207 nm to 205.5 nm with associate an increase of molar ellipticity as indicated in **fig. 36**. The percentages of α-helix, ß-sheet and random coil were performed using the neural network CDNN and the Greenfield's formula (**tab. 3**). The analysis with the neural network using k2d is not accuracy.

	C-ter		C-ter-SDS 0.005%		C-ter-SDS 0.01%		C-ter-SDS 0.05%	
	CDNN	Greenfield eq.	CDNN	Greenfield eq.	CDNN	Greenfield eq.	CDNN	Greenfield eq.
α-helix (%)	19.54%	33.7	19.95%	35.6	19.68%	35.1	19.18%	33.7
ß-sheet	38.36%	-	37.40%	-	37.43%	-	37.20%	-

(%)								
Random coil (%)	42.10%	-	42.58%	-	42.88%	-	43.65%	-
Total (%)	100%	-	100%	-	100%	-	100%	-
	C-ter-SDS 0.1%		C-ter SDS 0.5%		C-ter SDS 1%			
	CDNN	Greenfield eq.	CDNN	Greenfield eq.	CDNN	Greenfield eq.		
α-helix (%)	19.00%	34.6	19.60%	37.5	19.30%	36.8		
ß-sheet (%)	37.35%	-	37.68%	-	37.65%	-		
Random coil (%)	43.70%	-	42.68%	-	43.05%	-		
Total (%)	100%	-	100%	-	100%	-		

Tab. 3. C-ter is the abbreviation of C-terminal domain.

The calculated percentage values of the secondary structure elements using CDNN are not reliable because there are not variations in presence of different SDS concentrations. However, the increase of the molar ellipticity around 208 nm and the shift of the peak are probably due to the increase of the random coil.

In order to study the shape at low resolution of the C-terminal domain in presence of SDS, small angle neutron scattering experiments were performed. These experiments were carried out using ^{2}H labelled C-terminal domain because there was more contrast compared to background. To obtain the maximum yield of labelled protein, expression tests in M9 minimal medium were performed. The growth rate at two different ampicillin concentrations and at increasing IPTG concentrations is reported in **fig. 37**.

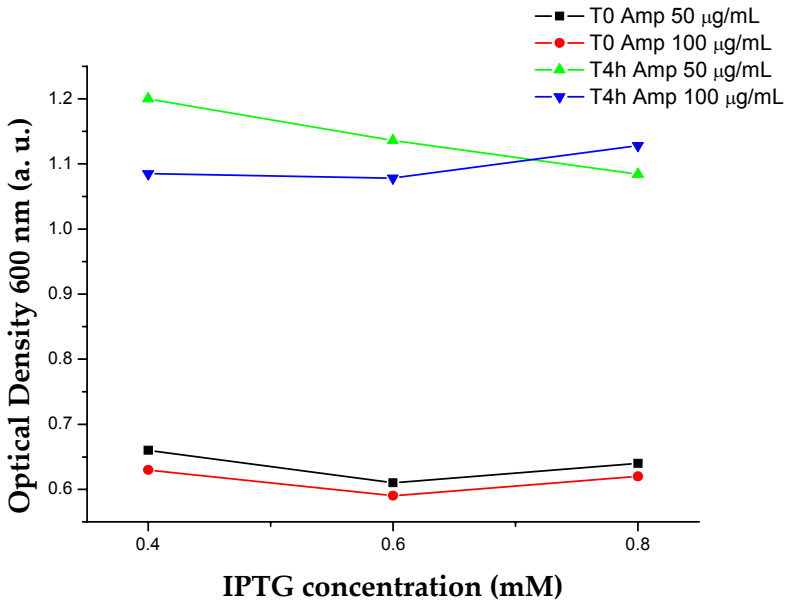

Fig. 37. Growth curves of the *E. coli* BL21 (DE3) for the expression of C-terminal domain in M9 minimal medium.

The growth curves in absence of IPTG (red and black) are very similar indicating that bacteria there are not sensitive to the ampicillin concentrations. Once added IPTG, the bacterial growth is favourite using 0.4 mM of IPTG and ampicillin 50 μg/mL. Cellular extracts collected at various time of growth were analyzed by 12% SDS-PAGE as shown in **fig. 38**.

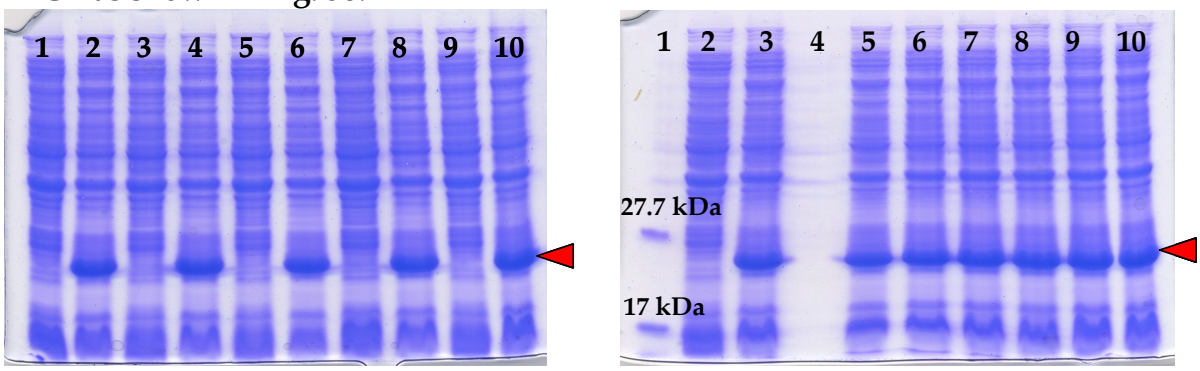

(a) (b)

Fig. 38. (a), 12% SDS-PAGE of cellular extracts. Lane1: T0 (IPTG 0.4 mM), ampicillin 50 μg/mL; lane 2: after 4 h of induction with IPTG 0.4 mM in presence of ampicillin 50 μg/mL; lane 3: T0 (IPTG 0.6 mM), ampicillin 50 μg/mL; lane 4: after 4 h of induction with IPTG 0.6 mM in presence of ampicillin 50 μg/mL; lane 5: T0 (IPTG 0.8 mM), ampicillin 50 μg/mL; lane 6: after 4 h of induction with IPTG 0.8 mM in presence of ampicillin 50 μg/mL; lane 7: T0 (IPTG 0.4 mM), ampicillin 100 μg/mL; lane 8: after 4 h of induction with IPTG 0.4 mM in presence of ampicillin 100 μg/mL; lane 9: T0 (IPTG 0.6 mM), ampicillin 100 μg/mL; lane 10: after 4 h of induction with IPTG 0.6 mM in presence of ampicillin 100 μg/mL. (b), 12% SDS-PAGE of cellular extracts and the comparison between bacterial lysate at different IPTG and ampicillin concentrations after an induction of 4 hours. Lane 1: molecular mass markers (low range SDS-polyacrylamide gel electrophoresis standards, SIGMA); lane 2: T0 (IPTG 0.8 mM), ampicillin 100 μg/mL; lane 3: after 4 h of induction with IPTG 0.8 mM in presence of ampicillin 100 μg/mL; lane 4: empty; lane 5: T4h of induction with IPTG 0.4 mM and ampicillin 50 μg/mL; lane 6: T4h of induction with IPTG 0.6 mM and ampicillin 50 μg/mL; lane 7: T4h of induction with IPTG 0.8 mM and ampicillin 50 μg/mL; lane 8: T4h of induction with IPTG 0.4 mM and ampicillin 100 μg/mL; lane 9: T4h of induction with IPTG 0.6 mM and ampicillin 100 μg/mL; lane 10: T4h of induction with IPTG 0.8 mM and ampicillin 100 μg/mL. Red arrow indicates the C-terminal domain.

Maximum yield of expression was obtained using IPTG 0.4 mM, ampicillin 100 μg/mL, at 30 °C for 4 hours. CaM affinity column was used to purify the ^{2}H labelled C-terminal domain. The yield was the same of that obtained in LB medium (16 mg/L). In order to calculate the scattering length density was necessary to know the percentage of deuteration of the protein. Therefore, reverse phase chromatography (**fig. 39**) and ESI mass spectrometry (**fig. 40**) were performed.

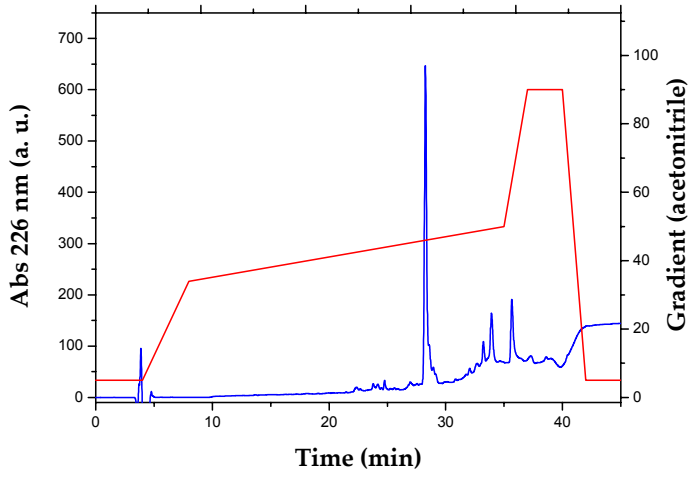

Fig. 39. Reverse phase chromatogram of purified ^{2}H C-terminal domain; red line represents the non linear gradient of acetonitrile used for the elution.

The first one eluted peak corresponds to the ^{2}H labelled C-terminal domain while the other peaks with bigger retention times are impurities present in column.

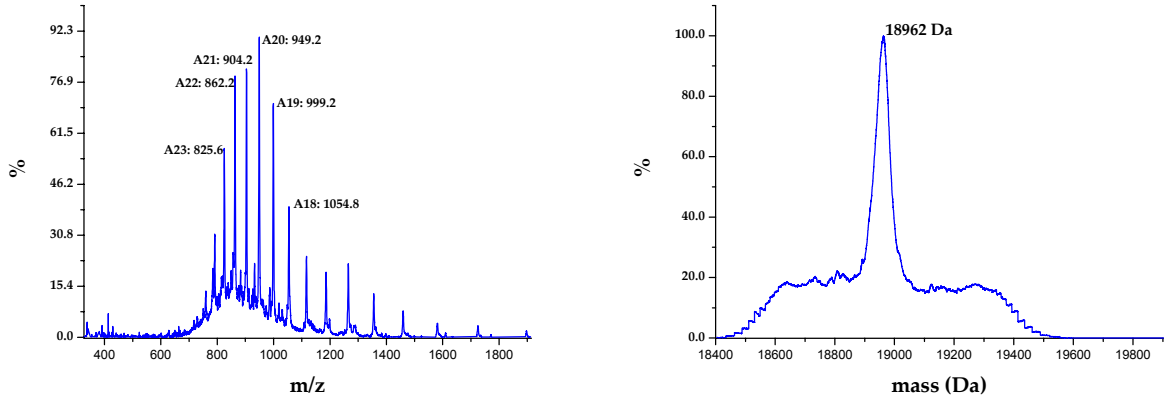

(a) (b)

Fig. 40. (a) Multi-charge ESI spectrum of the purified ^{2}H C-terminal domain. (b) Single-charge ESI spectrum of the purified ^{2}H C-terminal domain (deconvoluted spectrum).

^{2}H labelled C-terminal domain has a molecular weight of 18962 Da. All parameters necessary to calculate the scattering length density curve are reported below:

Exchangeable ^{1}H	287
Unchangeable ^{1}H	129
^{2}H	827
Total ^{1}H	1243
Percentage of deuteration	86.5%

The percentage of deuteration was calculated on the total unchangeable ^{1}H.

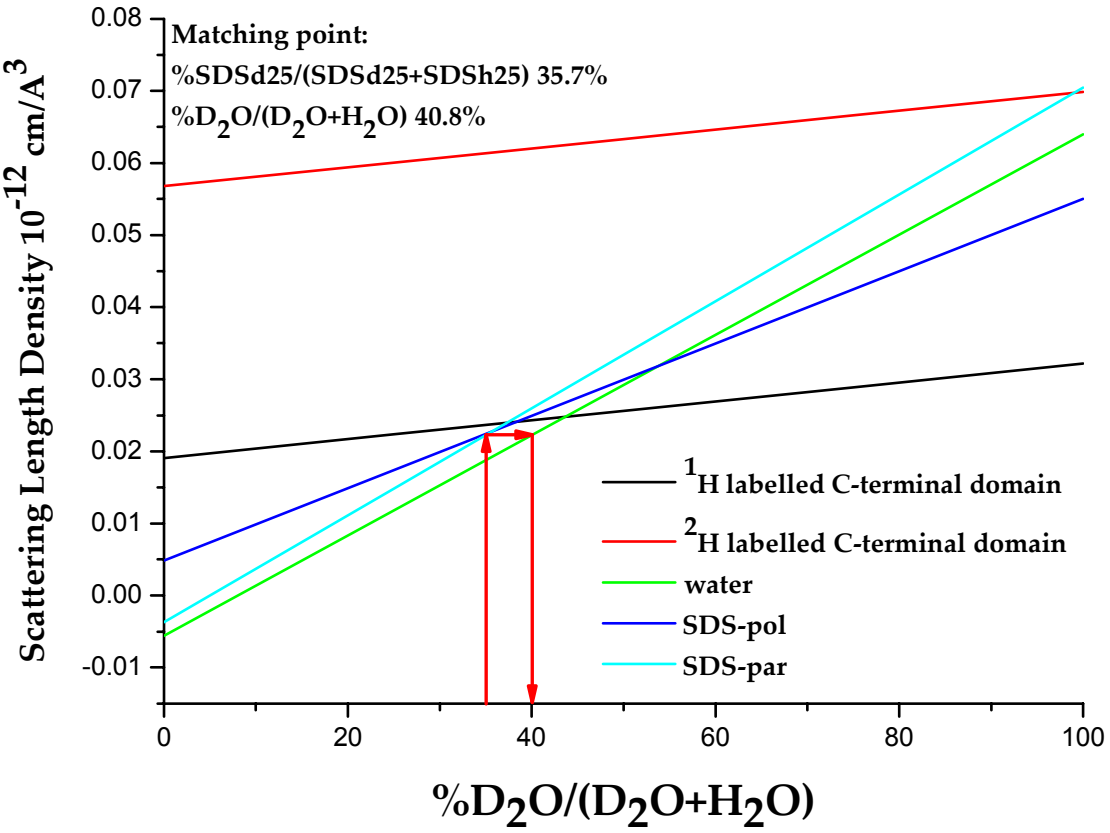

Fig. 41. Scattering length density plot of the ^{1}H labelled C-terminal domain, ^{2}H labelled C-terminal domain, water, SDS polar portion, SDS paraffinic portion.

Matching point was obtained for scattering length density value of 0.022755391 10^{-12} cm/Å^3 with a molar fraction of SDSd25 of 35.7% and a volumetric fraction of D_2O of 40.8% (**fig. 41**). The contrast (ϱ) is the difference between the scattering length density of the ^{2}H protein (red line) and the matching point scattering length density. SANS experiments were performed in matching point conditions and the experimental curves were normalized subtracting the incoherent scattering, due to spin incoherence of ^{1}H, calculated by Porod's law at high Q values [**65**]:

$$I(q) = B + C\,Q^{-4}$$

where I (q) represents the intensity of the scattering (cm^{-1}), B the incoherent scattering factor, C the Porod's constant and Q the scattering parameter described as $4\pi\sin\theta/\lambda$ (Å^{-1}). Once normalized, the background was subtracted from the curves of protein containing samples and the Kratky plots were drawn (**fig. 42**) to study the compactness.

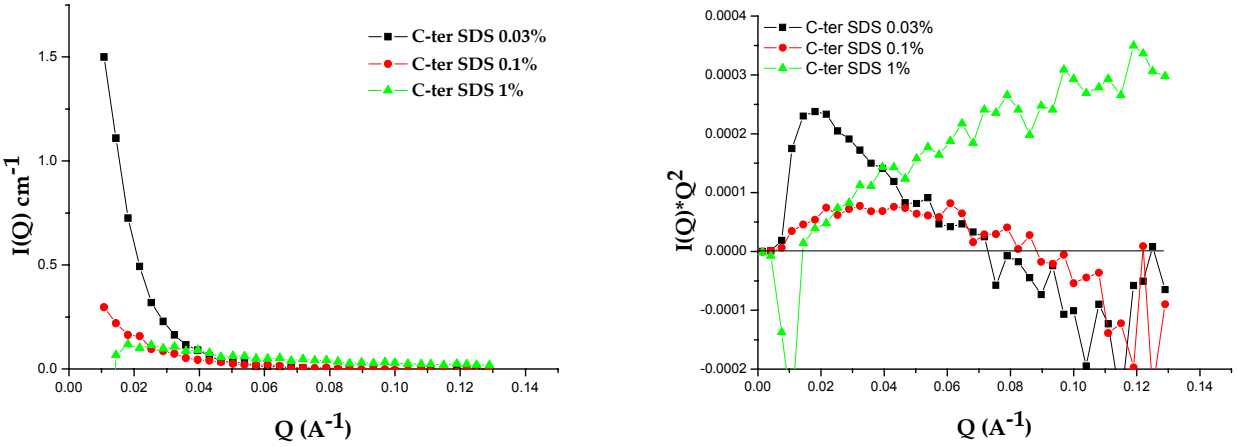

(a) (b)

Fig. 42. (a), C-terminal domain scattering patterns in presence of SDS 0.03% (black line), 0.1% (red line) and 1% (green line). (b), Kratky plots of the C-terminal domain in presence of SDS 0.03% (black line), SDS 0.1% (red line) and SDS 1% (green line).

C-terminal domain scattering patterns indicate that in presence of SDS concentration below the CMC (0.03%) the intensity at angle zero, I(0), is higher than the I(0) of the C-terminal domain in presence of SDS at the CMC (0.1%). I(0) is proportional at the molecular weight therefore below the CMC the protein is aggregate. The signal of the C-terminal domain in presence of SDS 1% is very low therefore is very difficult to analyze this curve. Kratky plots show that the protein in the presence of SDS 0.03% and 0.1% is compact while the C-terminal domain in presence of SDS 1% is not compact.

The curves are analyzed using GNOM program, with a rod-like model, to find the gyration radius of the ^{2}H C-terminal domain. In the presence of SDS below the CMC the gyration radius is 54.52 ± 3.056 Å with an I(0) of 0.2103E-01 ± 0.1458E-02 Å. In the presence of SDS concentration around the CMC the gyration radius is 26.68 ± 3.382 Å with an I(0) of 0.3418E-02 ± 0.3674E-03 Å. The GNOM fits are reported in **fig. 43**.

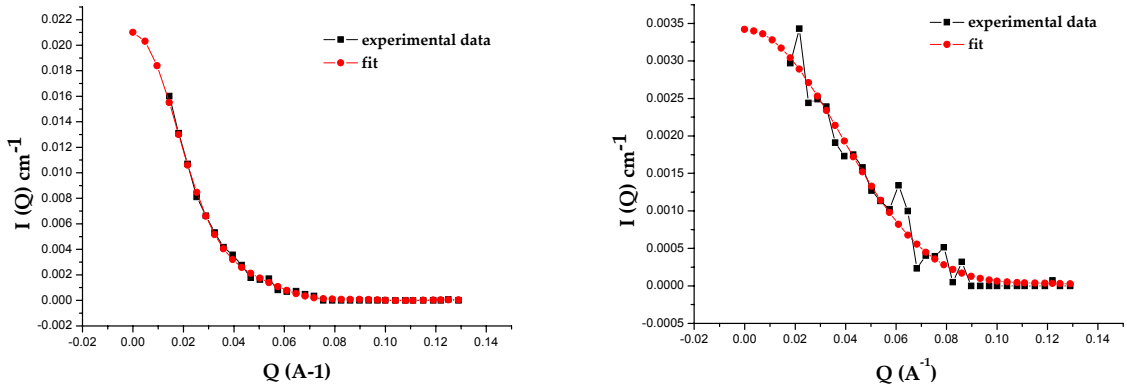

(a) (b)

Fig. 43. (a), scattering curves of the experimental data (black line) and of the GNOM fit (red line) of C-terminal domain in presence of SDS concentration below the CMC; (b), scattering curves of the experimental data (black line) and of the GNOM fit (red line) of C-terminal domain in presence of SDS concentration around the CMC

GNOM output has been used to predict *ab initio* the shape of the C-terminal domain at low resolution using DAMMIN program. A total of 30 runs of DAMMIN have been executed per each experimental curve because of the stochastic nature of the program and the average model has been calculated. The result is reported in **fig. 44**.

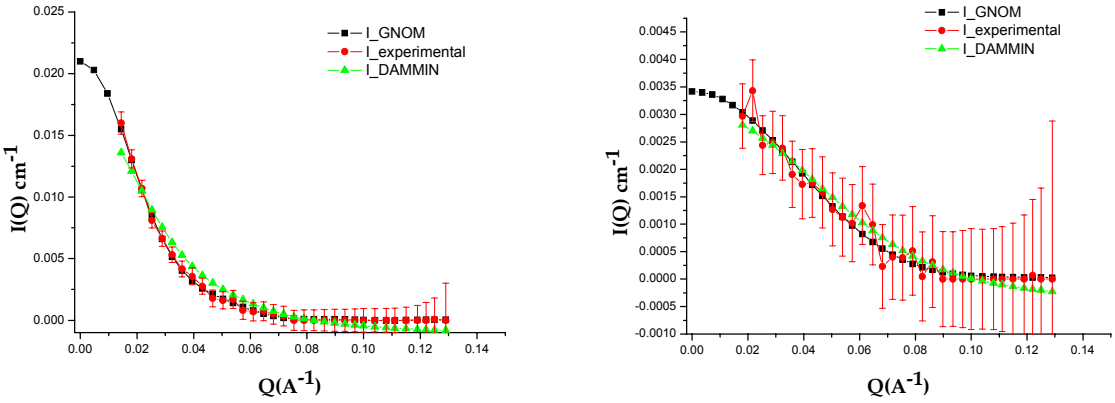

(a) (b)

Fig. 44. (a), scattering curves of the experimental data (red line), of the GNOM fit (black line) and DAMMIN fit (green line) of the C-terminal domain in presence of the SDS concentration below the CMC; (b), scattering curves of the experimental data (red line), of the GNOM fit (black line) and DAMMIN fit (green line) of the C-terminal domain in presence of the SDS concentration around the CMC

DAMAVER has been used to calculated the average of all the DAMMIN models and the resulting 3D reconstruction of the C-terminal domain in presence of SDS concentrations below (0.03%) and around the CMC (0.1%) is reported in **fig. 45**.

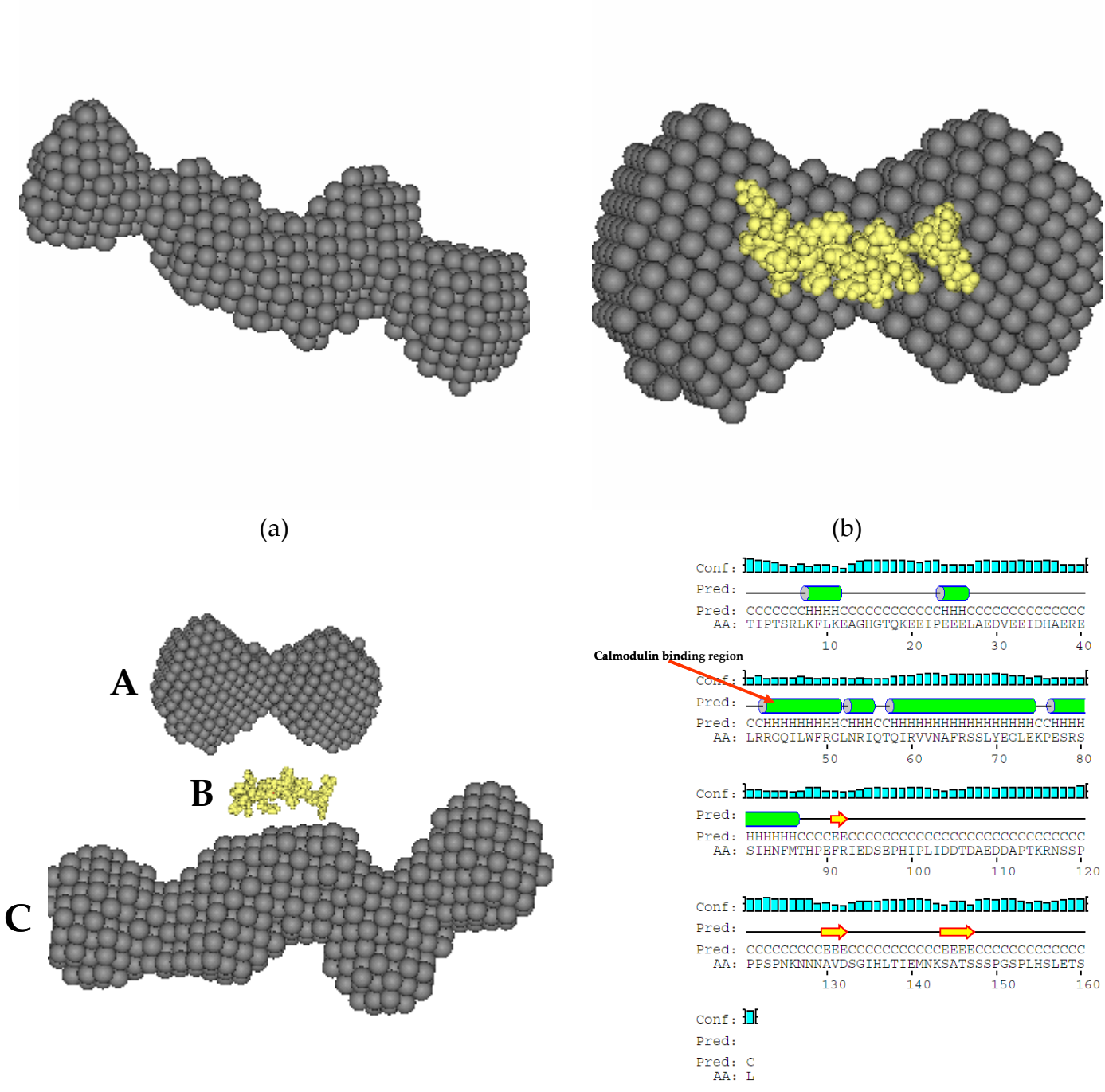

Fig. 45. (a), 3D reconstruction of the C-terminal domain shape at low resolution in the presence of SDS concentration of 0.03%; (b), 3D reconstruction of the C-terminal domain shape at low resolution in presence of SDS concentration of 0.1%. The yellow structure represents the C28W calmodulin binding region of the C-terminal domain; (c), scaled 3D reconstructions of the C-terminal domain in the presence of SDS concentration around the CMC (A), below the CMC (C) and the C28W calmodulin binding region inside the C-terminal domain (B); (d), prediction of the C-terminal domain secondary structure

In the presence of SDS concentration below the CMC, the C-terminal domain is in aggregate form as also demonstrated by native-PAGE while around the CMC, it has a hourglass form. The central cross section of the hourglass could corresponds to the calmodulin binding region that have an α-helix structure [**31**] and the down and

upstream parts could be unstructured and therefore flexible as predicted by PSIPRED (http://bioinf.cs.ucl.ac.uk/psipred/).

6 Calmodulin: expression, purification, structural characterization and binding experiments with the C-terminal domain of PMCA 1b

6.1 Materials and Methods

The expression vector containing the human CaM coding sequence was kindly provided by Dr. Joachim Krebs (Department of NMR-based Structural Biology, Göttingen, Germany; Institute of Biochemistry, Swiss Federal Institute of Technology (ETH), Zurich, Switzerland). The CaM nucleotidic sequence was cloned in the pET28b expression vector, without His-tag regions, using specific primers with NotI (GC↓GGCCGC) and NdeI (CA↓TATG) restriction sites at the 5′ and 3′ sides respectively (**fig. 46**).

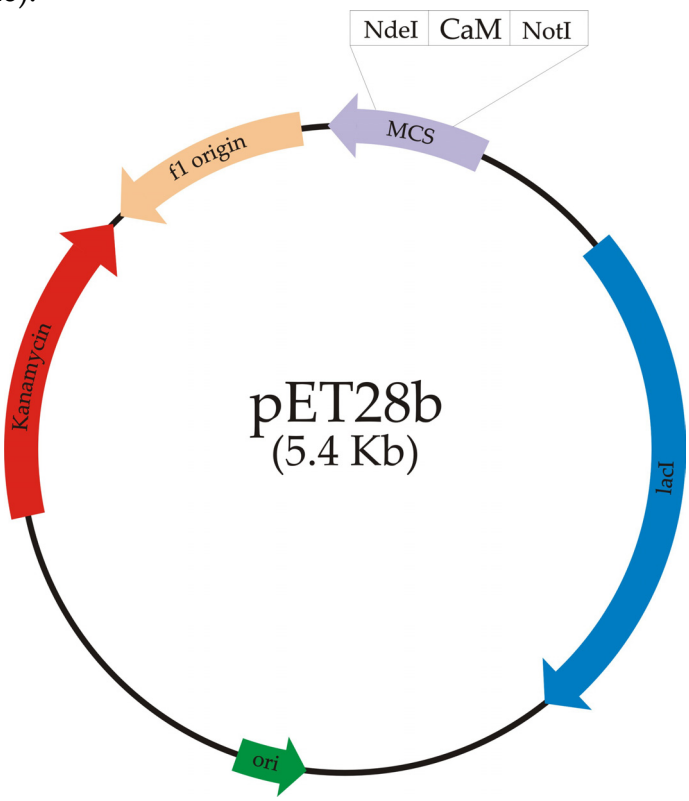

Fig. 46. pET28b map (Novagen)

6.1.1 Tests for expression of the recombinant CaM

Competent *E. coli* BL21 (DE3) cells were transformed with 1 µL (293 ng) of pET28b-CaM, streaked on LB agar plate containing kanamycin (Kan) 25 µg/mL and incubated at 37 °C overnight. Clones were inoculated in three Erlenmeyer flasks

containing 25 mL of LB, kanamycin 25 μg/mL and incubated at 37 °C until an optical density (OD_{600}) of 0.6. The expression tests were carried out at increasing concentration of IPTG: 0.4 mM, 0.6 mM, 0.8 mM at 30 °C for 5 hours. 1 mL of each culture was collected every hour and centrifuged at 2700g (Beckman Coulter Microfuge® 18 Centrifuge) at 4 °C for 5 minutes. The pellets were stocked at -20 °C for next SDS PAGE analysis.

6.1.2 Large-scale expression of the recombinant CaM

Once obtained the best conditions to produce recombinant CaM, large-scale inductions were made. To this aim, clones were inoculated in 500 mL of LB-kanamycin 25 μg/mL until an OD_{600} of 0.6 and induced with IPTG 0.6 mM at 30 °C for 5 hours. The growth was stopped at 4 °C for 30 minutes and the bacteria were centrifuged at 2700g (Beckman TJ-25 Centrifuge) for 30 minutes. The CaM containing pellet was stored at -80 °C.

6.1.3 Purification of CaM

The bacterial pellet containing CaM, previously stored at -80°C, was resuspended with 20 mL of Tris-HCl 50 mM, EDTA 1 mM, PMSF 1 mM and 20 μL of protease inhibitor cocktail (4-(2-aminoethyl)benzenesulfonyl fluoride, bestatin, pepstatin A, E-64, and phosphoramidon), pH 7.5. *E. coli* BL21 cells were disrupted by French Press (Inlabo American Instrument Company) applying three passes at 1000 psi (68.95 bar). The lysate was boiled at 100 °C for 3 minutes and centrifuged at 15871g (Beckman Coulter Allegra 64R Centrifuge) for 30 minutes to separate the soluble and insoluble fractions. The soluble fraction was filtered using a 0.22 μm cut off filter whereas the insoluble fraction, containing inclusion bodies, was stored at -20 °C for next SDS-PAGE analysis. The filtered material was incubated with 10 mL of Phenyl-Sepharose 4B resin previously equilibrated with Tris-HCl 50 mM, EDTA 1 mM, pH 7.5. The suspension was stirred at 4 °C for 2 hours and then centrifuged at 200g for 5 minutes (4236 centrifuge ALC). The CaM containing supernatant, added with $CaCl_2$ 2 mM, was loaded onto Phenyl-Sepharose 4B resin (flow rate 0.5 mL/min) equilibrated with Tris-HCl 50 mM, $CaCl_2$ 1 mM, pH 7.5 in FPLC system, for a second step of purification. Unbound proteins were washed with the equilibration buffer at a flow rate of 1 mL/min while CaM was eluted with a solution composed by Tris-HCl 50 mM, EGTA 2 mM, pH 7.5, flow rate 1.5 mL/min. The CaM containing fractions were pooled and applied to anionic exchange column (Resource Q®, Pharmacia Biotech) to separate contaminant DNA. CaM was eluted with a NaCl linear gradient 0-100% in 30 minutes, flow rate 1 mL/min. When necessary the purified CaM was dialysed using benzoylated cellulose dialysis bags (D7884-10FT, SIGMA) with cut off of 1000 Da.

6.1.4 Gel Filtration Chromatography

In order to study the purity and the monodispersity of the purified CaM, gel filtration chromatography in HPLC system was applied. A volume of 320 μL of purified CaM was loaded onto the Superdex™ 75 HR 10/30 prep grade column (Pharmacia LKB Biotechnology) with a flow rate of 0.5 mL/min. Commercial CaM

(P0809, SIGMA) was used as control. All peaks were analysed by UV/vis spectroscopy (Diode Array mod. 8452A, Hewlett Packard).

6.1.5 Reverse phase HPLC and mass spectrometry

Reverse phase HPLC chromatography was performed followed by mass spectrometry analysis. A C18 Phenomenex Jupiter (250 x 4.6 mm) column connected to the security guard C18 pre-column (Phenomenex Inc., Torrance, CA, USA) was used for this purification step. The column was equilibrated with 95% of solvent A (H2O mQ and 1% Trifluoroacetic acid, TFA) and 5% of solvent B (acetonitrile and 0.085% TFA). CaM (15 μg) was loaded onto reverse phase column and the protein was eluted with the gradient indicated below:

Time (minutes)	0	5	12	42	44	49	50	53	56
% B	5	5	30	55	95	95	5	5	Stop

The chromatography was carried out with a flow rate of 1 mL/min and the elution was observed at 226 and 280 nm corresponding to the absorption of the peptide bond and of aromatic amino acids respectively. The fraction of CaM was collected and lyophilized using a Savant Speed Vac concentrator. The CaM was resuspended in 20 μL of solution made from 49% H2O mQ, 50% acetonitrile and 1%formic acid for electrospray ionization mass spectrometry experiment using the Mariner System 5220 (Applied Biosystem) spectrometer, in collaboration with Dr.ssa. Polverino De Laureto (C.R.I.B.I., University of Padova).

6.1.6 Determination of the CaM extinction coefficient

CaM extinction coefficient in Tris-HCl 50 mM, EGTA 2mM, pH 7.5 was determined by bicinchoninic acid assay (BCA assay). Standard curve was prepared by diluting standard solutions of bovine serum albumin.

The BCA reagent is made by mixing 1 part of reagent B (4% cupric sulphate) and 50 parts of reagent A (sodium carbonate, sodium bicarbonate, bicinchoninic acid and sodium tartrate in 0.1 M sodium hydroxide). For the assay 1 mL of BCA reagent plus 50 μL of either BSA standard solutions or CaM were used throughout. All samples were incubated at 37 °C for 30 minutes and cooled in ice to stop the reaction. The developed colour was quantified at 562 nm using a spectrophotometer UV/vis mod. 8452A Diode Array of the Hewlett Packard. Each data point was obtained as average between two replicates. CaM concentration was calculated using the equation of the standard curve and its extinction coefficient at 276 nm determined by Lambert-Beer law.

6.1.7 Native-PAGE

Several studies have highlighted a calcium-dependent change in the electrophoretic mobility of CaM in the presence of sodium dodecyl sulphate (SDS) [**66**]. This observation suggests that the ability of CaM to bind calcium can be assayed by testing the mobility of the protein in presence or absence of calcium. Therefore, native PAGEs at 15% in the presence of $CaCl_2$ or EGTA were performed. The

composition of the native gels is reported in **tab. 4**. A volume of 10 μL of loading buffer 5X (glycerole 100%, Bromophenol blue) was added to 40 μL of CaM (1.43 μg/μL). Then, 20 μL of the mixture were loaded onto gels that were run at 20 mA each and at 4 °C using a BIORAD mini Protean 3 cell in Glycine 0.192 M, Tris 25 mM, $CaCl_2$ 2 mM or EGTA 5 mM, pH 8.3. Egg albumin (P01012) was used as positive control because it has an isoelectric point (pI) of 5.19 that is similar to the pI of CaM, 4.1 and a molecular weight of 42881.2 Da. Gels were stained with Blue Comassie for 40 minutes and then destained with a solution made from 10% acetic acid, 45% methanol and 45% water.

	Native PAGE with EGTA		Native PAGE with $CaCl_2$	
	Resolving Gel 15%	Stacking Gel 4%	Resolving Gel 15%	Stacking Gel 4%
Acrylamide 40%	3750 μL	500 μL	3750 μL	500 μL
Bisacrylamide 1.6%	2930 μL	391 μL	2930 μL	391 μL
Tris 1.5 M pH 8.8 (4x)	2500 μL	1250 μL	2500 μL	1250 μL
EGTA	19.01 mg (5 mM)	9.50 mg (5 mM)	-	-
$CaCl_2$ 1 M	-	-	20 μL	10 μL
TEMED	7 μL	3.5 μL	7 μL	3.5 μL
APS 10%	70 μL	35 μL	70 μL	35 μL
H_2O	743 μL	2821 μL	743 μL	2821 μL
Total Volume	10 mL	5 mL	10 mL	5 mL

Tab. 4. Native-PAGE composition

6.1.8 Circular dichroism

To study the secondary structure of purified CaM, far UV (196-250 nm) circular dichroism spectra were recorded at room temperature on JASCO J-715 spectrophotometer using 0.1 cm pathlength cells. Data were analysed with the jwstda32 software.

All spectra were recorded in Tris 50 mM, EGTA 2 mM, CaM 0.196 mg/mL and at three different calcium concentrations: 0 μM, 2 mM and 3 mM (**tab. 5**).

Using these conditions, the values of free calcium in solution were calculated with MAXCHELATOR program.

	CaM	Ca-CaM (6.3 μM)	Ca-CaM (1 mM)
CaM 0.196 mg/mL (μL)	200	199.6	199.4
Ca^{2+} (1M) (μL)	0	0.4	0.6
[CaM] mg/mL	0.196	0.196	0.195
Total volume (μL)	200	200	200

Tab. 5. Composition of the solution for CD experiments of recombinant CaM.

The percentages of α-helix, ß-sheet and random coil were calculated using two different softwares based on neural network, CDNN and k2d, and the formula described by Greenfield and Fasman [**67**]. CDNN was trained with a dataset of 13 spectra related to proteins of known structure, (**tab. 6**) that are dominated by the secondary structure of the protein. k2d was trained with 18 proteins of known structure (**tab. 6**).

Proteins CDNN	α-helix (%)	ß-sheet (%)	Random coil (%)	Proteins k2d	α-helix (%)	ß-sheet (%)	Random coil (%)
Cytochrome C	38	17	45	adenylate kinase	54.6	12.9	32.5
Flavodoxin	38	40	22	alpha-Chymotrypsin	7.6	24.6	67.8
GAPDH	30	36	34	carboxypeptidase A	34.9	15.6	47.9
Hemerythrin	75	11	14	concanavalin A	5.1	44.7	50.2
Hemoglobin	75	14	11	Cytochrome C	38	17	45
Lactate Dehydrogenase	41	28	31	elastase	9.6	34.2	56.2
Lysozyme	36	41	23	insulin			
Myoglobin	78	12	10	Lactate Dehydrogenase	41	28	31
Polyglutamic Acid	100	0	0	Lysozyme	36	41	23
Ribonuclease	24	47	29	Myoglobin	78	12	10
Subtilisin NOVO	31	21	48	nuclease	26.5	30.9	42.6
Thermolysin	32	38	30	Papain	25.5	17	57.5
Triosephosphate Isomerase	52	25	23	parvalbumin	55.4	0	44.5
				Ribonuclease	24	47	29
				ribonuclease S	18.1	35.2	46.7
				Subtilisin NOVO	31	21	48
				Thermolysin	32	38	30
				trypsin inhibitor	71.4	0	28.6

Tab. 6. Secondary structures of the protein used in CDNN and k2d neural networks.

CD spectroscopy was also used to study the effect of SDS on the secondary structure of the purified CaM. Experimental conditions were described above whereas the sample compositions are reported in **tab. 7**. All measurements were recorded in Tris 10 mM, NaCl 0.15 M and $CaCl_2$ 2 mM, pH 7.5.

	Blank composition		Sample composition		
Sample name	Buffer (μL)	SDS 10% (μL)	CaM (μL)	SDS 10% (μL)	[CaM] mg/mL
CaM	200	-	200	-	0.2
CaM-SDS 0.01%	199.8	0.2	199.8	0.2	0.1998
CaM-SDS 0.05%	199	1	199	1	0.199
CaM-SDS 0.1%	198	2	198	2	0.198
CaM-SDS 0.5%	190	10	190	10	0.19
CaM-SDS 1%	180	20	180	20	0.18

Tab. 7. Composition of the solution for CD experiments of recombinant CaM in presence of SDS.

Buffer: Tris 10 mM, NaCl 0.15 M, $CaCl_2$ 2 mM, pH 7.5.

SDS 10% in Tris 10 mM, NaCl 0.15 M, $CaCl_2$ 2 mM, pH 7.5.

6.1.9 Binding experiments

These experiments were aimed to define the capability of Ca^{2+}-CaM to bind the monomeric form of the C-terminal domain of human PMCA1b in the presence of SDS. The C-terminal domain (0.32 mg/mL) was incubated, in presence of increasing SDS concentration (0-1.5%), with 500 μL of Calmodulin-Sepharose 4B previously equilibrated with Tris 50 mM, NaCl 0.15 M and $CaCl_2$ 2 mM, pH 7.5. The mixture was stirred at room temperature for 2 hours. Then, the suspension was decanted and the supernatant containing the unbound C-terminal domain was stored at -20°C. The resin was washed three times with 1 mL of Tris 50 mM, NaCl 0.15 M and $CaCl_2$ 2 mM, pH 7.5 to remove the unbound C-terminal domain still present into the resin. Each wash was carried out at room temperature for 30 minutes and the supernatants were stored at -20°C. The bound C-terminal domain was eluted with five volumes (500 μL each) of Tris 50 mM, NaCl 0.15 M, EGTA 2 mM, pH 7.5. Also in this case, each wash was carried out at room temperature for 30 minutes and the supernatants were stored at -20 °C. Five washes were necessary to bring down the calcium concentration below the affinity constant of CaM for calcium. The supernatants stored at -20 °C were analysed by SDS-PAGE.

6.1.10 SDS-PAGE with silver staining

The binding experiments described in the section above were analyzed by SDS-PAGE. The different samples were applied to a 12% SDS-PAGE and run at 20 mA each at 4 °C using a BIORAD mini Protean 3 cell in Tris 25 mM, Glycine 0.192 M, SDS 0.1%, pH 8.3 followed by silver staining. After the run, as indicated below, the gels were:

- Fixed: 1 hour treatment with fixing solution (absolute ethanol 40% and acetic acid 10 %);
- Sensitized: 30 minutes treatment with sensitizing solution (absolute ethanol 30%, sodium acetate anhydrous 6.8%, sodium thiosulphate 0.2% and glutaraldehyde 0.125%);

- Rinsed three times for 10 minutes with H_2O mQ
- Silver stained: 30 minutes treatment in silver solution (silver nitrate 0.25% and formaldehyde 0.015%);
- Rinsed two times for 1 minute with H_2O mQ
- Developed: treatment with developing solution (sodium carbonate 2.5% and formaldehyde 0.0074%) until the appearance of the bands;
- Stopped: 10 minutes treatment with stopping solution (EDTA 1.5%);
- Rinsed three times for 5 minutes with H_2O mQ
- Preserved: treatment with preserving solution (absolute ethanol 30% and glycerol 4%)

6.2 Results

In order to verify that the CaM coding sequence inside the pET28b was correct, the plasmid was sequenced at BMR Genomics of University of Padova. The result of sequencing was translated (http://www.expasy.ch/tools/dna.html) and the sequence corresponding to CaM was aligned with the human CaM sequences (http://www.ebi.ac.uk/Tools/clustalw/index.html) (**fig. 47**).

```
hCaM            MADQLTEEQIAEFKEAFSLFDKDGDGTITTKELGTVMRSLGQNPTEAELQDMINEVDADG 60
AAH47523.1      MADQLTEEQIAEFKEAFSLFDKDGDGTITTKELGTVMRSLGQNPTEAELQDMINEVDADG 60
NP_005175.2     MADQLTEEQIAEFKEAFSLFDKDGDGTITTKELGTVMRSLGQNPTEAELQDMINEVDADG 60
CAG46818.1      MADQLTEEQIAEFKEAFSLFDKDGDGTITTKELGTVMRSLGQNPTEAELQDMINEVDADG 60
                ************************************************************

hCaM            NGTIDFPEFLTMMARKMKDTDSEEEIREAFRVFDKDGNGYISAAELRHVMTNLGEKLTDE 120
AAH47523.1      NGTIDFPEFLTMMARKMKDTDSEEEIREAFRVFDKDGNGYISAAELRHVMTNLGEKLTDE 120
NP_005175.2     NGTIDFPEFLTMMARKMKDTDSEEEIREAFRVFDKDGNGYISAAELRHVMTNLGEKLTDE 120
CAG46818.1      NGTIDFPEFLTMMARKMKDTDSEEEIREAFRVFDKDGNGYISAAELRHVMTNLGEKLTDE 120
                ************************************************************

hCaM            EVDEMIREADIDGDGQVNYEEFVQMMTAK 149
AAH47523.1      EVDEMIREADIDGDGQVNYEEFVQMMTAK 149
NP_005175.2     EVDEMIREADIDGDGQVNYEEFVQMMTAK 149
CAG46818.1      EVDEMIREADIDGDGQVNYEEFVQMMTAK 149
                ******************************
```

Name	Location
AAH47523.1 (CALM1)	14q24-q31
CAG46818.1 (CALM2)	2p21.3-p21.1
NP_005175.2 (CALM3)	19q13.2-q13.3

Fig. 47. Alignment of sequenced recombinant CaM with the three cellular isoforms of CaM coded by CALM1, CALM2 and CALM3 genes. In inset is also reported the locus of each isoform.

The bacterial growth curves of competent *E. coli* BL21 (DE3) cells transformed with the expression vector pET28b-CaM, are shown in **fig. 48**. The curves in presence of different amounts of IPTG are remarkable similar demonstrating that there is no toxicity by IPTG to the culture at the concentrations used.

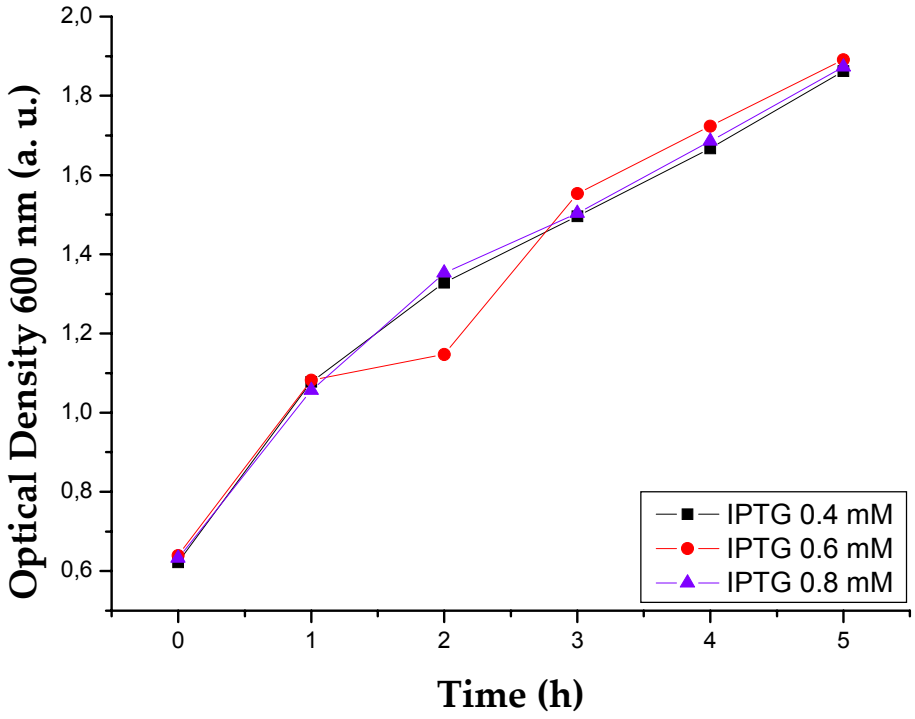

Fig. 48. Growth curves of the *E. coli* BL21 (DE3) strain for the expression of CaM

SDS-PAGE analysis of cellular extracts obtained at various time of growth shows an increase of CaM expression. Levels of CaM as function of time (**fig. 49**, panel A, B, C) and as function of IPTG concentration (**fig. 49**, panel D, E) indicate that the maximum yield of protein is obtained inducing the bacteria with IPTG 0.6 mM for 5 hours.

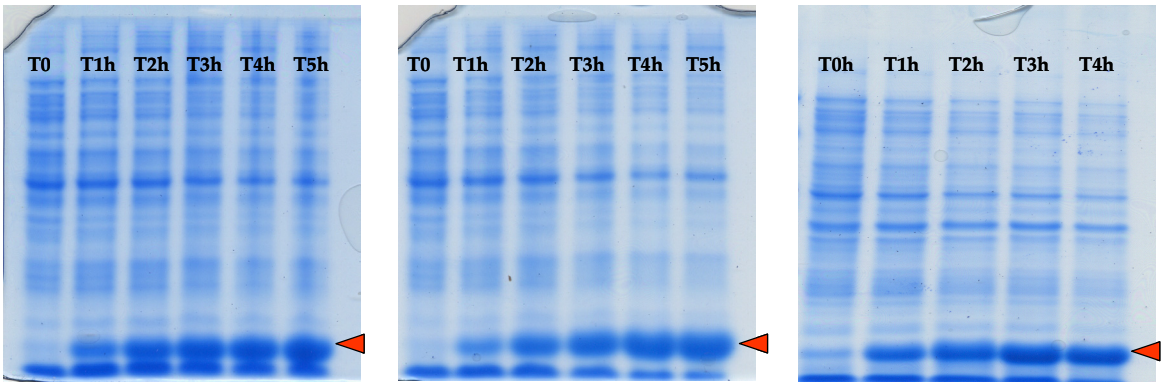

(a) (b) (c)

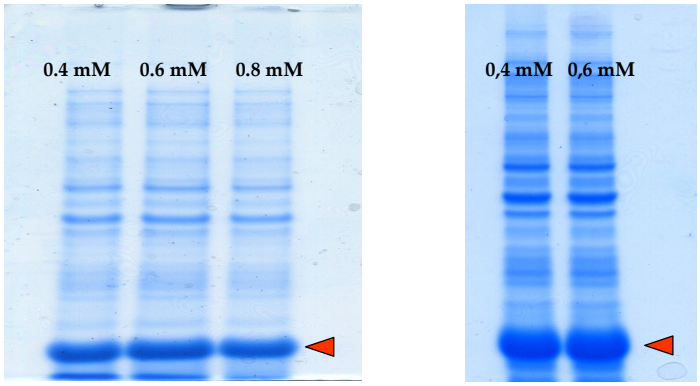

(d) (e)

Fig. 49. Expression tests of the recombinant CaM at different concentrations of IPTG: 0.4 mM (a), 0.6 mM (b) and 0.8 mM (c). T0 is the positive control whereas T1h, T2h, T3h, T4h and T5h correspond to the bacterial lysate collected after 1, 2, 3, 4 and 5 hours. Gels in panel (d) and (e) represent the total proteins after an induction of 4 hours and 5 hours respectively at different IPTG concentrations. Arrow indicates the CaM.

The CaM was purified as indicated in 6.1.3. All hydrophobic proteins were eliminated in the first step because they remain bound to the resin. In the presence of Ca^{2+}, the CaM exposes a hydrophobic region. Therefore, in the second step performed in presence of calcium ion, all polar proteins were eliminated whereas the CaM remains bound to the phenyl groups. EGTA, a specific calcium chelator, was used to elute the bound CaM because it produces apo-CaM that is unable to the bind to hydrophobic resin. The gel (**fig. 50**) refers to different steps of purification procedures.

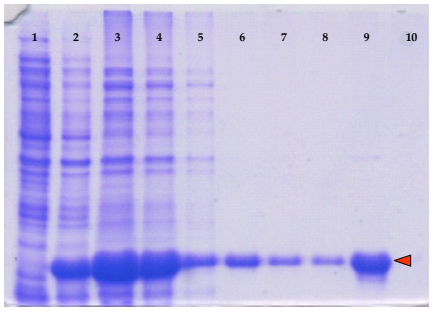

Fig. 50. SDS-PAGE of all samples collected at each purification step: 1- negative control ($OD_{600\ nm}$ ~ 0.6), 2- after 5h of induction with IPTG 0.6 mM, 3- after lysis by French Press and boiling at 100 °C for 3 minutes, 4- supernatant after the first purification step by Phenyl-Sepharose 4B in presence of EDTA, 5, 6, 7- washes with the equilibration buffer (Tris-HCl 50 mM, $CaCl_2$ 1 mM, pH 7.5), 8, 9- elution with EGTA, 10- wash with equilibration buffer.

Lane 1 represents the cellular extract before the induction with IPTG. Lane 2 represents the cellular extract after 5 hours of induction with IPTG 0.6 mM. Lane 3 represents the same extract of lane 2 after French Press and heat stress. Lane 4 refers to the same material of lane 3 after the first purification step in the presence of EDTA. Lanes 5-7 represent the wash-out of the column; the bands still present could be due

to the saturation of the resin. The bound CaM was eluted by single step of EGTA as shown in **fig. 51**. The peak was collected and applied to the same gel in lane 9. No other proteins were eluted from the resin as shown by the chromatogram and lane 10.

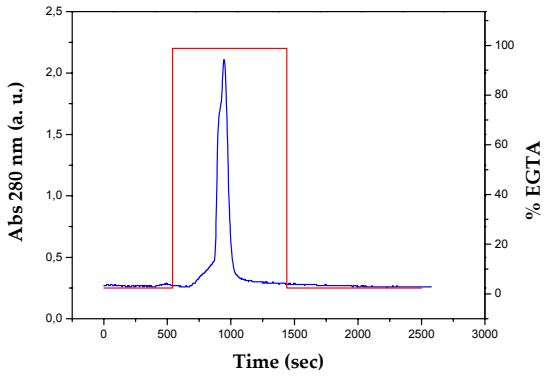

Fig. 51. Chromatogram of elution of the CaM in presence of EGTA (red line).

UV/vis spectroscopy has highlighted the presence of absorption at 260 nm, probably due to contaminant DNA (**fig. 52**).

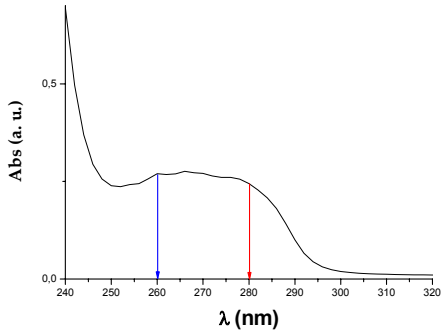

Fig. 52. UV/vis spectrum of the purified CaM.

In order to verify the presence of DNA and to establish whether it was free or bound to the CaM a gel filtration chromatography was performed (**fig. 53**).

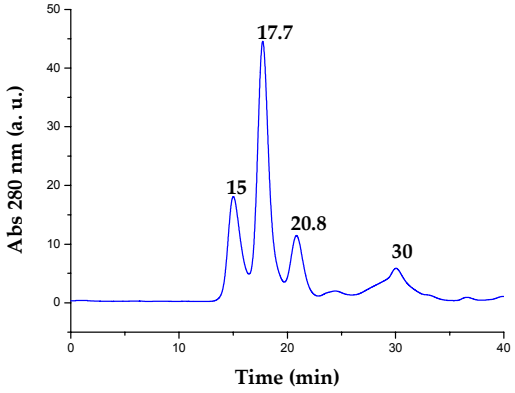

Fig. 53. Chromatogram of the CaM gel filtration; retention times are reported above each peak.

Gel filtration shows four peaks at different retention times: 15 min, 17.7 min, 20.8 min and 30 minutes. Each peak was analyzed by UV/vis spectroscopy as indicated in **fig. 54**.

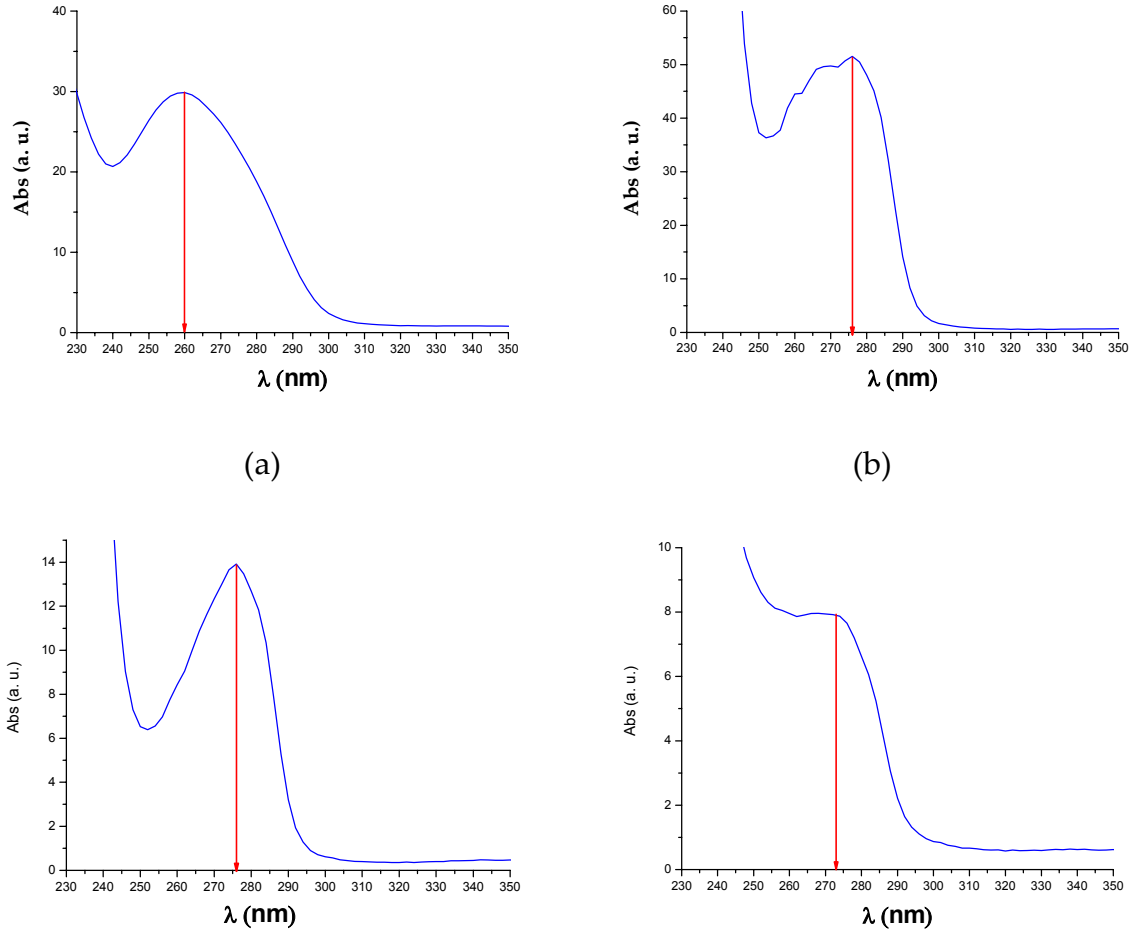

Fig. 54. (a) UV/vis spectrum of the peak with a retention time of 15 minutes, (b) UV/vis spectrum of the peak with a retention time of 17.7 minutes, (c) UV/vis spectrum of the peak with a retention time of 20.8 minutes and (d) UV/vis spectrum of the peak with a retention time of 30 minutes.

The first peak with a retention time of 15 minutes shows an absorption maximum at 260 nm indicating the presence of DNA whereas the other three peaks have spectra with an absorption maximum at 276 nm and typical modulations of phenylalanine. The second peak (17.7 minutes) corresponds to the CaM while other two peaks, with elution times of 20.8 and 30 minutes, represent proteolytic fragments of the CaM as suggested by their higher retention times and SDS-PAGE shown in **fig. 55**.

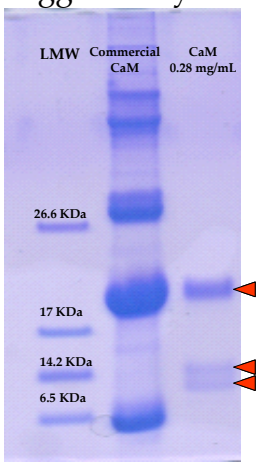

Fig. 55. SDS-PAGE of the CaM after the gel filtration; the two bands around 14 KDa could be due to the degradation and to correspond at the third and fourth peaks in the gel filtration chromatogram.

Anionic exchange chromatography was used to separate the CaM from contaminant DNA (**fig. 56**).

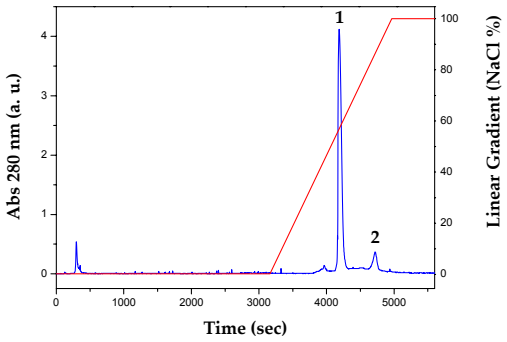

Fig. 56. Chromatogram of anionic exchange of the recombinant CaM; red line represents the linear gradient of NaCl.

The two peaks are eluted with the applied gradient: the first one corresponds to CaM as demonstrated by SDS- PAGE and UV/vis spectrum (**fig. 57**) while the second corresponds to contaminant DNA because there is not band in SDS-PAGE. Typical modulations of phenylalanine are visible because the primary sequence of the CaM presents 8 residues of this amino acid, 2 residues of tyrosine and devoid of tryptophan.

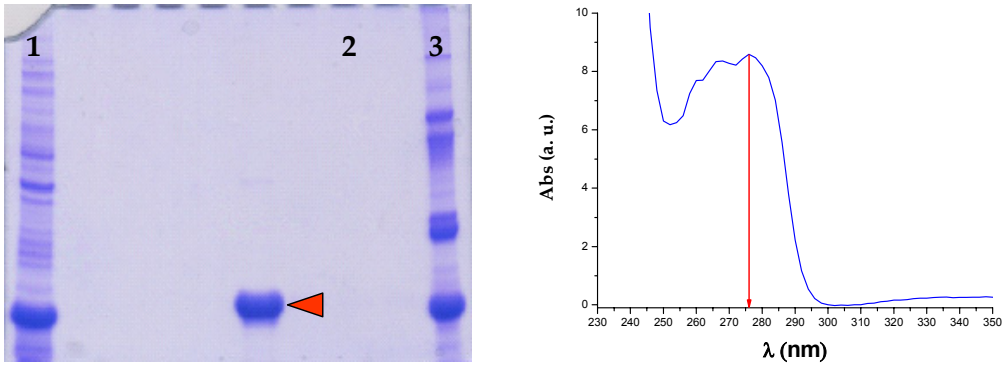

(a) (b)

Fig. 57. (a) SDS-PAGE performed after the anionic exchange: 1- positive control (after 5h of induction), red arrow- purified CaM corresponding to the gel filtration peak, 2- second peak obtained in anionic exchange chromatography and 3- commercial CaM. (b) UV/vis spectrum of the gel filtration peak.

In order to analyse the monodispersity of the purified CaM a gel filtration chromatography was performed (**fig. 58**).

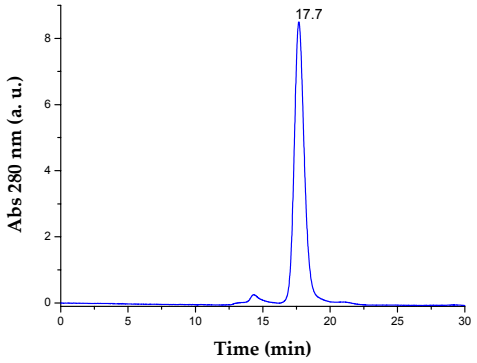

Fig. 58. Gel filtration chromatogram of the purified CaM.

Purified CaM was present in monodisperse form as indicated by the presence of only one peak in gel filtration chromatography. Retention time of CaM (17.7 minutes) was compared with the retention time of the commercial CaM as shown in **fig. 59**. The chromatogram of commercial CaM presents two peaks probably due to the presence of proteins with a higher molecular weight than CaM as shown in **fig. 55**.

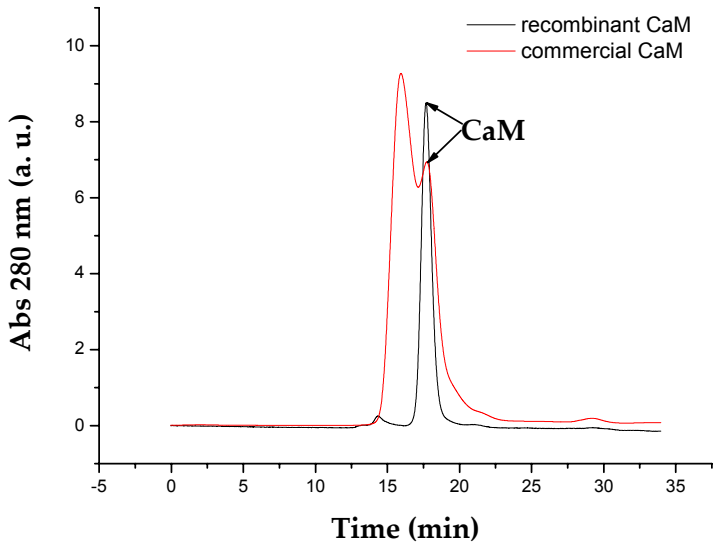

Fig. 59. Comparison between the gel filtration chromatograms of the recombinant CaM and commercial CaM.

In order to confirm that the purified protein corresponds to the CaM a reverse phase chromatography (**fig. 60**) followed by electrospray mass spectrometry analysis were performed (**fig. 61**).

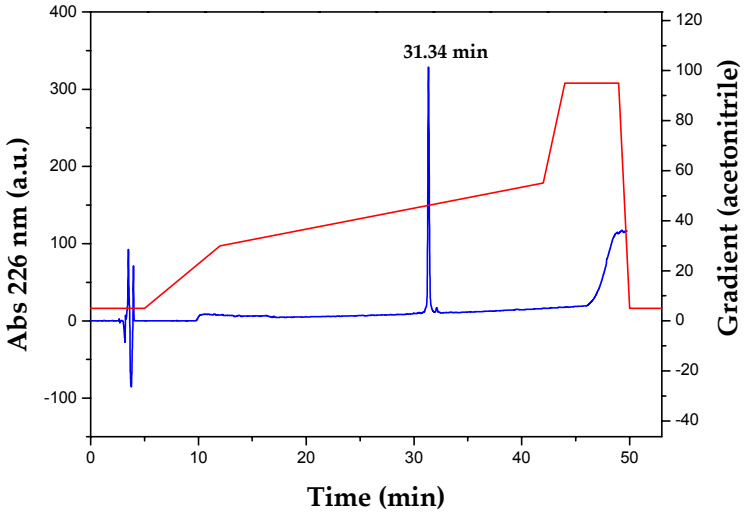

Fig. 60. Reverse phase chromatogram of purified CaM; red line represents the gradient of acetonitrile used for the chromatography.

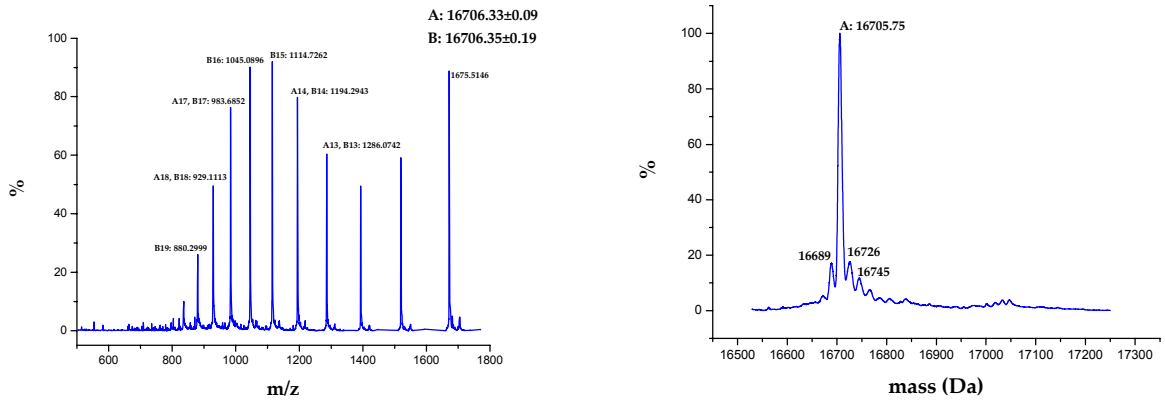

(a) (b)

Fig. 61. (a) Multi-charge ESI spectrum of the purified CaM. (b) Single-charge ESI spectrum of the purified CaM (deconvoluted spectrum).

The recombinant CaM has a molecular weight of 16706.34 Da that differs from the calculated molecular weight (16837.5 Da) of 132 Da probably due to the lack of the initial residue of methionine.

CaM extinction coefficient was determined by bicinchoninic acid assay. Standard curve is reported in **fig. 62** together with the equation of the linear regression whereas the values of absorption of the CaM are reported in **tab. 8**. Lambert-Beer law was used to calculate the extinction coefficient at 276 nm (ε): 3089 M^{-1} cm^{-1}. Experimental ε is quite different from the calculated ε 2748 M^{-1} cm^{-1}. Theoretical ε was calculated using an absorption values at 276 nm of 1362 M^{-1} cm^{-1} and 3 M^{-1} cm^{-1} for tyrosine and phenylalanine respectively.

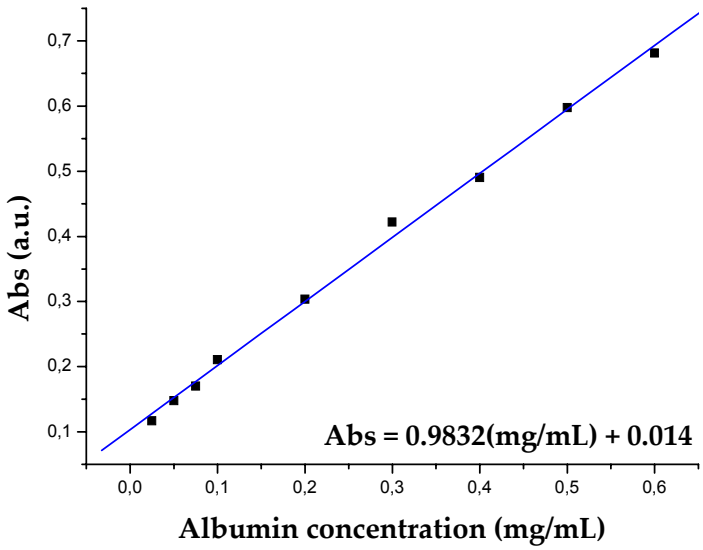

Fig. 62. Standard curve necessary to determine the CaM concentration by bicinchoninic acid assay; in graphic is also reported the equation of the linear regression.

Abs CaM	Abs CaM	Average Abs	Relative Abs	ε M^{-1} cm^{-1}
0.6858	0.7041	0.6950	0.6056	3089

Tab .8. Values of absorption of CaM after the reaction with BCA reagent.

As a test for activity of recombinant protein, the conformational changes upon addition of Ca^{2+} ions have been studied. To this aim, circular dichroism and native PAGE experiments were performed. CD spectrum of calcium free CaM shows a mixture of α-helix, ß-sheet and random coil because the molar ellipticity at 208 nm and 222 nm are different. In particular, the molar ellipticity at 208 nm is larger than that at 222 nm with a ratio of 1.1. In the presence of 6.3 μM and 1 mM of free calcium, the CD spectra of CaM are characterized by an increase of the α-helix contribution and the ratio between the molar ellipticity at 208 nm and 222 nm is equal to 1. In the presence of an excess of free calcium (1 mM), the values of molar ellipticity at 208 nm and 222 nm are reduced of 8% compared to the values obtained in presence of 6.3 μM of free calcium. In addition, the molar ellipticity at 198 nm of calcium free CaM is smaller than calcium-CaM complex (**fig. 63**).

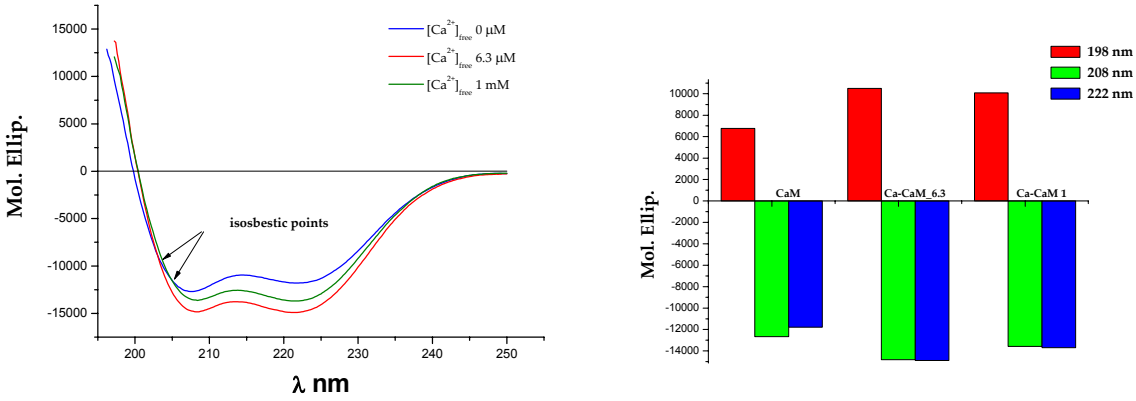

(a) (b)

Fig. 63. (a) Circular dichroism spectra of CaM in absence and in presence of calcium. (b) Molar ellipticity of apo and holo-CaM at 198 nm, 208 nm and 222 nm.

CD spectra in absence or in presence of calcium ion are different as also indicated by isosbestic points at 203 nm and 204 nm. The percentages of α-helix, ß-sheet and random coil were calculated using CDNN, k2d and the Greenfield-Fasman's formula. The results were compared with the values of percentages obtained by X-ray crystallographic structures of CaM (1cll.pdb and 1cfd.pdb) available in PDBsum database (http://www.ebi.ac.uk/pdbsum/) (**tab. 9**).

	CaM				Ca (6.3 μM)-CaM				Ca (1 mM)-CaM			
	CDNN	k2d	Greenfield eq.	PDBsum	CDNN	k2d	Greenfield eq.	PDBsum	CDNN	k2d	Greenfield eq.	PDBsum
α-helix (%)	36.7	31	57.4	56.1	46.5	53	64.8	64.6	42.3	39	60.6	64.6
ß-sheet (%)	31.5	15	-	6.8	26.4	10	-	2.8	28.4	16	-	2.8
Random coil (%)	30.1	54	-	37.2	24.6	37	-	32.6	26.9	44	-	32.6
Total (%)	98.4	100	-	100.1	97.5	100	-	100	97.6	99	-	100

Tab. 9. Prediction of secondary structure elements calculated by CDNN, k2d and Greenfield's formula.

Recombinant CaM increases its percentage of α-helix after the addition of calcium ions as also demonstrated by crystallographic structures (**fig. 64**). However, in presence of an excess of free calcium ions (1 mM) this rise is smaller than the rise in presence of 6.3 μM of a free calcium concentration.

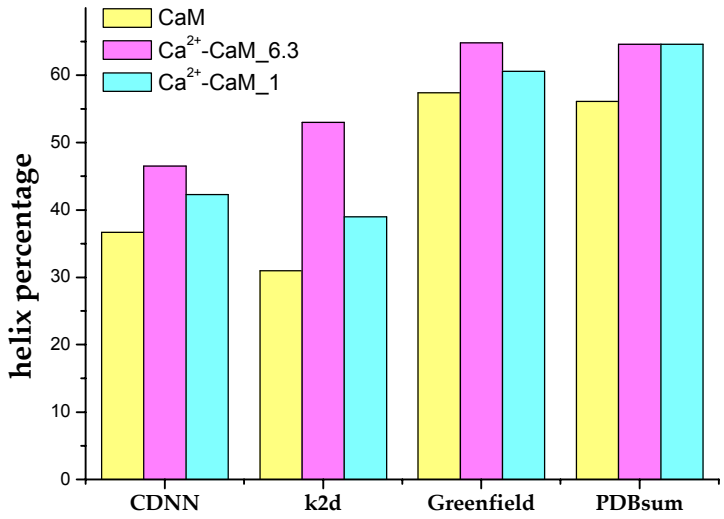

Fig. 64. Trend of helix percentage in presence of calcium, calculated using neural networks (CDNN and k2d), the Greenfield's formula and by PDB files.

Native PAGEs of CaM have shown a different electrophoretic mobility in presence and in absence of calcium ions (**fig. 65**).

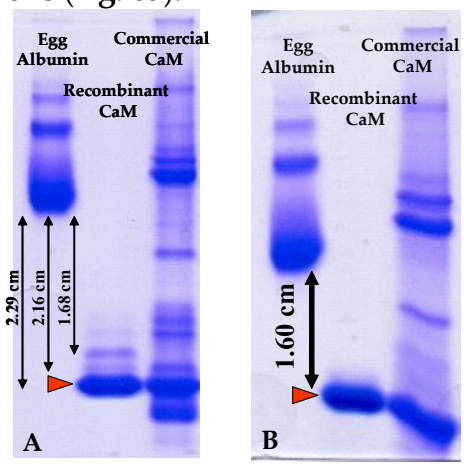

(a) (b)

Fig. 65. (a) Native PAGE of CaM in presence of EGTA 5 mM; the first lane corresponds to the positive control (egg albumin), the second lane is the purified CaM and the third lane is the commercial CaM. (b) Native PAGE in presence of $CaCl_2$ 2 mM; the composition of each lane is the same of the (a).

Apo-CaM has a higher mobility than the holo-CaM and this effect could be due to a different rearrangement of tertiary structure. Indeed, SAXS studies [**68**] have highlighted that apo-CaM has a gyration radius of 20.6 Å whereas, the holo-CaM has a gyration radius of 21.5 Å and maximum vector lengths of 58 Å and 62 Å respectively. In EGTA native PAGE there are additional bands that could represent different molar ratios between calcium and CaM.

Recombinant CaM was used to perform binding experiments with the human C-terminal domain of PMCA1b in presence of SDS. In order to study the effects on CaM CD spectra in presence of calcium ions and SDS were recorded. Ca^{2+}-CaM without SDS was used as control. The secondary structure of the protein in the latter conditions is characterized by α-helix because the values of molar ellipticity at 208 nm and 222 nm are equal. In the presence of SDS below the CMC (0.1%) there is a shift of the peak from 208 nm to 207.2 nm and a decrease of the molar ellipticity at 222 nm (**fig. 66**).

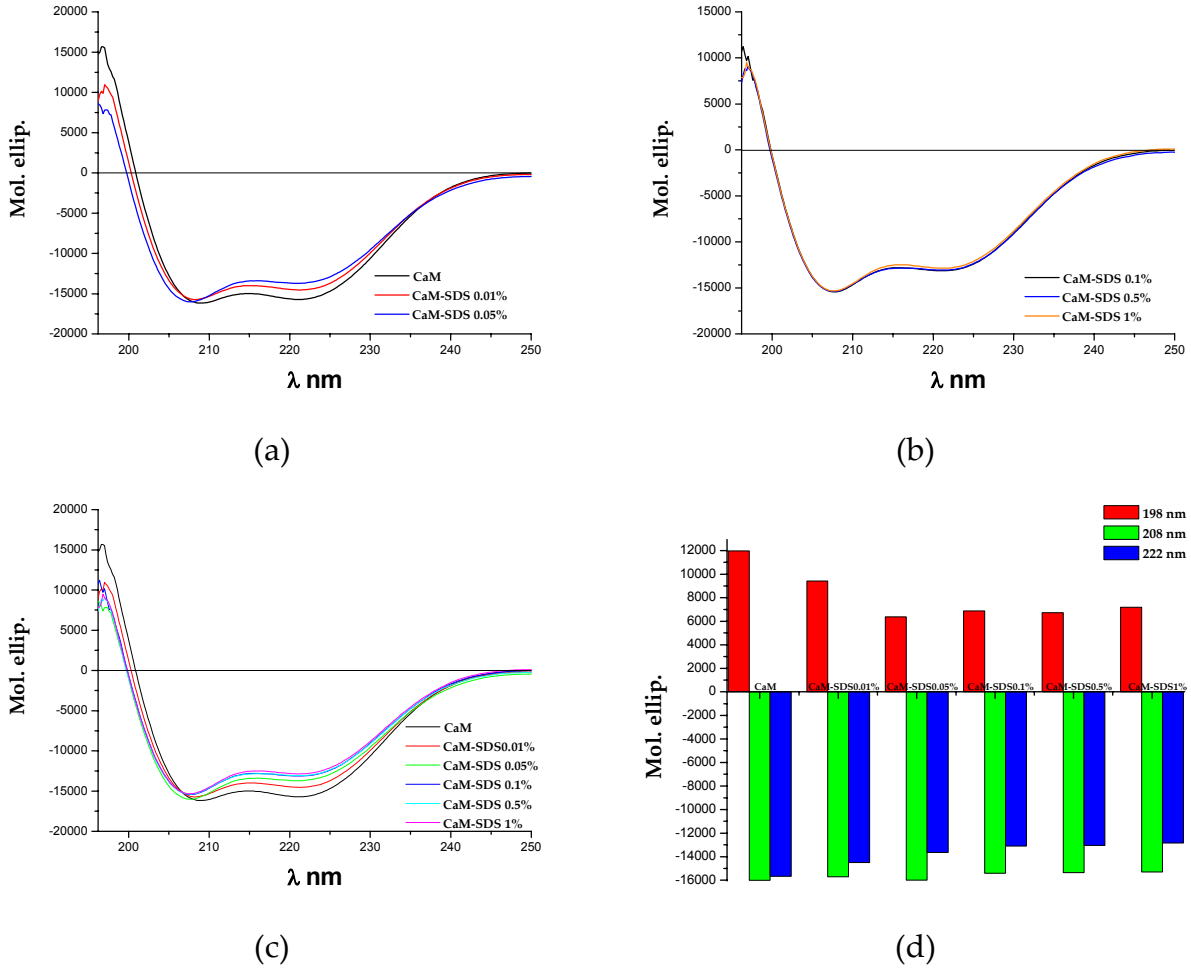

Fig. 66. (a) CD spectra of purified CaM below the CMC. (b) CD spectra of purified CaM above the CMC. (c) Overall CD spectra. (d) Molar ellipticity of CaM at 198 nm, 208 nm and 222 nm in presence of increasing concentration of SDS.

The molar ellipticity at 198 nm is also reduced. All these data highlight the mild loss of α-helix contribution and the increase of random coil as also indicated by the ratio between molar ellipticity at 208 nm and 222 nm (**tab. 10**). Above the CMC, there are not changes in the CD spectra of CaM (**fig. 66**). The percentages of α-helix, ß-sheet and random coil were always calculated using the neural networks CDNN, k2d and the Greenfield's formula. The results are reported in **tab. 11**.

	CaM	CaM-SDS 0.01%	CaM-SDS 0.05%	CaM-SDS 0.1%	CaM-SDS 0.5%	CaM-SDS 1%
Ratio 208nm/222nm	1.02	1.08	1.17	1.18	1.18	1.19

Tab. 10. Ratio between molar ellipticity at 208 nm and 222 nm

	CaM			**CaM-SDS 0.01%**			**CaM-SDS 0.05%**		
	CDNN	k2d	Greenfield eq.	CDNN	k2d	Greenfield eq.	CDNN	k2d	Greenfield eq.
α-helix (%)	51.0	60	68.9	47.3	59	67.9	47.3	57	68.9
ß-sheet (%)	24.4	7	-	26.0	7	-	26.0	8	-
Random coil (%)	22.4	33	-	24.0	34	-	24.0	35	-
Total (%)	97.8	100	-	97.3	100	-	97.3	100	-
	CaM-SDS 0.1%			**CaM-SDS 0.5%**			**CaM-SDS 1%**		
	CDNN	k2d	Greenfield eq.	CDNN	k2d	Greenfield eq.	CDNN	k2d	Greenfield eq.
α-helix (%)	43.5	56	66.9	43.4	54	66.7	42.8	49	66.5
ß-sheet (%)	27.9	9	-	28.0	11	-	28.3	13	-
Random coil (%)	25.9	34	-	25.9	35	-	26.2	38	-
Total (%)	97.3	99	-	97.3	100	-	97.3	100	-

Tab. 11. Prediction of secondary structure elements calculated by CDNN, k2d and Greenfield's formula.

In order to study whether the C-terminal domain of the human PMCA1b in presence of SDS, necessary to maintain this domain in monomeric form, is still able to interact with the CaM binding experiments were performed. The results are shown in **fig. 67**.

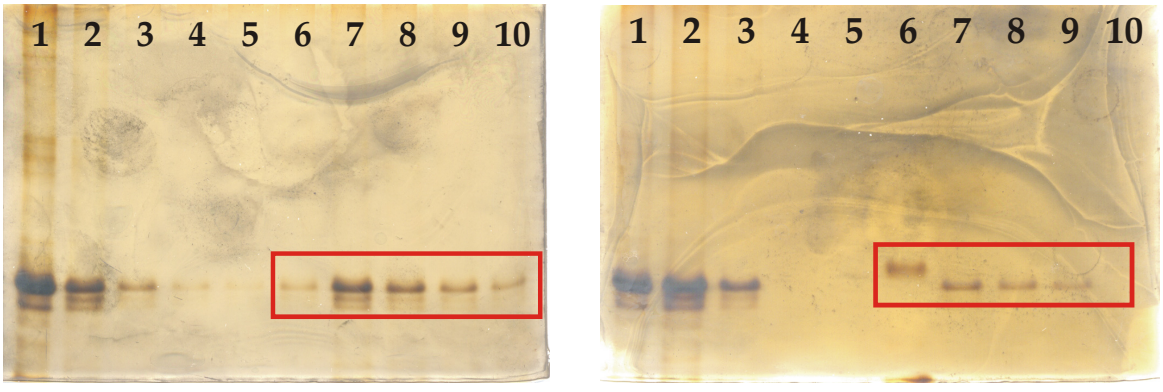

(a) (b)

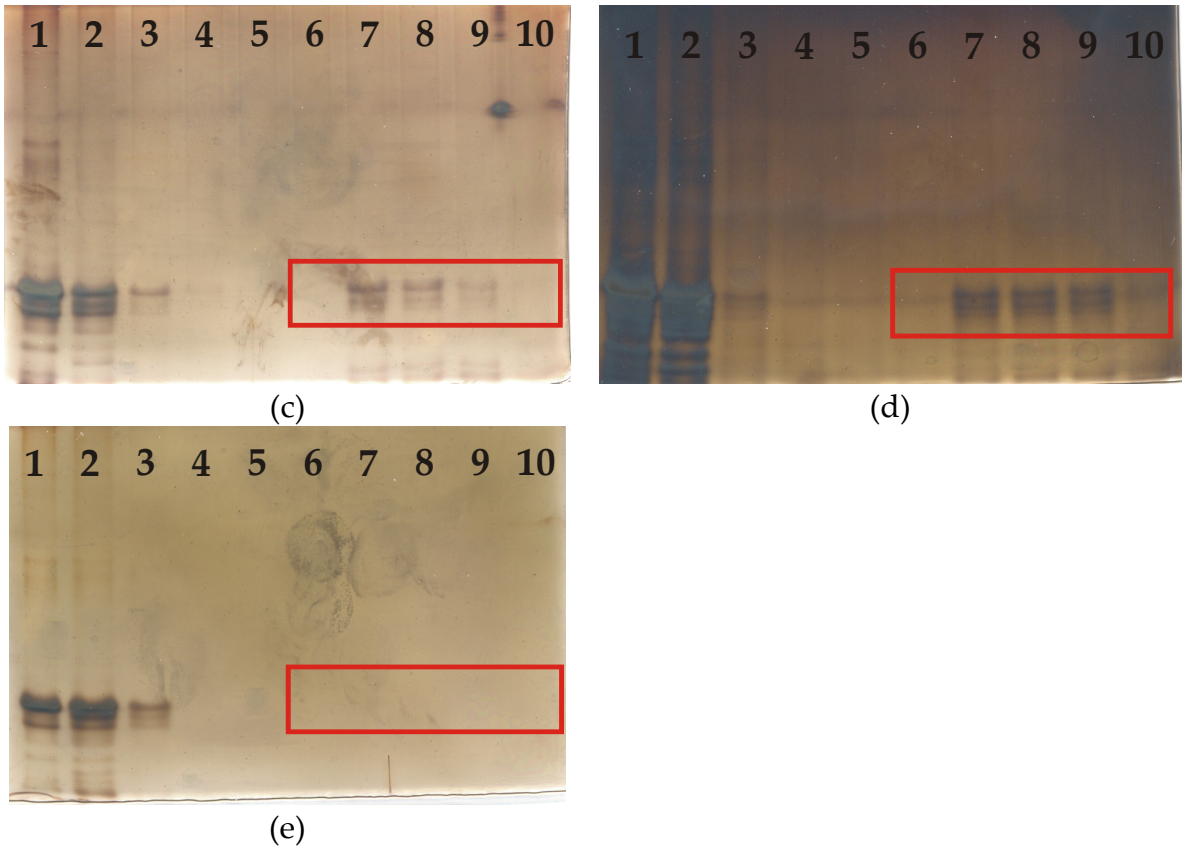

Fig. 67. (a) SDS-PAGE of the binding experiment between C-terminal domain and CaM (positive control). (b) SDS-PAGE of the binding experiment between C-terminal domain and CaM in presence of SDS 0.01%. (c) SDS-PAGE of the binding experiment between C-terminal domain and CaM in presence of SDS 0.02%. (d) SDS-PAGE of the binding experiment between C-terminal domain and CaM in presence of SDS 0.03%. (e) SDS-PAGE of the binding experiment between C-terminal domain and CaM in presence of SDS 0.04%. The loading order is the same in all gels: 1- 20 μL of the purified C-terminal domain (0.33 mg/mL), 2- 20 μL of the supernatant collected after the binding, 3- 20 μL of the first wash, 4- 20 μL of the second wash, 5- 20 μL of the third wash, 6- 20 μL of the first step of elution of the bound C-terminal, 7- 20 μL of the second step of elution of the bound C-terminal, 8- 20 μL of the third step of elution of the bound C-terminal, 9- 20 μL of the fourth step of elution of the bound C-terminal, 10- 20 μL of the fifth step of elution of the bound C-terminal.

In **fig. 67** only the most significant gels of the binding experiments are reported. CaM is able to interact with the C-terminal domain only in presence of low SDS concentration (0.03%). In the presence of SDS 0.04% there is not binding between the C-terminal domain and CaM as highlighted by lack of bands in the 6^{th} – 10^{th} lanes. In fact, the lowest concentration of SDS necessary to maintain the C-terminal domain in monomeric form corresponds to the CMC (0.1%).

7 Discussion and Conclusions

PMCAs are P-type pumps employed to keep low cytosolic calcium concentration (50-100 nM). They constitute a high affinity, low capacity system for the calcium homeostasis. PMCAs can be activated by several mechanisms such as the interaction with Ca^{2+}-CaM, the interactions with acidic phospholipids and fatty acids, the phosphorylation by kinases A and C, the proteolysis by calpain and the oligomerization. Each activation mechanism involves the cytosolic C-terminal domain also called regulatory domain. This domain represents the main characteristic that distinguishes the PMCAs from all other P-type pumps. In this domain there is also the splicing site C and the consensus sequence for the interaction with PDZ domain containing proteins such as members of the MAGUKs family.

Which is the role of the alternative splicing in the structure and activity of the C-terminal domain? Is the oligomerization a reversible process?

To date, there are not answers to these questions. In order to study the structure of the C-terminal domain and the reversibility of the oligomerization process, the C-terminal domain of the human PMCA1b has been cloned in the expression vector pET21b. Once expressed, using IPTG concentration of 0.4 mM at 30 °C for 4 hours, and purified by calmodulin affinity chromatography, the C-terminal domain has been characterized by ESI mass spectrometry and N-terminal sequencing. The recombinant C-terminal domain has a molecular weight of 18.134 kDa even if there is a small fraction that has a molecular weight of 18.176 kDa probably due to an acetylated form. This molecular weight differs from that calculated of 132 Da because of the lack of the initial methionine as also demonstrated by N-terminal sequence: TIPT. However, threonine is the first amino acid downstream of the last transmembrane segment. C-terminal domain contains two calcium binding sites with affinity constants of 30 nM and 300 nM respectively. This domain does not present an EGTA resistant calcium binding site as demonstrated by atomic absorption measurements of the protein dialysed against an EGTA containing solution. The calculated ratio Ca^{2+}/protein was 0.00058. In order to study the secondary structure of the C-terminal domain in absence or in presence of free calcium CD experiments were performed. Apo-C-terminal domain and holo-C-terminal domain show the same secondary structure that is composed by about 20% α-helix around, 42% random coil and 38% ß-sheet. The recombinant C-terminal domain has a strong tendency to aggregate. This observation is in agreement with the known mechanism of pump activation through oligomerization of the whole protein in its physiological membrane environment by interaction of the C-terminal domains of two molecules. The *in vitro* studies by negative staining electron microscopy show the formation of filaments longer than 100 nm and a cross section radius of around 8.75 nm. This

aggregation severely hampers the structural studies in solution. Therefore, several conditions have been used to study the reversibility of the oligomerization process and to stabilize the monomeric form such as ionic strength (NaCl), kosmotropic ions (SCN^-) and competitor agents (imidazole and tryptophan) but no solubilizing effect on oligomers was obtained as shown by SAXS and EM experiments. The aggregated states observable with the SAXS technique have not permitted subsequent tertiary structure determination of the domain in solution. These information indicate that the interactions between monomers to form oligomers are due to hydrophobic interfaces and that the tryptophan, involved in the stabilization of the interaction with Ca^{2+}-CaM is not essential for the oligomerization process. Ionic detergent such as sodium dodecyl sulphate (SDS), that is a good phospholipid mimetic system, is able to dissociate the oligomers and to stabilize the monomeric form of the C-terminal domain as shown by EM and native-PAGE. No effect was obtained using non ionic detergent such as NP40 and TRITON X-100 as shown by native-PAGE. The minimal SDS concentration necessary to maintain the C-terminal domain in monomeric form was 0.1% that corresponds to the critical micellar concentration (CMC). Since SDS is known to induce protein denaturation, it was necessary to compare the secondary structure in the presence and absence of this agent. In presence of SDS concentration below the CMC the shape of the CD spectra is similar to that the C-terminal domain without SDS (control) while in presence of SDS at the CMC or above the CMC there is a loss in ß-contribution and an small increase of the random coil.

The presence of a mixed phase including water and micelles of detergent prevent the applicability of Small Angle X-Ray Scattering methods to obtain a low resolution structural reconstruction of the molecule. The X-Ray are scattered by the electrons from all electron-dense molecules in solution making it impossible to discern between empty SDS micelles and protein-bound SDS micelles as well as protein molecules eventually unbound [**65**]. A convenient approach in the case of heterogeneous phases is the Small Angle Neutron Scattering. This method is based on a neutron beam, rather than on X-Ray radiation. Neutrons are scattered by the nuclei and a marked difference exist between the scattering length of ^1H ($-0.3742 \cdot 10^{-12}$ cm) and ^2H ($0.6671 \cdot 10^{-12}$ cm) [**63**]. It is therefore possible, by applying a contrast variation approach, to match the scattering density of SDS with that of the solvent. The scattering density of the protein can be conveniently maximized by ^2H labeling. Under these conditions, SANS experiments will report the scattering of only the protein molecules since it differs from that of all other species (solvent and SDS micelles) under the beam [**63**]. Thus, in order to determine the tertiary structure in presence of SDS, Small Angle Neutron Scattering (SANS) experiments were performed. These experiments were performed at the matching point conditions (D_2O/D_2O+H_2O = 40.8% and SDSd25/SDSd25+SDSh25 = 35.7%) to mask the buffer and SDS contributions and subtract them (background) from ^2H protein scattering. The ^2H C-terminal domain was expressed in the same conditions described above for the ^1H C-terminal domain, purified by calmodulin affinity chromatography and analyzed by ESI mass spectrometry (18962 Da) to determine the percentage of

deuteration (86.5%) necessary for the calculation of the contrast of SANS experiments.
The data analysis was carried out using GNOM and DAMMIN programs to determine the gyration radius (Rg) and to perform *ab initio* modeling respectively. Both gyration radii of the C-terminal domain in the presence of SDS concentration below and around the CMC were calculated using a rod-like model because these solutions were most reliable than those relative to a spherical model. The Rg of the C-terminal domain in presence of SDS concentration below the CMC is 54.52 ± 3.056 Å larger than the Rg of the C-terminal domain in presence of SDS concentration around the CMC that is 26.68 ± 3 Å. The *ab initio* modeling shows that the monomeric C-terminal domain (SDS 0.1%) presents a hourglass form (average of 30 runs) with the central cross section compatible with that of an α-helix. This part could correspond at the α-helix of the C28W calmodulin binding region while the downstream and upstream regions could be random coil as also predicted by PSIpred. The high mobility of these unstructured parts could determine the hourglass model. These results are in agreement with previous work showing that the consensus sequences for the physiological interactors such as kinases A and C, PDZ domains and calpain are typically present in random coil regions [**60**]. Furthermore, the regions upstream and downstream of the calmodulin binding region are rich in negatively charged amino acids that could produce electrostatic repulsions with the negative heads of acidic phospholipids of the plasma membrane.

The C-terminal domain is still able to interact with calmodulin in the presence of SDS?

To study the interaction between the C-terminal domain and the CaM in the presence of SDS, binding experiments were performed. CaM used in these experiments was expressed using IPTG 0.6 mM at 30°C for 5 hours, purified by hydrophobic interaction chromatography and anionic exchange and characterized by ESI mass spectrometry and circular dichroism. Mass spectra shows, also in this case, the lack of the initial methionine (16706.34 Da *vs* 16837.5 Da) while the CD spectra highlight that the recombinant CaM is folded and active because in presence of free calcium it become prevalently folded in α-helix as demonstrated by X-ray crystallographic structures. This procedure allows to obtain the protein with high yield and with much higher purity as compared with commercial preparations. Furthermore, the optimization of the expression and purification protocol will permit future studies using recombinant site-directed mutated protein forms.
The capacity of the recombinant wild-type CaM to bind calcium ions was also tested in native PAGEs in presence of EDTA or free calcium. This experiment is based on the different electrophoretic mobility exhibited by apo-CaM and holo-CaM [**66**]; in absence of free calcium the electrophoretic mobility was larger than that in the presence of free calcium. This difference is due to structural rearrangements that bring the apo-CaM to be more compact than the holo-CaM as demonstrated by crystallographic structures and also by SAXS data [**68**].

In order to study the effect of SDS on Ca^{2+}-saturated CaM (Ca^{2+}-CaM), CD experiments were performed. Upon increasing the SDS concentration, there is a small decrease of the molar ellipticity at 222 nm and at 198 nm associated with a mild shift of the peak at 208 nm toward smaller wavelengths. However, the secondary structure of Ca^{2+}-CaM in the presence of SDS appears to be preserved.
Binding experiments between the C-terminal domain and the Ca^{2+}-CaM in the presence of increasing concentrations of SDS were performed. These experiments show that the C-terminal domain binds the Ca^{2+}-CaM up to a SDS concentration of 0.03%. At this SDS concentration only a small fraction of the C-terminal domain is in monomeric form. In the presence of the minimal SDS concentration necessary to stabilize the C-terminal domain in the monomeric form, SDS 0.1%, there is not binding with Ca^{2+}-CaM. This could be due to a competition phenomenon between Ca^{2+}-CaM and SDS for the same binding region, for a local alteration of the tertiary structure in presence of SDS that prevents the binding or because of an electrostatic repulsion between the SDS-C-terminal domain and SDS-Ca^{2+}-CaM complexes.
From these data it is possible to conclude that the oligomerization is a reversible process. Physiological interactors such as acidic phospholipids or fatty acids, that have similar properties of SDS, can be involved in the maintenance of the C-terminal domain in monomeric form. However, this regulation pathway seems to exclude possible interactions with Ca^{2+}-CaM. Oligomers have a high affinity constant for calcium ions (Km around 52 nM) that is comparable with the cytosolic calcium concentration in the resting cell (50-100 nM). Therefore, oligomers could be present in all cellular types and active also in the resting cells to control all small variations of calcium concentration. Oligomers could be localized in membrane rafts rich of uncharged or zwitterionic phospholipids such as phosphatidylcholine whereas monomers could be localized in membrane rafts rich in acidic phospholipids. Moreover, Tang et al. [**69**] have demonstrated that the PMCA activity is higher when the pump is reconstituted with ordered lipids such as lens fiber lipid than when it is reconstituted with disordered lipids. These data could be explained considering that the movements of the phospholipids in fluid membranes prevent the formation of the oligomers.
Another interesting working hypothesis could be put forward based on the *in vivo* reversibility of the oligomerization process by acidic phospholipids or fatty acids. In the resting cells, PMCAs can stay in two different forms: in autoinhibited monomeric form and in an activated oligomeric form. After a stimulus, the cytosolic calcium concentration increases and small amphipathic molecules such as diacylglycerol (DAG), known to activate other enzymes such as protein Kinase C, produced by the signaling transduction could interact with oligomers and dissociate them. As a result, a decrease of the Km for calcium around 0.25 μM will occur, thus allowing the onset of the calcium wave (**fig. 68**).

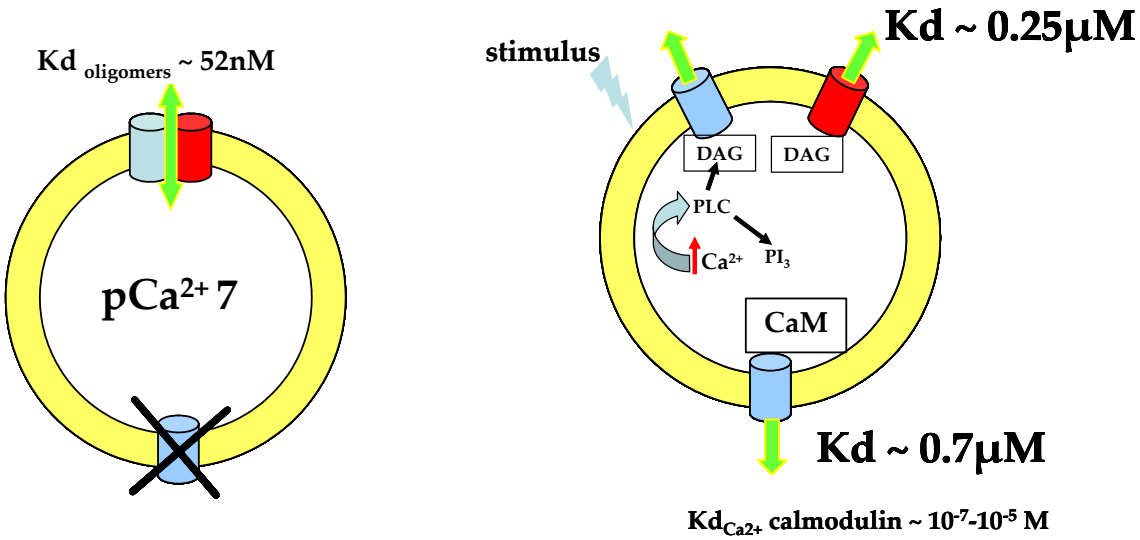

(a) (b)

Fig. 68. (a), schematic resting cell with the autoinhibited monomeric PMCA form and activated oligomeric PMCA form. The KdCa2+ value of the oligomers is similar to the cytosolic calcium concentration in resting cells; (b), schematic cell after a stimulus: the autoinhibited monomeric PMCA form is activated by CaM while the activated oligomeric PMCA form is dissociated in two monomers by DAG decreasing the affinity for calcium to a value around 0.25 µM.

These results open many other questions concerning the spatial and temporal events following a stimulus that carry at the development of the calcium wave following a specific cellular response. It will be very interesting to analyze in detail, step by step, the kinetics of activation of all calcium depending enzymes involved in the signaling transduction and of the PMCAs.

8 References

1. Gomperts, B. D., Kramer, I. M., Tatham, P. E. R. (2003) Signal transduction. Elsevier Academic Press, 1st edn

2. Williams, R. J. P. (1976). Calcium in Biological Systems. Cambridge Univ. Press

3. Levine, B.A., Williams, R. J. P. (1982). Role of Calcium in Biological Systems. L. J. Anghileri and A. M. T. Anghileri, eds., CRC Press

4. Campbell, A. K. (1983). Intracellular calcium: Its Universal Role as Regulator. Wiley

5. Bertini, I., Gray, H. B., Lippard, S. J., Valentine, J. S. (1994). Bioinorganic Chemistry, University Science Books

6. Nelson, M. R., Chazin, W. J. (1998). Structures of EF-hand Ca^{2+}-binding proteins: Diversity in the organization, packing and response to Ca^{2+} Binding. *BioMetals* **11**, 297-318

7. Lewit-Bentley, A., Rety, S. (2000). EF-hand calcium-binding proteins. *Current Opinion in Structural Biology* **10**, 637-643

8. Bhattacharya, S., Bunick, C.G., Chazin, W. J. (2004). Target selectivity in EF-hand calcium binding proteins. *Biochimica et Biophysica Acta* **1742**, 69-79

9. Carafoli, E., Klee, C. (1999) Calcium as a Cellular Regulator, Oxford University Press, New York

10. Van Eldik, L., Watterson, D. M. (1998) Calmodulin and Signal Transduction, Academic Press

11. Palmgren, M. G., Axelsen, K. B. (1998). Evolution of P-type ATPases. *Biochimica et Biophysica Acta* **1365**, 37-45

12. Taglietti, V., Casella, C. Elementi di Fisiologia e Biofisica della Cellula, La Gogliardica Pavese s. r. l

13. Strehler, E. E., Zacharias, D. A. (2001). Role of Alternative Splicing in Generating Isoform Diversity Among Plasma Membrane Calcium Pumps. *Physiological Reviews* **81**, 21-50

14. Brandt, P., Ibrahim, E., Bruns, G. A. P., Neve, R. L. (1992). Determination of the nucleotide sequence and chromosomal localization of the ATP2B2 gene encoding human Ca^{2+}-pumping ATPase isoform PMCA2. *Genomics* **14**, 484-487

15. Olson, S., Wang, M. G., Carafoli, E., Strehler, E. E., McBride, O. W. (1991). Localization of two genes encoding plasma membrane Ca^{2+}-transporting ATPases to human chromosomes 1q25-32 and 12q21-23. *Genomics* **9**, 629-641

16. Wang, M. G., Yi, H., Hilfiker, H., Carafoli, E., Strehler, E. E., McBride, O. W. (1994). Localization of two genes encoding plasma membrane Ca^{2+}-ATPases isoform 2 (ATP2B2) and 3 (ATP2B3) to human chromosomes 3p26→p25 and Xq28, respectively. *Cytogenet Cell Genet* **67**, 41-45

17. Zvaritch, E., James, P., Vorherr, T., Falchetto, R., Modyanov, N., Carafoli, E. (1990). Mapping of functional domains in the plasma membrane Ca^{2+} pump using trypsin proteolysis *Biochemistry* **29**, 8070-8076

18. Carafoli, E. (1994). Biogenesis: Plasma Membrane calcium ATPase: 15 years of work on the purified enzyme. *FASEB J.* **8**, 993-1002

19. Carafoli, E., Coletto, L., Brini, M. (2004). Plasma Membrane Calcium Pumps. *Handbook of ATPases*, 211-232

20. Adamo, H. P., Penniston, J. T. (1992). New Ca2+ pump isoforms generated by alternative splicing of rPMCA2 mRNA. *Biochem J.* **283**, 355-359

21. Szemraj, J., Kawecka, I., Bartkowiak, J., Zylinska, L. (2004). The effect of antisense oligonucleotide treatment of plasma membrane Ca^{2+}-ATPase in PC12 cells. *Cellular and Molecular Biology Letters* **9**, 451-464

22. Sasamura, S., Furukawa, K. I., Stiratori, M., Motomura, S., Ohizumi, Y. (2002). Antisense- Inhibition of Plasma Membrane Ca^{2+} Pump Induces Apoptosis in Vascular Smooth Muscle Cells. *Jpn. J. Pharmacol*. **90**, 164-172

23. Lee, W. J., Robinson, J. A., Holman, N. A., McCall, M. N., Roberts-Thomson, S. J., Monteith, G. R. (2005). Antisense-mediated Inhibition of the Plasma Membrane Calcium-ATPase Suppresses Proliferation of MCF-7 Cells. *The Journal of Biological Chemistry* **280** (29), 27076-27084

24. Zacharias, D. A., Dalrymple, S. J., Strehler, E. E. (1995). Transcript distribution of plasma membrane Ca^{2+} pump isoforms and splice variants in the human brain. *Molecular Brain Research* **28**, 263-272

25. Guerini, D. (1998). The significance of the isoforms of the plasma membrane calcium ATPase. *Cell Tissue Res* **292**, 191-197

26. Brandt, P., Neve, R. L., Kammesheidt, A., Rhoads, R. E., Vanaman, T. C. (1992). Analysis of the Tissue-specific Distribution of mRNAs Encoding the Plasma Membrane Calcium-ATPases and Characterization of an Alternately Spliced Form of PMCA4 at the cDNA and Genomic Levels. *The Journal of Biological Chemistry* **267** (7), 4376-4385

27. Zacharias, D. A., DeMarco, S. J., Strehler, E. E. (1997). mRNA expression of the four isoforms of the human plasma membrane Ca^{2+}-ATPase in the human hippocampus. *Molecular Brain Research* **45**, 173-176

28. Chicka, M. C., Strehler, E. E. (2003). Alternative Splicing of the First Intracellular Loop of Plasma Membrane Ca^{2+}-ATPase Isoform 2 Alters Its Membrane Targeting. *The Journal of Biological Chemistry* **278** (20), 18464-18470

29. James, P., Maeda, M., Fischer, R., Verma, A. K., Krebs, J., Penniston, J. T., Carafoli, E. (1988). Identification and Primary Structure of a Calmodulin Binding Domain of the Ca^{2+} Pump of Human Erythrocytes. *The Journal of Biological Chemistry* **263** (25), 2905-2910

30. Verma, A. K., Enyedi, A., Filoteo, A. G., Penniston J. T. (1994). Regulatory Region of Plasma Membrane Ca^{2+} Pump. *The Journal of Biological Chemistry* **269** (3), 1687-1691

31. Elshorst, B., Hennig, M., Försterling, H., Diener, A., Maurer, M., Schulte, P., Schwalbe, H., Griesinger, C., Krebs,J., Schmid, H., Vorherr,T., Carafoli, E. (1999). NMR Solution Structure of a Complex of Calmodulin with a Binding Peptide of the Ca^{2+} Pump. *Biochemistry* **38**, 12320-12332

32. Kessler, F., Falchetto, R., Heim, R., Meili, R., Vorherr, T., Strehler, E. E., Carafoli, E. (1992). Study of Calmodulin Binding to the Alternative Spliced C-terminal Domain of the Plasma Membrane Ca^{2+} Pump. *Biochemistry* **31**, 11785-11792

33. Niggli, V., Adunyah, E. S., Carafoli, E. (1981). Acidic Phospholipids, Unsaturated Fatty Acids, and Limited Proteolysis Mimic Effect of Calmodulin on the Purified Erythrocyte Ca^{2+}-ATPase. *The Journal of Biological Chemistry* **256** (16), 8588-8592

34. Missiaen, L., Raeymaekers, L., Wuytack, F., Vrolix, M., De Smedt, H., Casteels, R. (1989). Phospholipid-protein interactions of the plasma-membrane Ca^{2+}-transporting ATPase. *Biochemistry Journal* **263**, 687-694

35. Enyedi, A., Flura, M., Sarkadi, B., Gardos, G., Carafoli, E. (1987). The Maximal Velocity and the Calcium Affinity of the Red Cell Calcium Pump May Be regulated Independently. *The Journal of Biological Chemistry* **262** (13), 6425-6430

36. Filoteo, A. G., Enyedi, A., Penniston, J. T. (1992). The Lipid-binding Peptidi from the Plasma Membrane Ca^{2+} Pump Binds Calmodulin, and the Primary Calmodulin-binding Domain Interacts with Lipid. *The Journal of Biological Chemistry* **267** (17), 11800-11805

37. Caroni, P., Carafoli, E. (1981). Regulation of Ca2+-pumping ATPase of heart sarcolemma by a phosphorylation-dephosphorylation Process. *The Journal of Biological Chemistry* **256**, 9371-9373

38. Neyses, L., Reinlib, L., Carafoli, E. (1985). Phosphorylation of the Ca2+-pumping ATPase of Heart Sarcolemma and Erythrocyte Plasma Membrane by the cAMP-dependent Protein Kinase. *The Journal of Biological Chemistry* **260** (18), 10283-10287

39. James, P. H., Pruschy, M., Vorherr, T. E., Penniston, J. T., Carafoli, E. (1989). Primary Structure of the cAMP-Dependent Phosphorylation Site of the Plasma Membrane Calcium Pump. *Biochemistry* **28**, 4253-4258

40. Smallwood, J. I., Gügi, B., Rasmussen, H. (1988). Regulation of Erythrocyte Ca^{2+} Pump Activity by Protein Kinase C. *The Journal of Biological Chemistry* **263** (5), 2195-2202

41. Wang, K. K. W., Wright, L. C., Machan, C. L., Allen, B. G., Conigrave, A. D., Roufogalis, B. D. (1991). Protein Kinase C Phosphorylates the Carboxyl Terminus of the Plasma Membrane Ca^{2+} ATPase from Human Erythrocytes. *The Journal of Biological Chemistry* **266** (14), 9078-9085

42. Hofmann, F., Anagli, J., Carafoli, E. (1994). Phosphorylation of the Calmodulin Binding Domain of the Plasma Membrane Ca2+ Pump by Protein Kinase C Reduces Its Interaction with Calmodulin and with Its Pump Receptor Site. *The Journal of Biological Chemistry* **269** (30), 24298-24303

43. James, P., Vorherr, T., Krebs, J., Morelli, A., Castello, G., McCormick, D. J., Penniston, J. T., De Flora, A., Carafoli, E. (1989). Modulation of Erythrocyte Ca^{2+}-ATPase by Selective Calpain Cleavage of the Calmodulin-binding Domain. *The Journal of Biological Chemistry* **264** (14), 8289-8296

44. Goll, D. E., Thompson, v. F., Li, h., Wei, W., Cong, J. (2003). The Calpain System. *Physiological Reviews* **83**, 731-801

45. Kosk-Kosicka, D., Bzdega, T. (1988). Activation of the Erythrocyte Ca^{2+}-ATPase by Either Self-association or Interaction with Calmodulin. *The Journal of Biological Chemistry* **263** (34), 18184-18189.

46. Kosk-Kosicka, D., Bzdega, T., Wawrzynow, A. (1989). Fluorescence Energy Transfer Studies of Purified Erythrocyte Ca^{2+}-ATPase. *The Journal of Biological Chemistry* **264** (33), 19495-19499.

47. Levi, V., Rossi, J. P. F. C., Castello, P. R., Flecha, F. L. G (2002). Structural Significance of the Plasma Membrane Calcium Pump Oligomerization. *Biophysical Journal* **82**, 437-446.

48. Vorherr, T., Kessler, T., Hofmann, F., Carafoli, E. (1991). The Calmodulin-binding Domain Mediates the Self-association of the Plasma Membrane Ca^{2+} Pump. *The Journal of Biological Chemistry* **266** (5), 22-27

49. Levi, V., Rossi, J. P. F. C., Castello, P. R., Flecha, F. L. G (2000). Oligomerization of the plasma membrane calcium pump involves two regions with different thermal stability. *FEBS Letters* **483**, 99-103

50. Kosk-Kosicka, D., Bzdega, T., Johnson, J. D. (1990). Fluorescence Studies on Calmodulin Binding to Erythrocyte Ca^{2+}-ATPase in Different Oligomerization States. *Biochemistry* **29**, 1875-1879

51. Kosk-Kosicka, D., Bzdega, T. (1990). Effects of Calmodulin on Erythrocytes Ca^{2+}-ATPase Activation and Oligomerization. *Biochemistry* **29**, 3772-3777

52. Fujimoto, T. (1993). Calcium Pump of the Plasma Membrane Is Localized in Caveolae. *Journal of Cell. Biology* **120**, 1147-1157

53. Hammes, A., Oberdorf-Maass, S., Rother, T., Nething, K., Gollnick, F., Linz, K. W., Meyer, R., Hu, K., Han, H., Gaudron, P. (1998). Overexpression of the sarcolemmal calcium pump in the myocardium of transgenic rats. *Circ. Res.* **83**, 877-888

54. Fujimoto, T., Nakade, S., Miyawaki, A., Mikoshiba, K., Ogawa, K. (1992). Localization of inositol 1, 4, 5-triphosphate receptor-like protein in plasmalemmal caveolae. *Journal of Cell Biology* **119**, 1507-1513

55. Kim, E., DeMarco, S. J., Marfatia, S. M., Chishti, A. H., Sheng, M., Strehler, E. E. (1998). Plasma Membrane Ca^{2+} ATPase Isoform 4b Binds to Membrane-associated Guanylate Kinase (MAGUK) Proteins via Their PDZ (PSD-95/Dlg/ZO-1) Domains. *The Journal of Biological Chemistry* **273** (3), 1591-1595

56. DeMarco, S. J., Strehler, E. E. (2001). Plasma Membrane Ca^{2+} ATPase Isoforms 2b and 4b Interact Promiscuously and Selectivity with Members of the Membrane-associated Guanylate Kinase Family of PDZ (PSD-95/Dlg/ZO-1) Domain-containing Proteins. *The Journal of Biological Chemistry* **276** (24). 21594-21600

57. Ranganathan, R., Ross, E. M. (1997). PDZ domain proteins: Scaffold for signalling complexes. *Current Biology* **7**, R770-R773

58. Cabral, J. H., Petosa, C., Sutcliffe, M. J., Raza, S., Byron, O., Poy, F., Marfatia, S. M., Chisthi, A. H., Liddington, R. C. (1996). Crystal structure of a PDZ domain. Nature 382, 649-652

59. Doyle, D. A., Lee, A., Lewis, J., Kim, E., Sheng, M., MacKinnon, R. (1996). Crystal structures of a complexed and peptide-free membrane protein-binding domain: molecular basis of peptide recognition by PDZ. *Cell* **85**, 1067-1076

60. Jeleń, F., Oleksy, A., Śmietana, K., Otlewski, J. (2003). PDZ domains – common players in the cell signaling. *Acta Biochimica Polonica* **50** (4), 985-1017

61. Schuh, K., Uldrijan, S., Telkamp, M., Röthlein, N., Neyses, L. (2001). The plasma membrane calmodulin-dependent calcium pump: a major regulator of nitric oxide synthase I. *The Journal of Cell Biology* **155** (2), 201-205

62. Mungrue, I. N., Bredt, D. S. (2004). nNOS at a glance: implications for brain and brawn. *Journal of Cell Science* **117**, 2627-2629

63. Jacrot, B. (1976). The study of biological structures by neutron scattering from solution. *Rep. Prog. Phys.* **39**, 911-953

64. Hofmann, F., James, P., Vorherr, T., Carafoli, E. (1993). The C-terminal Domain of the Plasma Membrane Ca^{2+} Pump Contains Three High Affinity Ca^{2+} Binding Sites. The *Journal of Biological Chemistry* **268** (14), 10252-10259

65. Koch, M. H. J., Vachette, P., Svergun, D. I (2003). Small- angle scattering: a view on the properties, structures and structural changes of biological macromolecules in solution. *Quarterly Reviews in Biophysics* **36** (2), 147-227

66. Burgess, W. H., Jemiolo, D. K., Kretsinger, R. H. (1980). Interaction of calcium and calmodulin in presence of Sodium Dodecyl Sulphate. *Biochimica et Biophysica Acta* **623**, 257-270

67. Greenfield, N., Fasman, G. D. (1969). Computed Circular Dichroism Spectra for the Evaluation of Protein Conformation. *Biochemistry* **8** (10), 4108-4116

68. Seaton, B. A., Head,J. F., Engelman, D. M., Richards F. M. (1985). Calcium-Induced Increase in the Radius of Gyration and Maximum Dimension of Calmodulin Measured by Small- Angle X-ray Scattering. *Biochemistry* **24**, 6740-6743

69. Tang, D., Dean, W. L., Borchman, D., Paterson, C. A. (2006). The influence of membrane lipid structure on plasma membrane Ca^{2+}-Atpase activity. Cell Calcium **39**, 209-216

9 Supplementary material

Bacterial strains

E. coli strain used in all cloning steps was InvαF' that presents the following genotype: F', endA1, recA1, hsdR17 (rk-,mk+), supE44, thi-1, gyrA96, relA1, Φ 80 lacZΔM15, Δ(lacZYA-argF)U169, deoR.

E. coli strain used for the expression of recombinant proteins was BL21 (DE3) that presents the following genotype: F^{-}, ompT, hsdS (r_B^{-} m_B^{-}), gal dcm (DE3). DE3 indicates the presence of the λDE3 lysogen that brings the T7 RNA polymerase gene controlled by *lacUV5* promoter. BL21 strain is also deficient in the *lon* protease and lacks the ompT outer membrane protease that could degrade proteins during purification.

Culture medium and buffers

Culture medium

Liquid Luria-Bertani medium (LB)

Tryptone	10 g
Yeast extract	5 g
NaCl	10 g
Final volume	1 L

Solid Luria-Bertani medium

Tryptone	10 g
Yeast extract	5 g
NaCl	10 g
Bacto agar	15 g
Final volume	1 L

M9 Minimal Medium

5X M9 solution	200 mL
$MgSO_4$ 1 M	1 mL
$CaCl_2$ 1 M	0.1 mL
Sucrose 20%	20 mL
Final volume	1 L

5X M9 solution

$Na_2HPO_4 \cdot 7H_2O$	64 g
KH_2PO_4	15 g
NaCl	2.5 g
NH_4Cl	5 g
Final volume	1 L

Selective media were prepared adding to the solution ampicillin 100 μg/ mL or kanamycin 25 μg/ mL.

Buffers

Buffer Tris-Acetate EDTA (TAE)

Tris	40 mM

Glacial acetic acid	1.14 mL
EDTA pH 8.0	1 mM
Final volume	1 L

Buffer Tris-Acetate (TA)

Tris	40 mM
Glacial acetic acid	1.14 mL
Final volume	1 L

SDS-PAGE running buffer (pH 8.3)

Tris	25 mM
Glycine	0.192 M
SDS	0.1 %

SDS loading buffer (5X)

Tris	250 mM
SDS	5%
DTT	40 mM
MIA	20 mM
Glycerol 30° Bè	1 mL

Native running buffer (pH 8.3)

Tris	25 mM
Glycine	0.192 M

Molecular biology techniques

Preparation of competent cells

Single colony of InvαF′ or BL21 (DE3) *E. coli* cells was inoculated in 5 mL of LB and incubated at 37 °C overnight. 1 mL of the overnight cell culture was inoculated into 60 mL of fresh LB (in a 250 mL flask) and incubated at 37 °C to OD_{600}~ 0.5. The growth was stopped at 4°C for 30 minutes and the culture centrifuged at 2700g at 4 °C for 5 minutes. The pellet was resuspended in 30 mL of cold $CaCl_2$ 0.1 M and incubated in ice for 30 minutes. The suspension was centrifuged at 2700g at 4 °C for 5 minutes and the pellet resuspended with 2 mL of cold $CaCl_2$ 0.1 M, glycerol 20%. The suspension was incubated at 4 °C overnight and then the competent cells stored at -80 °C.

Transformation of chemical competent cells

Plasmid DNA was added to chemical competent cells that were before incubated in ice for 20 minutes and then at 42 °C for 90 seconds (heat shock). 900 µL of LB were added to the cells and the suspension incubated at 37 °C for 1 hour. Transformed cells were centrifuged at 2700g for 5 minutes and the pellet resuspended in 200 µL of LB. The suspension was streaked on LB agar plate containing the specific antibiotic (ampicillin or kanamycin) to select plasmid containing cells.

Ladder

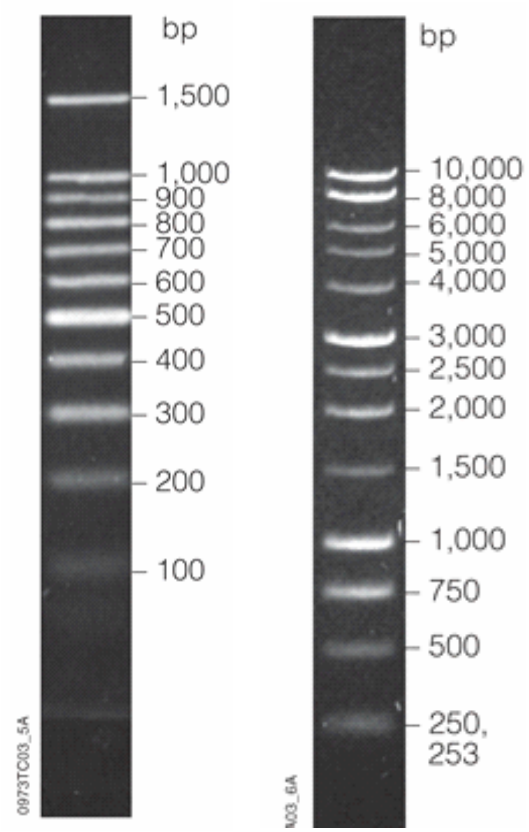

(a) (b)

(a) Promega ladder 100 bp
(b) Promega ladder 1 Kb